The modelling of flat fluidised photoreactors

Iatridis, D.

Award date:
1988

Awarding institution:
University of Bath

THE MODELLING OF FLAT FLUIDISED PHOTOREACTORS

Submitted by : D. Iatridis

for the degree of Ph.D. of

the University of Bath

1988

ProQuest LLC
789 East Eisenhower Parkway
P.O. Box 1346
Ann Arbor, MI 48106-1346

ACKNOWLEDGEMENTS

The author is sincerely grateful to the following persons and organisations for their contribution to this work.

1. Dr P.L. Yue for his supervision, advice and useful discussions throughout the present study.

2. The University of Bath for financial support through a research studentship.

3. Prof. L. Rizzuti, University of Palermo, for useful discussions.

4. Ministry of Economy of Greece for travel expenses and Prof. M Schiavello, University of Palermo for providing NATO funds in order a part of this research be presented in a NATO-ASI (Italy).

5. Technical staff, especially Mr T.B. Walton and J. Bishop for their technical assistance.

6. Friends and colleagues, especially Mr E. De Souza and Dr J. Dudley for transmitting their computing knowledge.

7. The author's Parents and Grandparents for their unfailing moral and financial support,

To

My Parents

CONTENTS

THE MODELLING OF FLAT FLUIDISED PHOTOREACTORS

Submitted by : D. Iatridis

for the degree of Ph.D. of

the University of Bath

1988

ACKNOWLEDGEMENTS

The author is sincerely grateful to the following persons and organisations for their contribution to this work.

1. Dr P.L. Yue for his supervision, advice and useful discussions throughout the present study.

2. The University of Bath for financial support through a research studentship.

3. Prof. L. Rizzuti, University of Palermo, for useful discussions.

4. Ministry of Economy of Greece for travel expenses and Prof. M Schiavello, University of Palermo for providing NATO funds in order a part of this research be presented in a NATO-ASI (Italy).

5. Technical staff, especially Mr T.B. Walton and J. Bishop for their technical assistance.

6. Friends and colleagues, especially Mr E. De Souza and Dr J. Dudley for transmitting their computing knowledge.

7. The author's Parents and Grandparents for their unfailing moral and financial support,

To

My Parents

CONTENTS

SUMMARY

The present research constitutes a systematic study towards the modelling and design of flat plate fluidised photoreactors. Light transmitted through a fluidised photoreactor (transmittance) and light reflected from the reactor (reflectance) have been measured by new optical techniques. These two important design variables were correlated with relevant fluidisation parameters.

The average light transmittance was found to increase with bed expansion, the square root of particle diameter and inversely with bed thickness. On the other hand, the average light reflectance was found to decrease with bed height and particle diameter. The correlations found for light transmittance and reflectance with the fluidised parameters were tested with experimental data using two types of particles of different optical characteristics. The form of these correlations was not affected by the type of particles used.

The light energy retained within a fluidised photoreactor, "light absorption", was evaluated by an energy balance from the measured values of light transmittance and reflectance. The light absorption data obtained were regressed for two different types of particles. For 13X zeolites the average light absorption by the bed was found to increase with the second power of bed height and the square root of particle diameter and reactor thickness. For Co-Mo-Al_2O_3 the average light absorption by the bed was found to increase with particle diameter and inversely with bed height.

A theoretical study was made using the light energy retained within the reactor to promote a photochemical reaction of first order with respect to reactant concentration and to light absorption.

The fluidised bed was treated as a single phase continuously stirred tank reactor (CSTR). The conversion of the reactant was found to increase with the light absorption and decrease with flow rate. This modelling approach may be extended to more complex hydrodynamic representation of a fluidised photoreactor and more complex reaction kinetics.

NOMENCLATURE

a'	coefficient in equation 2.4.2.	
a'_a	coefficient in absorption correlation for 13X zeolite particles (equation 6.7.1).	
a'_r	coefficient in reflectance correlation for 13X zeolite particles (equation 5.3).	
a'_t	coefficient in transmittance correlation for 13X zeolite particles (equation 4.2).	
$\dot{a}'''_\lambda$	local volumetric rate of energy absorption.	
A	reactant in equation 7.1.	
A'	absorptivity.	
b'	coefficient in equation 2.4.2.	
b'_a	coefficient in absorption correlation for 13X zeolite particles (equation 6.7.1).	mm^{-1}
b'_r	coefficient in reflectance correlation for 13X zeolite particles (equation 5.3).	$mm^{1/8}$
b'_t	coefficient in transmittance correlation for 13X zeolite particles (equation 4.2).	$mm^{1/2}$
B	product in equation 7.1.	
c	single albedo scattering.	
c'_a	coefficient in absorption correlation for Co-Mo-Al_2O_3 particles (equation 6.7.2).	
c'_r	coefficient in reflectance correlation for Co-Mo-Al_2O_3 particles (equation 5.4).	
c'_t	coefficient in transmittance correlation for Co-Mo-Al_2O_3 particles (equation 4.3).	
C	concentration of the absorbing medium.	
C_{as}	molar concentration of the absorbing species.	
C_A	final concentration of reactant A	$gr\text{-}mole/cm^3$
C_{Ao}	initial concentration of reactant A	$gr\text{-}mole/cm^3$
C_{O_2}	oxygen concentation	$mole/cm^3$

d	constant in the Lambert equation for the photoabsorption rate (equation 2.5.4).	
d_p	particle diameter.	mm
d_r	internal reactor thickness.	mm
d_p^o	constant for the normalisation of d_p.	mm
d_r^o	constant for the normalisation of d_r.	mm
d_a'	coefficient in absorption correlation for Co-Mo-Al_2O_3 particles (equation 6.7.2).	$mm^{-1/8}$
d_r'	coefficient in reflectance correlation for Co-Mo-Al_2O_3 particles (equation 5.4).	$mm^{1/8}$
d_t'	coefficient in transmittance correlation for Co-Mo-Al_2O_3 particles (equation 4.3).	$mm^{1/2}$
e_b	bubble voidage of the fluidised bed.	
$\dot{e}_\lambda'''$	local rate of energy absorption.	
E_r	fraction of local light reflectance, i.e. diffuse reflectance, at a given height (h) with respect to incident light.	
E_t	fraction of local light transmittance at a given height (h) with respect to incident light.	
$\bar{E}_t$	fraction of light transmittance with respect to empty reactor.	
$\hat{E}_a, \hat{E}_a^P$	fraction of mean light absorbed by the particles with respect to incident light.	
$\hat{E}_i$	fraction of mean incident light energy to the whole reactor with respect to incident light ($\hat{E}_i=1$).	
$\hat{E}_r$	fraction of mean light reflectance, i.e. diffuse reflectance, with respect to incident light.	
$\hat{E}_t, \hat{E}_t^{E+P}$	fraction of mean light transmittance through the whole reactor system with respect to incident light.	
$\hat{E}_a'$	volumetric rate of light absorption	$\mu J/cm^3 sec$

$\hat{E}_i'$	fraction of mean incident light energy at the inside of the rear wall of the reactor with respect to incident light.	
$\hat{E}_r'$	fraction of mean light reflectance of rear wall of the reactor with respect to incident light.	
$\hat{E}_a^E$	fraction of mean light absorbed by the empty reactor with respect to incident light.	
$\hat{E}_a^{E+P}$	fraction of mean light absorbed by empty reactor and particles (whole system) with respect to incident light.	
$\hat{E}_r^{E+P}$	fraction of mean light reflectance, i.e. specular and diffuse reflectance, from the whole reactor system with respect to incident light.	
$\hat{E}_r^{fw}$	fraction of mean light reflectance (specular) of front wall only with respect to incident light.	
$\hat{E}_t^{fw}$	fraction of mean light transmittance of front wall only with respect to incident light.	
F_{Ao}	mass flow rate of reactant A.	gr-mole/sec
h	local bed height.	mm
h'	Planck 's constant.	ergssec/molec
H	bed height.	mm
H'	height of irradiated section.	cm
H_{mf}	bed height at minimum fluidisation.	mm
I_o	incident light intensity at reactor wall.	einscm^{2}sec
$\bar{I}_a$	average absorbed power.	
k	kinetic constant.	cm^3/μJ
k_d	empirical coefficient depending on the optical properties of the system.	
l	light path lenght.	cm
l_s	single light path length.	cm

L	lenght of light source.	cm
m	optical thickness ($m=R_2\beta_{as}C_{as}$).	
P	specific photochemical power.	
Q	volumetric flow rate of reactant A.	cm^3/sec
Q'	light absorption rate.	eins/sec
Q_λ	light absorption rate in Yokota et al model(82).	$eins/cm^3sec$
r_A	consumption rate of reactant A.	$gr\text{-}mole/cm^3$
R'	reflectivity.	
R_1	radius of inner cylinder.	cm
R_2	radius of outer cylinder.	cm
s	linear coordinate.	
S	area of irradiated section.	cm^2
T'	transmissivity.	
u,U	superficial gas velocity.	mm/sec
u_{mb}	superficial gas velocity at which bubbles appear in the bed (minimum bubbling point).	mm/sec
u_{mf},U_{mf}	superficial gas velocity at point of incipient fluidisation (minimum fluidisation velocity).	mm/sec
V	total volume of the fluidised bed.	cm^3
W	width of irradiated section.	cm
x_A,X_A	fractional conversion of reactant A.	
z	axial distance along light source.	cm

GREEK

α	specific surface area.	cm^{-1}
β_{as}	molar absorptivity of the absorbing species.	
ΔP	pressure drop across the bed.	cm H_2O

ε	constant in the Lambert equation for the photoabsorption rate (equation 2.5.4).	
ε_G	gas hold-up.	
η	number of collisions.	
η'	absorption efficiency.	
η''	radiation efficiency.	
ϑ	spherical coordinate.	
λ	wavelength.	
μ	extinction coefficient.	
μ'	cosine of the angle between the direction of radiation and the positive axis $\dot{\tau}$ of the element considered.	
μ_e	effective absorption coefficient.	cm^{-1}
μ_L	absorption coefficient for liquid phase.	cm^{-1}
μ_λ	attenuation coefficient.	cm^{-1}
ν	frequency of radiation.	sec^{-1}
ξ	dimensionless axial distance.	
π	ratio of circumference to diameter of a circle (π=3.14).	
ρ	linear coordinate along the radiation path ($\rho=s/R_2$).	
σ	dimensionless radius of inner cylinder.	
σ	dimensionless radius of outer cylinder.	
τ	residence time of reactant A into the bed.	sec
τ'	optical variable.	
τ''	ratio of light energy vanished by dispersed phase.	
τ_n	residence time of reactant A in the compartment n (fig. 7.1).	sec

τ_{n-1}	residence time of reactant A in the compartment n-1 (fig. 7.1).	sec
τ_{n+1}	residence time of reactant A in the compartment n+1 (fig. 7.1).	sec
φ	spherical coordinate.	
ω	normalised radiation angle.	
Ω	solid angle.	

CHAPTER 1

INTRODUCTION

1.1 Background of research project

It has been more than sixty years since photochemical reactions became well known. However, the application of photochemical methods for the commercial production of chemicals appeared around the 1950's with the photohalogenation of hydrocarbons. Since then such commercial applications have stimulated considerable interest of research in the field of photochemical reaction engineering. Because of the trade secrecy, details on industrial photochemical processes are normally not available.

However, from researches carried out in different academic institutions, the discovery and investigation of efficient photochemical reactions in the laboratory scale have made some contributions to the possible conversion of solar energy into chemical energy. If these reactions are to be conducted in large scale, the engineering problems such as the design, operation and control of the photoreactors must be addressed.

Recently the production of hydrogen and ammonia has been successfully obtained by using efficient photocatalysts in gas-solid and gas-liquid-solid phase systems giving relatively high yields (25,26,100). These reactions have been conducted

in cylindrical and flat plate fluidised photoreactors. The flat plate fluidised photoreactor was found to give higher conversions than the cylindrical ones because of better utilisation of light energy by the photoreactants [25,26,100].

There is a need for further investigation and development into the modelling and design of such photoreactors. Thus the present study was conducted and the main objectives are summarised in section 1.2.

1.2 Objectives of Present Study

1. To measure the key variables which are required for the design of flat fluidised photoreactors. These variables are the light transmittance, reflectance and absorption.

2. To establish models which correlate these key variables with reactor parameters.

3. To show how these models of the key variables may be used in the modelling of photon driven reactions.

1.3 Organisation of Thesis

A literature review on photoreactions and photoreactors is given in Chapter 2. New experimental techniques and results of the measurement of light transmittance and reflectance as well as their influence by fluidisation parameters of the flat plate photoreactor are described in Chapters 3, 4 and 5. The light energy absorbed by the photoreactor is examined in Chapter 6.

The modelling of a hypothetical photoreaction using the absorbed energy is described in Chapter 7. The discussions, conclusions and recommendations of the present study are presented in Chapter 8.

CHAPTER 2

LITERATURE REVIEW OF PHOTOCHEMICAL REACTIONS AND PHOTOREACTORS

2.1 Homogeneous Photochemical Reactions

Homogeneous photochemical reactions have been investigated since the 1950's and are applied mainly to the photochlorination of organic compounds and the treatment of waste water. In 1951 Baginski[1] considered a liquid phase photochemical reaction between hydrogen sulphide and n-octene-1. However back mixing in the flow reactor thwarted a complete analysis of the data. The photochlorination of propane[2] and paraffin[3] have also been studied in cylindrical tubular flow reactors.

In 1970, Matsuura and Smith[4] studied the continuous photodecomposition of dodecylbenzene suflonate (DBS) as a process for water purification and as well as the photodecomposition of aqueous solutions of formic acid[5] as a model reaction for removing organic pollutants from water. In both studies a tubular flow reactor was used which was irradiated by a 1200 Watt mercury-vapour lamp. The calculated rate constants and quantum yields of the above systems agreed well with the experimental values.

Schorr and Smith[6] later developed a rate equation obtained by modelling differential reactor data for the photo-oxidation of organic pollutants in waste water. The

reaction rate which appeared to be of first order with respect to radiation absorbed by the photoreactants was found to be directly proportional to oxygen concentration (C_{O_2}) at low C_{O_2} but independent of C_{O_2} at high C_{O_2}. The quantum yield for the complete conversion of pollutants to carbon dioxide was reported to be 1.47×10^{-3}.

2.2 Heterogeneous Photochemical Reactions

Since the discovery of potential photoactive substances promoting chemical reactions, i.e. the so called photocatalysts, in the early seventies and the limited applicability of homogeneous photochemical reactions performed in gas or liquid phase for conversion of solar energy into chemical energy, the main research groups have now shifted to study the research of heterogeneous photochemical reactions. Among the heterogeneous photoreactions reported in the literature the splitting of water has been successfully obtained by using photoactive substances such as compound salts, semiconductors and zeolites.

The production of ammonia was another successful application of heterogeneous photoreactions which was obtained by the hydrogen produced from the splitting of water in nitrogen environment by using TiO_2 photocatalyst. Relatively high quantum yields for NH_3 production were obtained when titanium exchanged zeolites were used as photocatalysts. The evolution of CH_4 was also obtained from the combination of water gas and carbon dioxide over $SrTiO_3$-Pt.

Since a variety of substances showed photocatalytic action, Parmon and Zamaraev[7,8] classified them into three main groups, i.e. compound salts, semiconductors and zeolites. A discussion on their photocatalytic mechanism when in contact with chemicals will not be held here because the present study is concerned with the design of photoreactors. However, a selective literature survey was carried out and a summary of the research of heterogeneous photoreactions is reported in Tables 2.2.1 - 2.2.3.

2.3 Homogeneous Photoreactors

A photochemical reactor is a conventional chemical reactor which requires the exposure of the contents within reactor to light irradiation. Thus a photochemical reactor must have transparent walls if external irradiation is to reach the photoreacting species to promote the photochemical reaction.

If the photoreaction takes place in a single phase, then the reactor is referred to as a homogeneous photoreactor. For the modelling of such reactors the design equations involve the light absorption which is indispensible for any study towards the design of photoreactors. Thus a variety of modelling approaches have been considered by different researchers and mathematical formulations on light distribution and absorption have been proposed.

Before any mathematical formulation of light irradiation can be applied, knowledge of the path travelled by the rays emitted from the light source within the photoreactor must be known.

Author	Photoreaction	Photocatalyst/Light Source	Remarks	Ref.
Markham and Laidler	Evolution of H_2S	ZnO Ultra Violet lamp	Near Ultra Violet spectrum was used	9
Heidt and McMillan	Formation of H_2 and O_2 from water	Cerium (Ce^{4+}) ion salt. High intensity mercury arc lamp	Near Ultra Violet irradiation. 2% maximum quantum efficiency	10
Mann et al	Formation of H_2 and $[Rh_2(bridge)_4 Cl_2]^{2+}$ from $[Rh_2(bridge)_4 H_2]^{3+}$ Cl^- in 12M HCl solution	$[Rh_2(bridge)_4H_2]^{3+}$ Cl^- at 546nm irradiation	Quantum yield 0.004 ± 0.002	11
Kiwi and Gratzel	Evolution of H_2 from a dispersed platinum solution in polyvinyl alcohol	Dispersed platinum solution 450W Xenon lamp	400nm cut off filter Quantum yield 0.13	12

TABLE 2.2.1 Summary of research which used compound salts as photocatalysts

Author	Photoreaction	Photocatalyst/Light Source	Remarks	Ref.
Fujishima and Honda	Water cleavage	N-type TiO_2 at wavelength lesser than 415nm	Single crystal wafe of n-type rutile TiO_2. Quantum yield 10%	13
Schrauzer and Guth	Water cleavage	Mixture of rutile and anatase TiO_2	19.16 10^{-3} mmol/g of Ti/hr. Van Damme and Hall(15) were unable to reproduce the results	14
Hemminger et al	Evolution of CH_4 from gaseous H_2O and CO_2	$SrTiO_3$-Pt sandwich 500Watt high pressure mercury lamp	15 torr of CO_2 and 17 torr of H_2O were used. 15 torr of CH_4 was produced at 150 C.	16

TABLE 2.2.2 Summary of research which used semiconductors as photocatalysts

Author	Photoreaction	Photocatalyst/Light Source	Remarks	Ref.
Inoue et al	CO_2 reduction	Aqueous suspension of semiconductor powder (e.g. TiO_2, ZnO, CdS etc.) 500W Xe lamp	Quantum yield by using TiO_2. Aldehyde 5×10^{-4} Methanol 1.9×10^{-4}	17
Sakata et al	Water cleavage	$TiO_2 - RuO_2$	0.11 mmol of H_2 per 30mg of $TiO_2 - RuO_2$ for 120 hours were produced	18
Carr and Somorjai	Water cleavage	Platinized $SrTiO_3$ crystal	0.161 ml of H_2 at STP were produced. The reaction was carried out at 650 to 723 ^{o}C under illumination of high pressure discharge lamp	19
Augugliaro et al	Ammonia synthesis	Rutile TiO_2	$6.53 - 7.83 \times 10^{-3}$ mmol/ gr of Ti/hr	20
		Mixture of anatase and rutile TiO_2	5.04×10^{-3} mmol/ gr of Ti/hr	21

TABLE 2.2.2 (First page of continuation)

Author	Photoreaction	Photocatalyst/Light Source	Remarks	Ref
Yue et al	Ammonia synthesis	Iron doped titanium dioxide. Near UV irradiation	Quantum efficiency more than 10%. Mixing of photocatalyst with - A_2O_3 improved fluidisation behaviour and increased NH_3 production.	100
Miyama et al	Ammonia synthesis	Platinum and Eval	Eval is a copolymer of 32% mmol of ethylene and 68% mmol of vinyl alcohol. 2.8 mmol of NH_3 in 5 hours were produced	101
		Gap with Pt and Eval	7.5 mmol / 0.3 g cat. of NH_3 in 5 hours were produced	
Pichat et al	Oxidation of various compounds (e.g NH_3, propane etc.)	TiO_2 and other semi-conductor oxides UV light source	Gas - liquid phase photoreactor was used	102

TABLE 2.2.2 (Second page of continuation)

Author	Photoreaction	Photocatalyst/Light source	Remarks	Ref.
Kasal and Bishop	Formation of O_2 from water	Copper exchanged zeolite	Oxygen was produced at a temperature greater than 300 °C.	22
Jacob et al	Water cleavage	Silver exchanged zeolite	Mass spectrometer was used for hydrogen analysis.	23
		Magnesium exchanged zeolite X	The method of analysis was doubted by Schumacher (24)	
Schumacher and Leutwyler	Water cleavage	Silver exchanged zeolite A	Quantum Yield 0.6 for O_2 evolution	24
Khan et al	Water cleavage	Titanium exchanged 5A zeolite	1.15 mmol NH_3/gr of Ti/hr 0.77 mmol H_2/gr of Ti/hr Energy efficiency 19%	25
	Ammonia synthesis	Titanium exchanged 3A zeolite	0.31 mmol NH_3/gr of Ti/hr 8.07 mmol NH_3/gr of Ti/hr Energy efficiency 69.5%	26

TABLE 2.2.3 Summary of research which used zeolites as photocatalysts

Reflection, transmission, absorption and refraction of light by the photoreactor cause a change of direction or reduction of the light energy and must therefore be considered. However, if all the parameters mentioned above are taken into account the modelling problem becomes very complex. For this reason assumptions and simplifications are necessary for a solution of the light radiation distribution problem to be obtained. Thus the different modelling approaches employed are mainly characterised by the assumptions and simplifications made. The most commonly used are the (i) radial, (ii) partial diffuse, (iii) diffuse, (iv) line source and (v) extense source model.

In the radial model, the light rays are received by the photoreactor radially and travel only in planes normal to the reactor axis. In the partial diffuse model, light beams are received by the photoreactor from any direction. If the extension of light beam equals the reactor diameter then the diffuse model is obtained.

For the line source models different approaches have been considered. One approach is to consider each point of the line source emitting light on parallel planes. Another approach is to assume spherical emission from each point of the line source.

The extense source models provide rigorous models for the source as well as the reactor.

Alfano et al[45] have recently reviewed and classified the above outlined models. The 125 papers considered in their

review were classified according to incidence and emission models. The incidence models describe the radiant energy distribution in the vicinity of the reactor, while the emission models give mathematical formations of light energy distributions by considering the light source emission. These models as reported by Alfano et al[45] are given in Table 2.3.1.

A summary of the research on homogeneous photoreactors is reported in Table 2.3.2 and the individual work is discussed below.

The design of homogeneous photoreactors was first investigated in 1932, by Bhagwatt and Dhar[27] who developed a simplified radial model. In 1965, Hill and Felder[28] studied the light distribution and quantum yield for chain reactions in cylindrical, slab and an annular photoreactor. The following conditions of mixing were investigated: (i) no mixing, (ii) perfect lateral mixing without axial mixing and (iii) perfect mixing.

In 1967, Cassano at al[29] reviewed the progress on the design of photochemical reactors and pointed out the complexity of modelling multiphase photoprocesses in flow reactors. In this review they also pointed out that for any study on photoreactor design a priori knowledge of light distribution and hence of light absorption is required.

Later on Harano and Smith[30] used a tubular flow reactor to study the light intensity and radial concentration profiles for complex non chain reactions, again using the radial model. Laminar and plug flow were considered in the tubular reactor.

INCIDENCE MODEL	REFERENCES
Two-dimensional radial	37, 44, 46-48
Two-dimensional partially diffuse	37, 47
Two-dimensional diffuse	44, 49
Three-dimensional diffuse	38, 48
EMISSION MODEL	**REFERENCES**
Line source parallel plane	32, 34, 40, 50-52
Line source spherical	32-34, 51-54
Line source diffuse	40, 55
Extense source volumetric	56-60
Extense source superficial spherical	61-63
Extense source superficial diffuse	64

TABLE 2.3.1 Main radiation models as classified and reported by Alfano et al(45)

Author	Research Topic	Principles/Equations	Remarks	Ref.
Bhagwat and Dhar	Simplified radial model	Lambert law Rate eqns	First attempt in the reactor modelling	27
Hill and Felder	Chain reactions Cylindrical, slab and annular photoreactor	Lambert law Rate eqns Material balance	Conversion and yieldwere varied with reactor thick-ness and absorption coefficient	28
Cassano et al	Homogeneous reaction Annular, slab and cylindrical reactor	Lambert law Thermal energy eqn Radiation eqn Rate eqn.	Review paper	29
Harrano and Smith	Non - chain reaction Tubular flow reactor	Rate eqn. Radiation Eqn.	Discussion of the effect of operating variables on reactor performance	30
Harrano and Smith	Annular, flat-plate, and cylindrical reactor	Lambert law Material balance	Review paper	31

TABLE 2.3.2 Summary of the research in homogeneous photoreactors

Author	Research Topic	Principles / Equations	Remarks	Ref.
Skarbo and Williams	Tubular flow reactor Radial model	Lambert law Rate eqn.	Effect of internal light filtering to reactor performance	36
Williams and Ragonese	Tubular flow reactor Radial model Momochromatic radiation	Rate eqn. Light intensity eqn. Steady state Continuity eqn.	Radial diffusion of reactant increases conversion	35
Jacob and Dranoff	Chloroplatinic acid Annular well - mixed reactor	Lambert law Empirical convection factor	Relfection and refraction effects were neglected within reactor	32-34
Matsuura and Smith	Cylindrical photoreactor Radial, partial diffuse and diffuse models	Intersity profiles for radial and partial diffuse models. Rate eqns.	Average light intensity was used	37
Zolner III and Williams	Cylindrical reactor with elliptical reflector, 3-D diffuse model	Light diffusion eqn.	Matsuura et al (37) model was a limiting case of the 3-D diffuse model	38

TABLE 2.3.2 (First page of continuation)

Author	Research Topic	Principles/Equations	Remarks	Ref.
Akehata and Shirai	Annular photoreactor Radial, specular and diffuse line source model	Light intensity eqn. Radial scale-up	Results in agreement with those obtained by Jacob and Dranoff (32-34)	40
Roger and Villermaux	Cylindrical reactor Partial diffuse model	Intensity profile eqn. including the incident wall flux	A modification of the partial diffuse model proposed by Matsuura and Smith (37)	44, 43
Williams	Cylindrical photoreactor with elliprical reflector 3-D diffuse model	Light diffusion Eqn.	Experimental results compared with that predicted by Zolner III and Williams (38)	39
Costa	Cylindrical and Annular reactors. Radial and perfect mixing model	Mass balance Radiation and kinetic equations	Review paper	41
Sugawara et al	Batch and laminar 2-D flat-plate reactor Polychromatic diffuse model Monochromatic parallel light model	Lambert law Mass balance Rate eqns.	Homogeneous irreversible photochemical reaction was considered in the light distribution analysis	65

TABLE 2.3.2 (Second page of continuation)

Author	Research Topic	Principles/Equations	Remarks	Ref.
Bhatt-acharya and Deshpande	Cylindrical reactor Axially irradiated model	Mass and radiation equation	Mixing effect are not always beneficial for the axially irradiated reactor	66
Tournier et al	Cylindrical reactor Semi-empirical model	Light intensity equation	Good agreement obtained between experimental data and some simplified models (30,31,4,5,38) at only low optical densities	42
Roger and Villermaux	Cylindrical reactor Radial model 2-D and 3-D diffuse model 2-D and 3-D specular model	Basic laws of photo-metry, Lambert law	Absorption efficiency and average absorbed power were well correlated	44
Alfano et al	Incidence model Emission model	Lambert Law Eqn. Radiation eqns Mass balance eqns	The most important review paper on the radiation modelling of homogeneous photoreactors	45

TABLE 2.3.2 (Third page of continuation)

Later on the same authors[31] reviewed the design of various homogeneous photoreactors using the simplified radial model. In their review the steady state analysis, the optical thickness, the shape of reactor, the light intensity profile and the effect of mixing were discussed with respect to photoreactor design.

For the first time Jacob and Dranoff[32-34] attempted to use the combination of Lambert law and an empirical convection factor (non-radial model) in order to investigate the effect of light distribution and radial scale-up of the design of annular shaped, well-mixed photoreactors. Their experimental data were obtained by using chloroplatinic acid as the actinometer. The results gave satisfactory agreement with that predicted by the rigorous model based on a point to point integration. They also found that the light absorption characteristics might be combined with functional dependence of quantum efficiency, light intensity and wavelength distribution.

The effect of light distribution was experimentally investigated by Williams et al[35,36] applying the radial model for unidirectional and monochromatic radiation in a liquid phase tubular flow reactor under the following types of flow and mixing: (i) perfect radial and axial mixing, (ii) plug flow with perfect radial mixing, (iii) plug flow without radial mixing and (iv) laminar flow with no radial mixing. Their results showed that radial mixing of the photoreactants would increase the conversion for systems with both small and large optical densities.

A cylindrical photoreactor was used by Matsuura and Smith[37] to investigate experimentally light intensity profiles for testing radial, partial diffuse and diffuse models. Their two dimensional diffuse model, i.e. light travels in planes perpendicular to the cylindrical reactor axis, was extended by Zolner III and Williams[38] to a three dimensional diffuse model in order to accommodate the variation of radial and axial light intensities within the cylindrical reactor. Thus the Matsuura and Smith's[37] model became a limiting case of the three dimensional diffuse model.

A direct experimental verification of the 3-D diffuse model was later shown by Williams[39]. The light intensity at the reactor wall was accurately measured by using an actinometric technique. The quantum yields and reaction rates were evaluated and complied satisfactorily with the values predicted by the diffuse model. However, the results obtained were limited to the case of a cylindrical reactor with an elliptical reflector.

In 1972 Akehata and Shirai[40] proposed three line source models, i.e. the radial, specular and diffuse models, in an annular shape photoreactor. The light intensity distribution was evaluated by using the same actinometer used by Jacob and Dranoff[32]. The main assumptions were that the absorption coefficient and quantum yield were constant. The results of their work were found to be in agreement with those obtained by Jacob and Dranoff[32-34].

Costa[41] in 1977 gave a thorough analysis of the state of theoretical calculation, design, construction and operation of

cylindrical and annular photochemical reactors. Then in the same paper the advantages and disadvantages on the improvement of photoreactor designs were also discussed.

In the early eighties a semi-empirical model based on the experimental determination of light distribution in a cylindrical photoreactor was proposed by Tournier et al[42]. In their work they suggested that the local light energy distribution would be important in order to evaluate the main reaction rate and in the design of the photoreactor. The experimental results obtained were then used to investigate the validity of the radial model[30,31], the 2-D diffuse model[4,5], and the 3-D diffuse model[38]. Theoretical and experimental results agreed only for low optical densities.

The basic concepts of photometry were used by Roger and Villermaux[43] to study the modelling of monochromatic light absorption in photoreactors of different shapes. The Beer-Lambert law was reformulated allowing unambiguous determination of the radiation field inside the reactor, including the limiting cases of diffuse and unidirectional radiation. The incident light flux at the wall was determined by the relative geometric configuration of the lamp-reactor system including the characteristics of the emitted radiation. The exact expressions for the light intensity distribution and the absorption efficiency were derived later on by the same authors[44] under four different situations of emitted radiation at the reactor wall, i.e. the two and three dimensional diffuse emission and two and three dimensional specular emission.

The absorption efficiency (η') in each situation was found to be very close to the following simple expression:

$$\eta' = [1-\exp(-\mu d)] \qquad 2.2.1$$

where

μ = extinction coefficient

d = proportional to the reactor radius.

Using the previously published experimental results on the decomposition of tetrachloroplatinic acid[43], it was shown that the data could be equally well represented by any of the five models (including the simple radial one). They hence concluded that sophisticated mathematical models are useless for the design and scale-up of photoreactors for liquid-phase reaction considered by them[43]. They also concluded that the average absorbed power ($\bar{I}a$) might be calculated from the available specific photochemical power (P) by the following simple relationship:

$$\bar{I}_a = P[1-\exp(-\mu d)] \qquad 2.2.2$$

However it should be noted that the 2.2.1 and 2.2.2 correlations developed are restricted to the homogenous liquid-phase reactions considered. It should also be mentioned that the light transmittance and reflectance were neglected and that the light scattering effect which would be important when solids are present in the reactor has also been ignored in the modelling.

2.4 Heterogeneous Photoreactors

The average energy distribution in several irradiated stirred tank slurry reactors with the presence of phosphorescent slurry particles has been studied by Rudd[67]. A probabilistic approach was employed in developing a mathematical model which would isolate the effect due to individual important operating parameters of irradiated continuous stirred tank slurry reactors. A solution for the distributed energy was obtained in the terms of properties of the stirred reactor system, (e.g. size of reactor, order of reaction, rate constants, etc.), and the formulation obtained could be applied to a design problem.

Santarelli et al[68-71] attempted to model heterogeneous photoreactors by using the theory of radiant energy transfer. This approach has a very sound theoretical basis. However, the validity of these models has not been tested experimentally in any type of continuous flow reactors. The distribution of light intensity, the effects of light scattering and that of reflecting boundaries have been investigated for batch and continuous flow photoreactors. Rigorous and simplified approaches were applied to both cylindrical and flat plate reactors. However, the effect of light scattering was only considered in a bed with stationary particles. No attempt has been made to account for the effect of scattering in a bed with moving particles such as a fluidised bed photoreactor.

The integro-differential equation of the radiative transfer governing the light intensity distribution in the

photocatalytic parallel plate reactor was given[70] by:

$$\frac{1}{\mu'}\frac{\partial I(\tau',\mu')}{\partial \tau'} + I(\tau',\mu') = \frac{c}{2}\int_{-1}^{1} I(\tau',\mu')d\mu' \qquad 2.4.1$$

where

$I(\tau',\mu')$ = radiation intensity

τ' = optical variable

μ' = cosine of the angle between the direction of radiation and the positive axis τ of the element considered

c = single albedo scattering.

The exact solution of the above integro-differential equation 2.4.1 is formidable. However, some approximated solutions using semi-analytical techniques and numerical calculations have been proposed, e.g. integral transform methods[72,73] and projectional methods[74].

Akehata et al[75,76] considered two different situations in a flat plate photoreactor: a dilutely dispersed phase system and a concentrated dispersed phase system. For the dilutely dispersed phase system it was assumed that a single bubble within the hetergeneous medium was irradiated by parallel rays in its front face and its back face was irradiated by a completely diffused irradiation.

For the concentrated dispersed phase system a completely diffused irradiation was received by both faces of any single bubble

within the heterogeneous medium. Thus the above assumptions made it possible for a radiation balance including scattering, transmission and absorption coefficients to be applied to both systems.

The numerical solutions of the mathematical model were in good agreement with the experimental values obtained for the dilutely dispersed phase system. For the concentrated dispersed phase system the authors introduced a correcting factor to bring about an agreement between theoretical and experimental values.

In 1983 Rizzuti and Yue[77] attempted to study experimentally the light transmittance through an irradiated two-dimensional fluidised bed reactor containing photocatalytic particles. They have also successfully correlated the average light transmittance with the bubble voidage of bed, the particle diameter and reactor thickness. The experimental apparatus used in their work is given in Fig. 2.4.1 The correlation obtained had the following form:

$$\bar{E}_t = a' + b'\left(e_b\right)\left(\frac{d_p}{d_p^\circ}\right)^{0.5}\left(\frac{d_r}{d_r^\circ}\right)^{-1} \qquad 2.4.2$$

where

$\bar{E}_t$ = fraction of light transmittance with respect to empty reactor

a', b' = coefficients in equation 2.4.2

e_b = bubble voidage of the fluidised bed

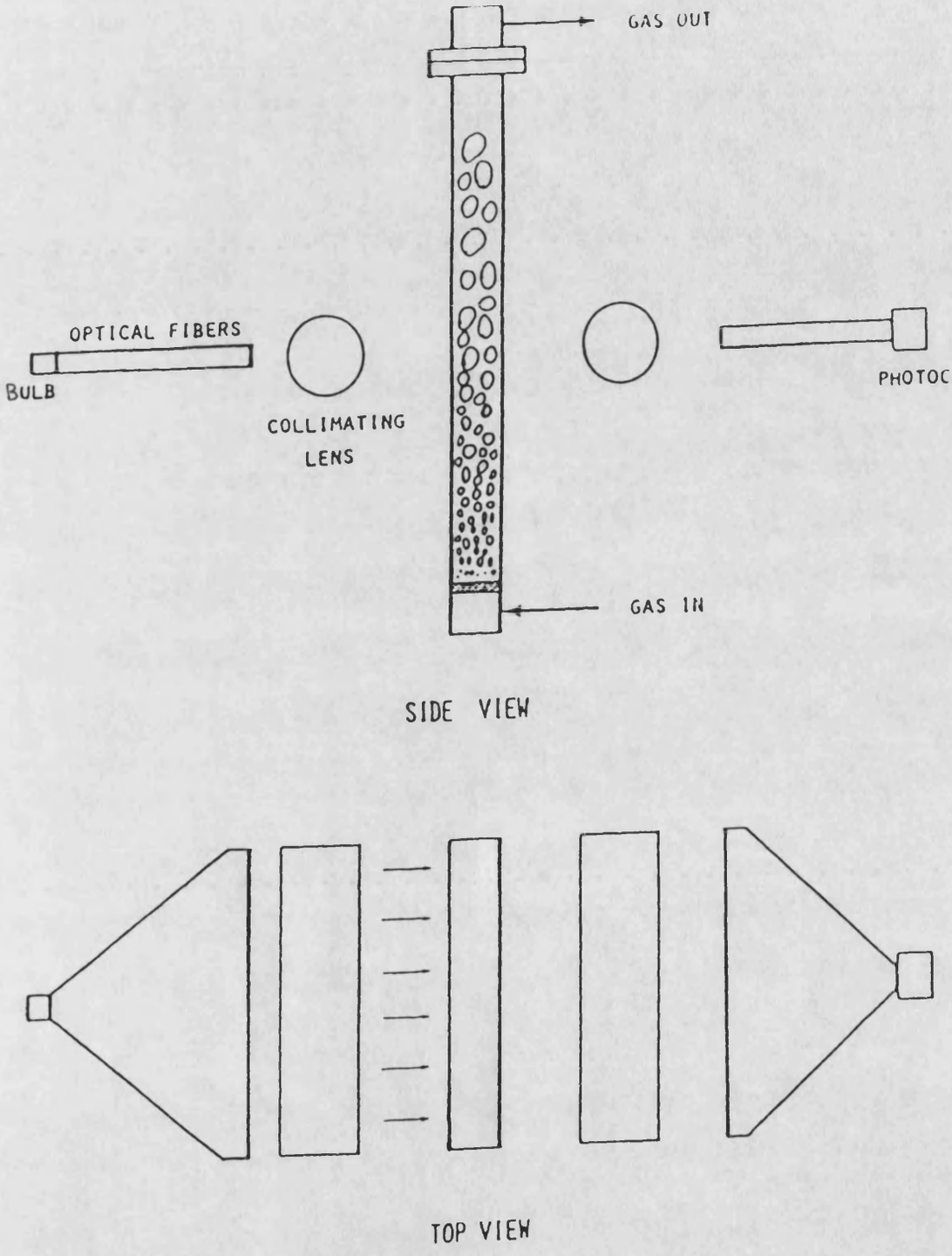

Figure 2.4.1. Experimental apparatus used by Rizzuti and Yue[77]

d_p = particle diameter (mm)

d_r = reactor thickness (mm)

d_p^o, d_r^o = constants for the normalization of d_p and d_r (mm)

The same authors[78] later on used the same light transmission technique to explain the gas flow patterns in a gas-solid fluidised bed reactor.

In 1986 Alfano et al[79] reviewed the present state of modelling the radiation field in heterogeneous media. In their review the radiation field models were classified into four different groups. These groups are (i) two flux model[75,76], (ii) distribution function model[81-83], (iii) Monte Carlo simulation model[71] and (iv) effective absorption coefficient model[82].

2.5 Light Absorption in Homogeneous Photoreactors

Since the volumetric rate of energy absorption is the most fundamental parameter for the modelling and design of photoreactors, the present section reports research which is related to the study of light absorption in homogeneous photoreactors.

Stramigioli et al[61] used an extensive light source with superficial emission, monochromatic light in an absorbing homogeneous medium in order to evaluate the local volumetric rate of energy absorption. They applied a radiation energy balance to the homogeneous medium and the local volumetric rate of energy absorption ($\dot{a}'''_\lambda$) was found to have the following expression:

$$\dot{a}_{\lambda}'''' = \frac{1}{2\pi}\int_{\varphi_1}^{\varphi_2}\int_{\vartheta_1}^{\vartheta_2} \exp[-m\rho]\sin\vartheta d\vartheta d\varphi \qquad 2.5.1$$

with $m = R_2\beta_{as}C_{as}$ $\qquad \rho = \frac{s}{R_2}$

where

m = optical thickness

R_2 = radius of the outer wall of the reactor

β_{as} = molar absorptivity of the absorbing species

C_{as} = molar concentration of the absorbing species

ρ = linear coordinate along the radiation path

s = linear coordinate

ϑ, φ = spherical coordinates

The spherical coordinates and the geometrical characteristics of the superficial emission model are shown in Fig. 2.5.1

The reflectivity and transmissivity of an absorbing slab which can lead to the evaluation of absorptivity (A') has been studied theoretically by Lii and Ozisik[84]. The effect of scattering by the photoabsorbing medium has also been included in their study. They applied radiative transfer theory to the evaluation of reflectivity (R') and transmissivity (T') and obtained the following expressions:

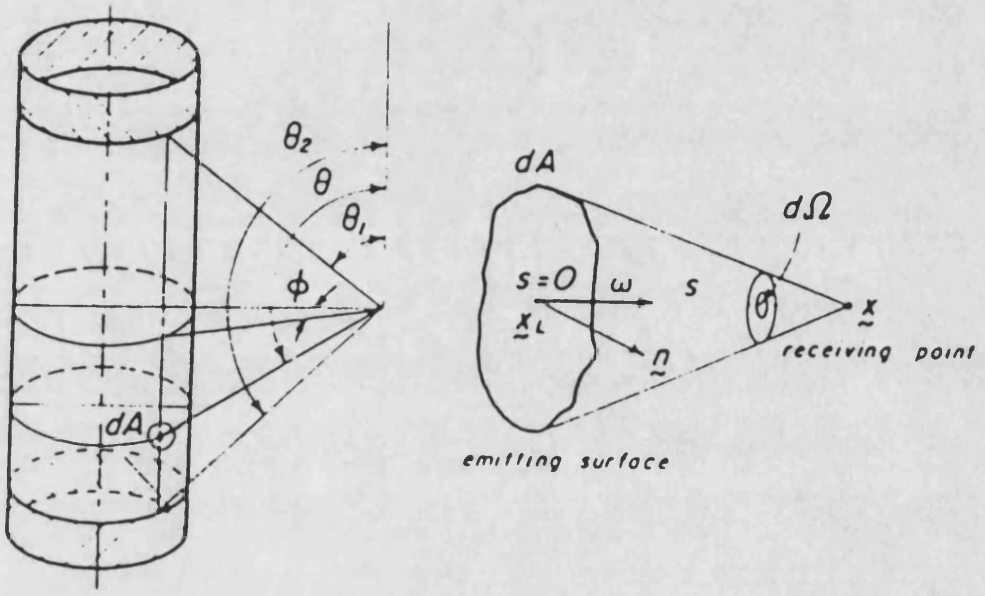

Figure 2.5.1. Geometrical characteristics of the superficial emission model by Santarelli et al[61]

$$R' = \frac{1}{2\pi}\left[G(0) + \frac{2}{3}\frac{dG(0)}{d\tau'}\right] \qquad 2.5.2$$

$$T' = -\frac{1}{3\pi}\frac{dG(\tau_o)}{d\tau'} \qquad 2.5.3$$

where $G(\tau')$ was a function of the radiation intensity ($I(\tau',\mu')$) and the radiant heat flux ($q(\tau')$). It was concluded that the absorptivity (A') of the slab could be determined from the $A'+R'+T'=1$ equation.

Sugawara et al[85] studied the light intensity distribution in a parallel plate reactor under laminar flow. The usual assumption that the reaction rate is proportional to the radiant energy absorption and that the validity of Beer's Law were adopted.

The same actinometric reaction was used by Shirotsuka et al[86-89] who made a distinction between models using monochromatic light source and polychromatic light source[88]. They found good agreement between experimental results and that resulted from their proposed model based on the assumption that the polychromatic photochemical reaction was a concurrence of reactions irradiated by monochromatic light. The same authors[87] derived a generalised power law expression for the photochemical reaction rate by using the following equation:

$$\mu(C) = \epsilon C^d \qquad 2.5.4$$

where

C = concentration of the absorbing medium

ϵ, d = constants in the Lambert equation for the photoabsorption rate.

Thus Beer's law is a special case when d is equal to 1. The experimental data agreed with the calculated rates using d=1 and d=0.88 for wavelengths of 365 and 463 nm respectively.

2.6 Light Absorption in Heterogeneous Photoreactors

The absorption rate of light in a heterogeneous photochemical reactor has been studied by Yokota et al[80]. The method proposed was based on the light path length and collision number distribution within the reactor. The theoretical predictions of light absorption rate were compared with the experimental results obtained by the photoreduction of the potassium ferrioxalate.

The photoreactor was irradiated with parallel rays. The dispersed phase was introduced under the form of vertical cylinders. A schematic representation of the photoreactor and the light path distribution is shown in Figure 2.6.1. Thus radiation scattering was produced on a horizontal plane perpendicular to the vertical cylinders. Reflection, transmission and refraction were caused by the dispersed phase. Finally the light absorption rate in the heterogeneous photoreactor considered was given by the following equation:

$$Q' = SI_0 \int_0^{\infty} f_2(\eta) \left\{ 1 - \int_0^{\infty} f(l_s/\eta) e^{-\mu l_s} dl_s \right\} \times \frac{1 - \left\{ \tau'' \int_0^{\infty} f(l_s/\eta) e^{-\mu l_s} dl_s \right\}^{\eta}}{1 - \tau'' \int_0^{\infty} f(l_s/\eta) e^{-\mu l_s} dl_s} \times d\eta \qquad 2.6.1$$

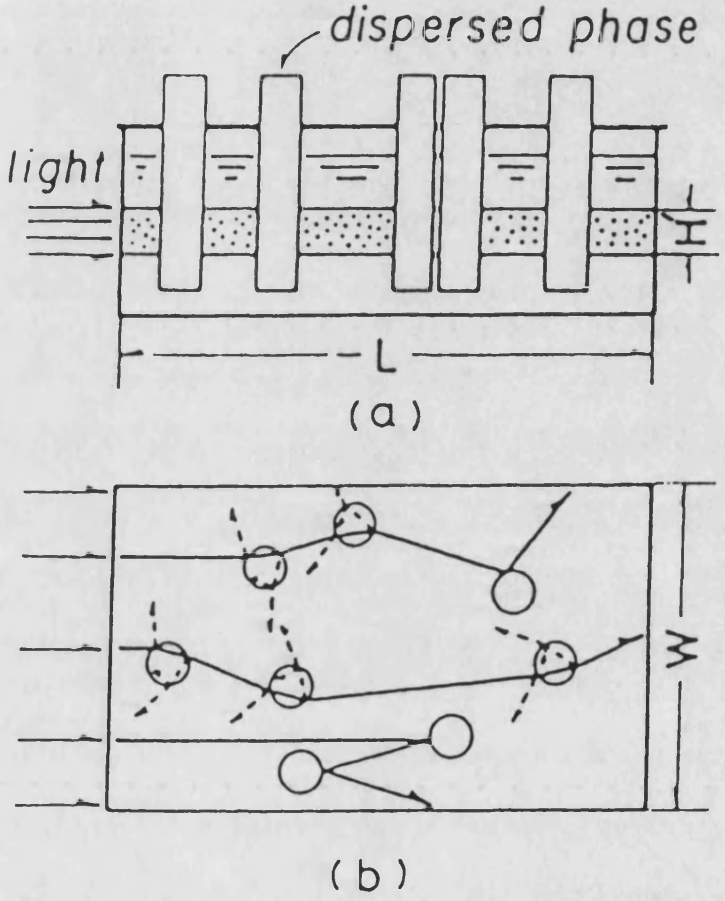

Figure 2.6.1. Experimental rectangular photoreactor used by Yokota et al[80] a) front view of photoreactor b) light path through the dispersed phase

with $S=WxH$

where

Q = light absorption rate — eins/sec

S = area of irradiated section — cm^2

W = width of irradiated section — cm

H' = height of irradiated section — cm

Io = incident light intensity at reactor wall — $eins/cm^2 sec$

$f_2(\eta)$ = marginal density function for collision number

$f(l_s/\eta)$ = conditional density function of single light path length at collision number n — cm^{-1}

μ = attenuation coefficient — cm^{-1}

l_s = single light path length — cm

τ'' = ratio of light energy vanished by dispersed phase

η = number of collisions

Later on the same authors[81] used a similar experimental apparatus to study the effect of light filtering by dispersed phase on the light absorption rate in a heterogeneous photochemical reactor. The experimental results obtained from the photoreduction of potassium ferrioxalate agreed well with the calculated values based on the statistical method previously proposed[80]. Thus it was concluded that the method has been proved to be applicable to a heterogeneous photochemical reactor with light filtering by a dispersed phase.

In 1981 Yokota et al[82] proposed a new statistical approach to estimate the light absorption rate in a gas-liquid photochemical reactor in which the light rays were scattered by bubbles. The estimation of light absorption rate was based on the probability distribution function of the light path length in the reactor zone by using Monte Carlo technique. The use of the actinometric reaction of photoreduction of potassium ferrioxalate confirmed the agreement between experimental and estimated values of the light absorption rate. The proposed formulation for the light absorption rate was given by the following equation:

$$Q_\lambda = \frac{4\sigma_1}{\sigma_2^2 - \sigma_1^2}\left(\frac{I_{\omega,\lambda}}{L}\right)\frac{1}{\eta''}\int_0^1\int_{-0.5}^{0.5}\cos^2(\pi\omega)\times$$

$$\times\left\{1-\exp(-\mu_\lambda l)\right\}d\omega d\xi \qquad 2.6.2$$

with $\xi = \frac{z}{L}$, $\omega = \frac{\vartheta}{\pi}$, $\sigma_1 = \frac{R_1}{L}$, $\sigma_2 = \frac{R_2}{L}$, $\eta = \frac{2}{\pi}\tan^{-1}\left(\frac{L}{R_1}\right)$

where

Q_λ	=	light absorption rate	eins/cm^3 sec
σ_1	=	dimensionless radius of inner cylinder	
σ_2	=	dimensionless radius of outer cylinder	
R_1	=	radius of inner cylinder	cm
R_2	=	radius of outer cylinder	cm
L	=	length of light source	cm

$I_{\omega,\lambda}$ = incident light intensity at inner cylinder wall — eins/cm² sec

η'' = radiation efficiency

ω = normalized radiation angle

μ_λ = attenuation coefficient — cm^{-1}

l = light path length — cm

ξ = dimensionless axial distance

z = axial distance along light source — cm

Otake et al[90,91] investigated the applicability of an effective absorption coefficient in a rectangular shape gas-liquid photoreactor as shown in Fig. 2.6.2. The following equation for the effective absorption coefficient (μ_e) was proposed:

$$\mu_e = \mu_L(1-\epsilon_G) + k_d a \qquad 2.6.3$$

where

μ_L = absorption coefficient for liquid phase — cm^{-1}

ϵ_G = gas hold-up

k_d = empirical coefficient depending on the optical properties of the system.

a = specific surface area — cm^{-1}

The scattering effects in photosensitised reactions for continuous processes have been studied by Spandoni et al[71] using the Monte Carlo approach. They found that scattering effects reduces the reactant conversion. They also suggested that the local rate of

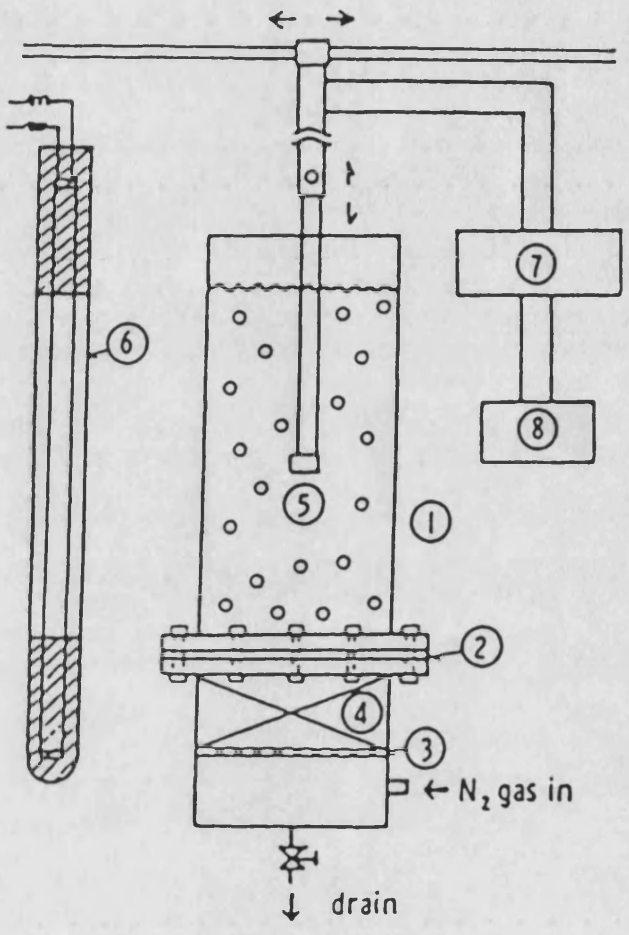

① bubble column
② porous or perforated plate
③ distributor
④ 4 mmØ Raschig ring
⑤ probe
⑥ low-pressure mercury lamp
⑦ DC power source
⑧ recorder

Figure 2.6.2. Experimental apparatus of the rectangular photoreactor used by Otake et al[91]

energy absorption ($\dot{e}'''_\lambda$) could be evaluated by integrating the integro-differential equation of the light intensity distribution. Thus the general formulation for $\dot{e}'''_\lambda$ was given as follows:

$$\dot{e}'''_\lambda(x) = k_\lambda \int_{4\pi} I_{\lambda\omega}(x) d\Omega \qquad 2.6.4$$

where

k_λ = absorption coefficient

$I_{\lambda\omega(x)}$ = radiation intensity

Ω = solid angle

2.7 Type of Photoreactors

For the selection of a conventional chemical reactor knowledge of the mode of operation, i.e. batch, continuous, of the phases involved, i.e. single phase, multi-phase, of heat exchange, of mixing and flow characteristics and of material of construction are required.

For the selection of a photoreactor in addition to the previous requirements the light source as well as the geometrical configuration of the photoreactor must be considered. The light source provides the light intensity and the correct wavelength for the activation of the specific photoreaction intended. However, the light source and the geometrical configuration of the photoreactor must be coupled in such a way that the light energy distribution within the photoreactor is sufficient for the promotion of the selected photoreaction.

In 1985 Yue[93] discussed the modelling and design of photoreactors. He pointed out the importance of reactor geometry and the spatial relation between reactor and light source. From the reactor geometry aspect, the following three simple geometries have been used: (i) cylindrical in which the irradiation can be normal to or axially aligned with the flow of reactants. (ii) parallel plate in which the light energy mainly travels in parallel planes normal to the direction of flow and (iii) annular photoreactor in which the emission of light is perpendicular to the inner reactor wall.

The popular annular photoreactor arrangement is shown in Fig. 2.7.1[93]. The photoreactants flow within the annular space of the reactor. The light source is positioned in the geometrical axis of the annular and a coolant is used to remove the heat generated by the lamp. The use of a coolant in a jacket on the outside surface of the photoreactor removes the heat generated by the photoreaction.

The flat plate fluidised bed photoreactor is shown in Fig. 2.7.2 In this type of photoreactor the photoreactants are fed from the bottom and fluidisation enchances contact between reactants photoratalyst and photons. This type of photoreactor has been shown to be more efficient than a cylindrical one with respect to the conversion obtained under the same conditions of irradiation[25,26,100].

Another type of photoreactor is the falling film reactor. This type of reactor has the advantage of direct exposure of photoreactants to light irradiation without the need of a reactor wall between light-source flow reactants. However, such reactors are limited to low flow rates. Fig. 2.7.3 shows such a photoreactor designed by Braun[94].

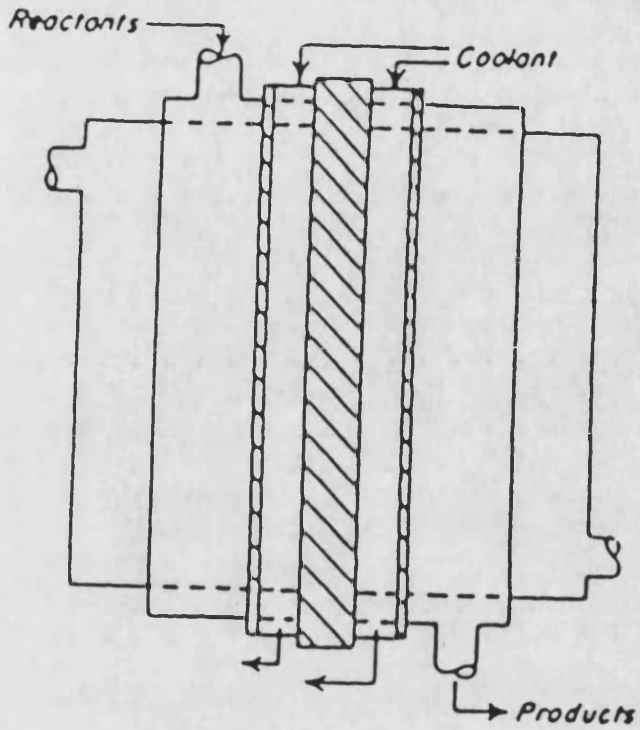

Figure 2.7.1. Annular type photoreactor as reported by Yue[93]

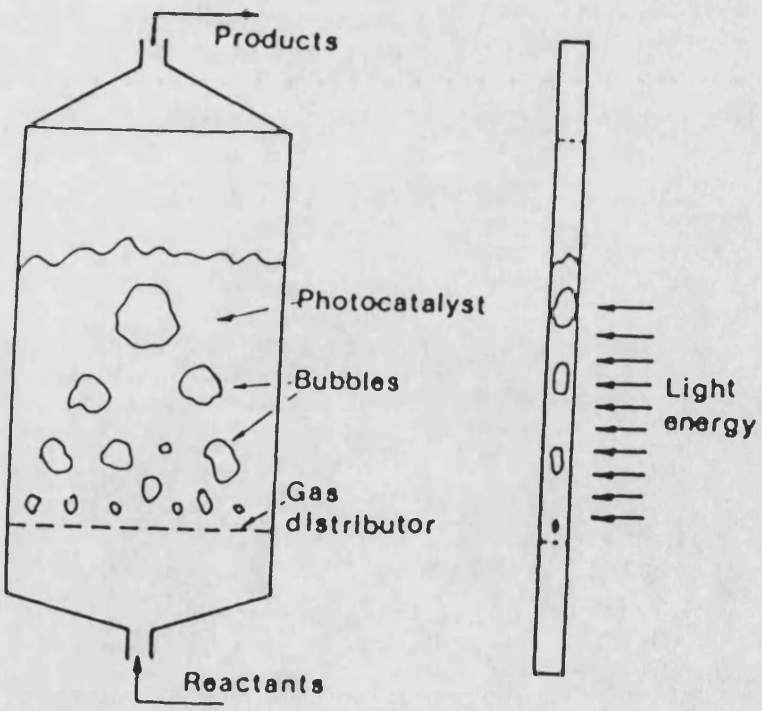

Figure 2.7.2. Two-dimensional fluidised bed photoreactor as reported by Yue[93]

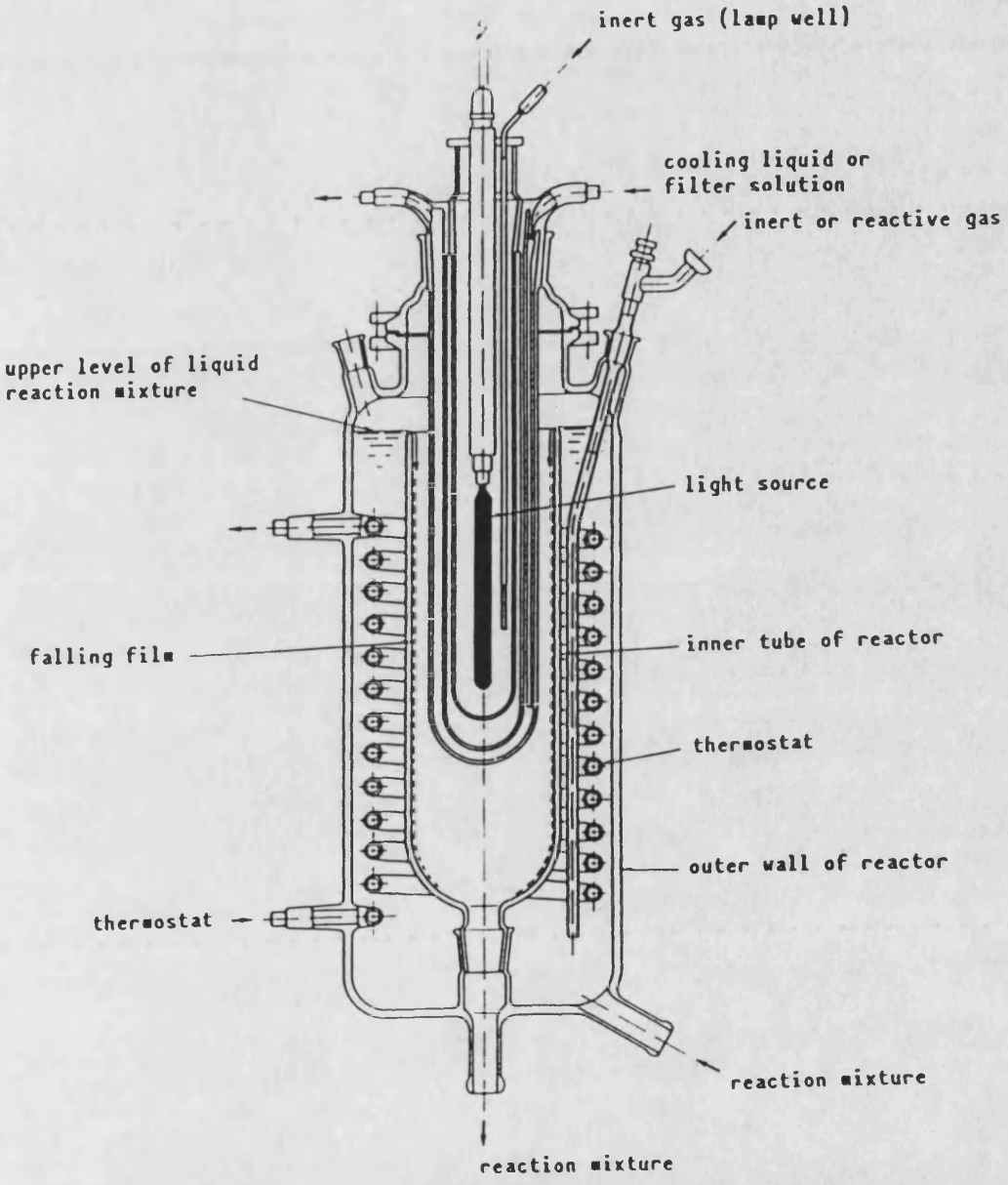

Figure 2.7.3. Falling film photoreactor of Braun-De Meijere[94]

The same type of photoreactor has been used by Movahed[103] to investigate the oxidation of aqueous phenol solutions ultra violet radiation with Ozone in the gas phase. The experimental results showed poor utilisation of Ozone by the liquid phase. This is in contrast with high utilisation of O_3 obtained by using a bubble column with immersed ultra violet lamp.

2.8 Fluidised Bed Reactors

Fluidised bed reactors have an important role in industrial processes especially because of the advantages for gas-solid operations with respect to fixed bed reactors. These advantages are (i) temperature uniformity due to fluidisation, (ii) solid particles can be continuously added and removed from the system. The last feature is especially relevant for solid catalysed reactions in which the deactivated catalyst requires regeneration.

Other advantages of the fluidised bed reactor include the possibility of operating over a wide range of flow rates and for a fixed superficial gas velocity, the pressure drop across the fluidised bed is less than that of fixed bed.

However, there are disadvantages such as backmixing of both solids and gas leading to lower conversions, by-pass of gas via bubbles, and attrition, erosion and agglomeration problems. In the present study fluidised bed reactors were used for gas solid photoreactions, the advantages of which have already been pointed out in section 2.2.

The study of fluidised bed reactors is a vast field of research and the literature produced is voluminous. Many models have been proposed[96-99] to explain the phenomena involved and the variables which influence the performance of fluidised bed reactors. Single, two and three phase models have been considered by different researchers to explain the behaviour of fluidised bed reactors.

In the single phase model the gas and the solid particles are considered intimately mixed without segregation into dilute and dense phases. In practice however, this is not true because the gas is split into different phases. Thus the hydrodynamic behaviour of fluidised beds is better explained by models in which the flow patterns of gas and solids are taken into account. Such models are the two and three phase models. These models have been discussed and classified by Grace[95,96] according to the selection of the phases and the assumptions made by different research groups.

A schematic representation of two and three phase models is given in Fig. 2.8.1. However, these models are not reviewed here in detail because the model chosen in this work is that of the single-phase type where the detailed hydrodynamics and transfer processes are not considered separately.

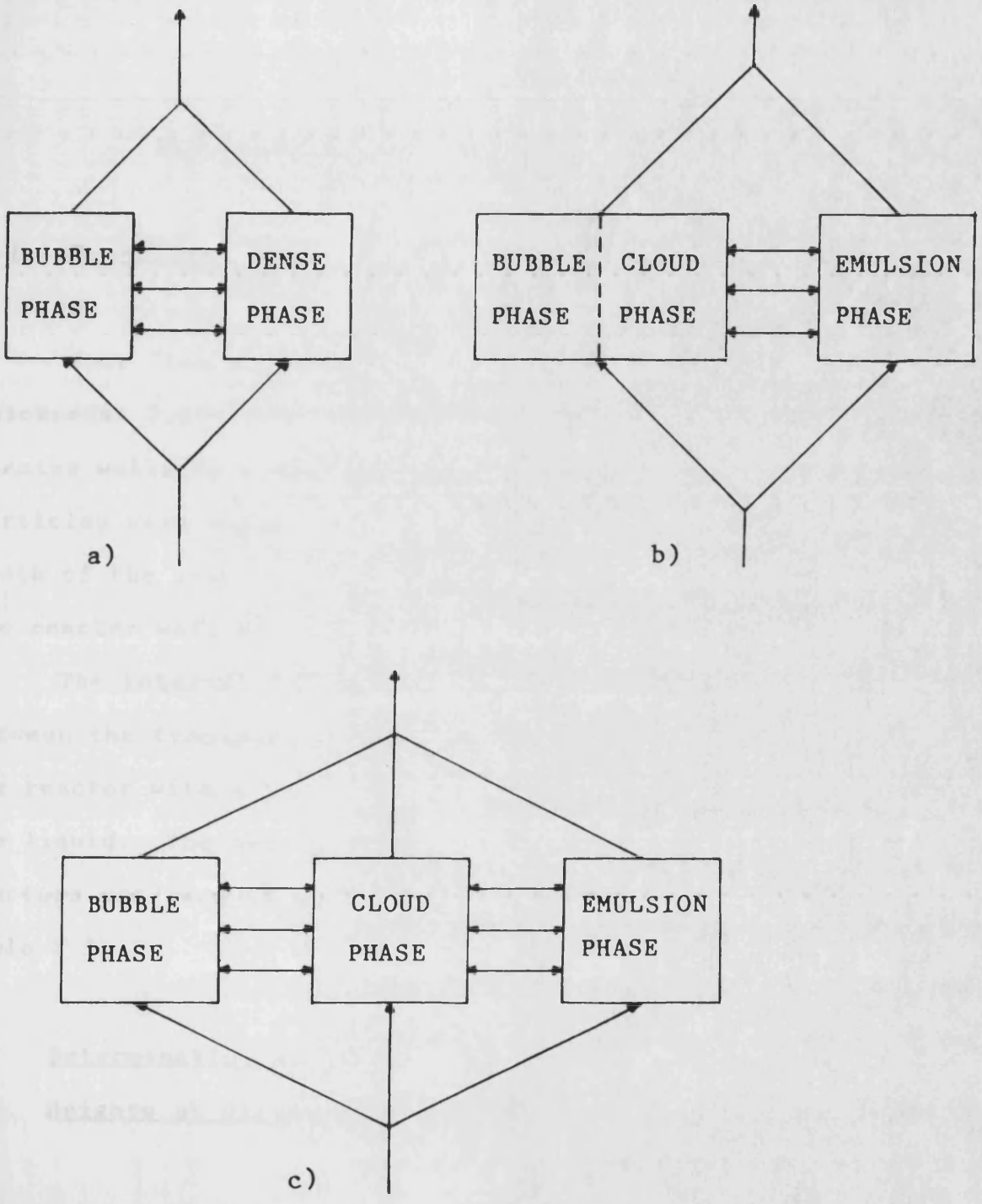

Figure 2.8.1. Phases selection for fluidised bed reactor models as reported by Grace[96], a) and b) two-phase models, c) three-phase models

CHAPTER 3

EXPERIMENTAL EQUIPMENT AND PROCEDURES OF ANALYSIS

3.1 Two-Dimensional Fluidised Bed Reactors

Four "two dimensional" fluidised bed reactors of internal thickness: 2.45, 3.41, 4.10 and 5.30 mm were used. The transparent reactor walls were made of 2 mm thick soda-lime glass. The particles were supported on a porous sintered plate distributor. The width of the reactors was approximately 60 mm and the total height of the reactor wall was 320 mm above the distributor.

The internal thickness of the reactor, i.e. the internal gap between the transparent walls, was determined accurately by filling the reactor with a known volume of water and measure the height of the liquid. The height of the bed at static conditions for all reactors used was 90 mm. The dimensions of the reactors are given in Table 3.1.

3.2 Determination of Minimum Fluidisation Velocities and Bed Heights at Different Flow Rates

Experimental determination of superficial gas velocity at the point of incipient fluidisation u_{mf} was obtained graphically, by plotting the bed pressure drop against superficial gas velocity. The gradient of the graph changes sharply at the point of minimum fluidisation. Thus the intersection of the two lines drawn through

Reactor	Internal Thickness (mm)	Width (mm)	Height (mm)
A	2.45	61	495
B	3.41	56.5	535
C	4.10	61	510
D	5.30	57.5	500

TABLE 3.1 Dimensions of Reactors

the experimental points in the fixed and fluidised regions gives the minimum fluidisation velocity.

The graph of bed pressure drop against superficial gas velocity for reactor A and 13X zeolite particles with mean diameter of 0.116 mm for the determination of u_{mf} is shown in figure 3.2.1. This method has been shown by Richardson[107] to give satisfactory results for the determination of u_{mf}.

The experimental equipment was leak tested before any measurements were made. At least two sets of data were collected for each bed used. The errors of the values of u_{mf} for all beds used were estimated to be less than 3%.

For all four reactors and all five particle sizes of 13X zeolites used and for all three reactors and three particle sizes of Co-Mo-Al_2O_3, the values of u_{mf} did not vary with the bed thickness. Linear regression analysis of the present data of u_{mf} showed that minimum fluidisation velocity varies approximately with the square of mean particle diameter, which is in agreement with the empirical correlations propose by Kunii and Levenspiel[106] and Wen and Yu[105]. Figure 3.2.2 shows the dependence between minimum fluidisation velocity and mean particle diameter for 13X zeolites and Co-Mo-Al_2O_3 particles.

The fluidisation parameter u_{mf} is useful for the comparison of different fluidised systems or when a number of variables are to be correlated, in order to establish a model of a fluidised system.

The bed heights at different fluidisation conditions were measured. A sliding sight-glass was mounted on the front wall of the reactor with two graduated scales attached to its edges. The bed

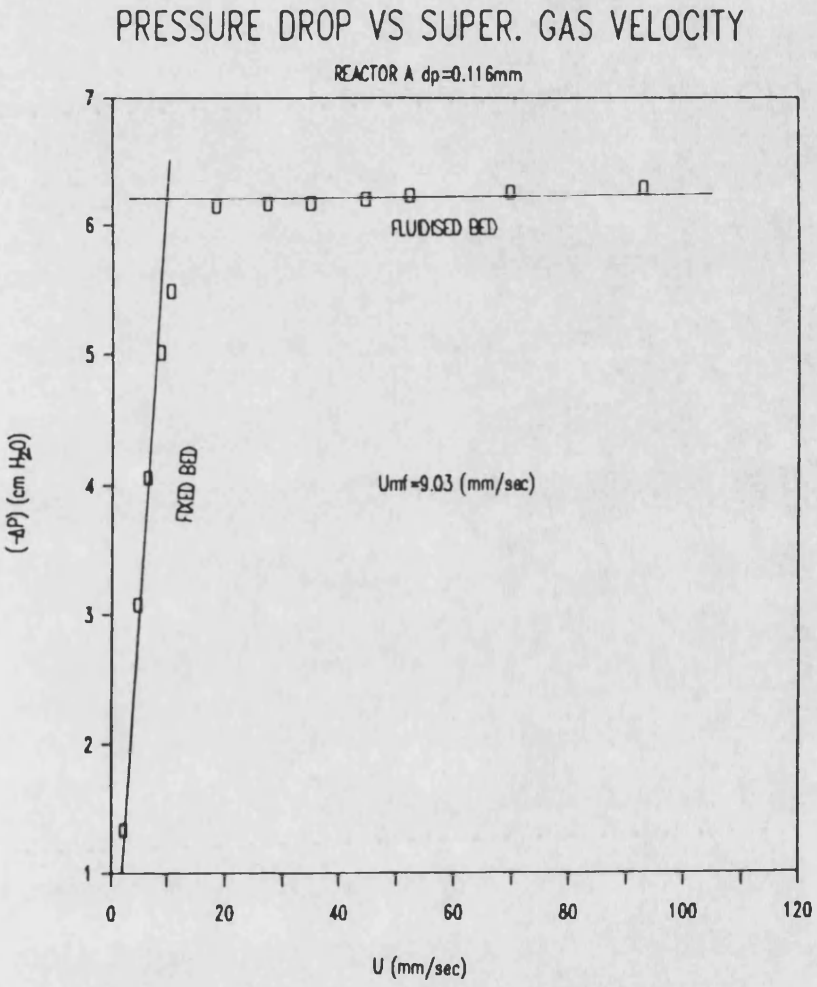

Figure 3.2.1. Typical graph of bed pressure drop versus superficial gas velocity for minimum fluidisation velocity determination. Reactor A, dp=0.116mm,13X zeolites

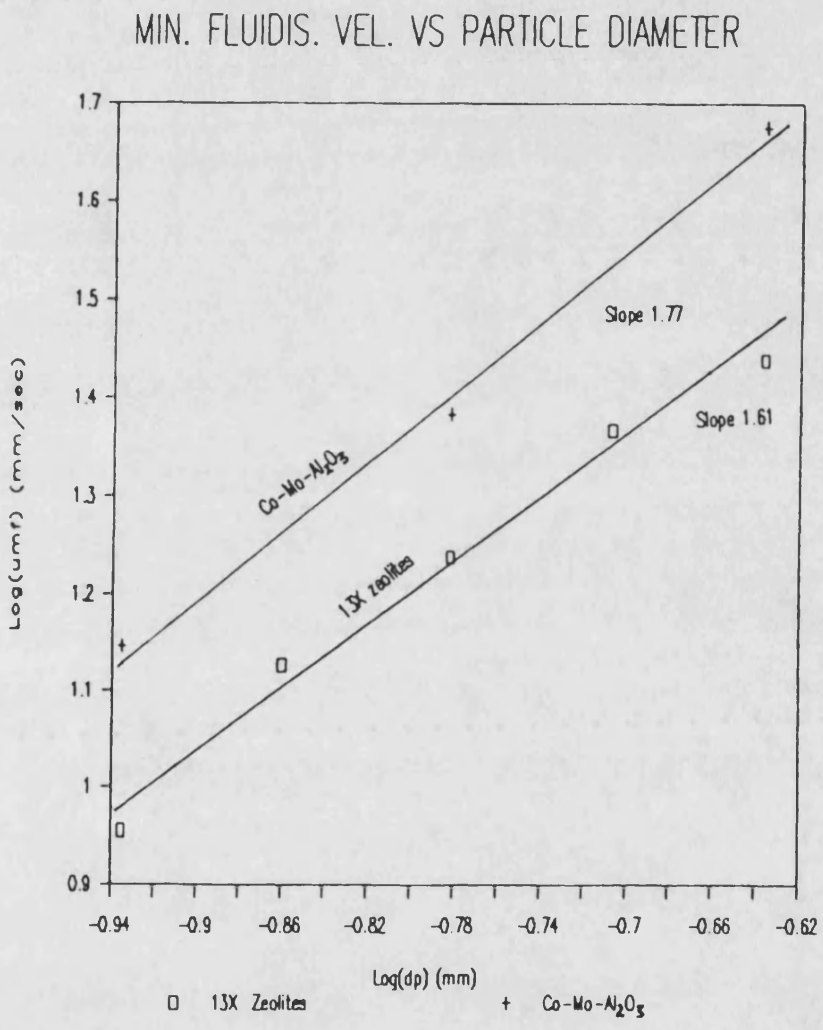

Figure 3.2.2. Logarithmic plot between minimum fluidising velocity and particle diameter for 13X zeolite and Co-Mo-Al_2O_3 particles

height was taken as the mean of the upper and lower fluctuations of the top of the fluidised bed surface determined by traversing the sight glass to obtain the best estimate of the locations of the bed surface.

The bed was first freely fluidised at a high flow rate. The flow was then gradually reduced until the bed reached incipient fluidisation. The bed height at the point of incipient fluidisation was taken as H_{mf}. The values of H_{mf} could be different if they were determined by increasing the flow rate from static bed conditions because of hysteresis effects. The range of errors of the measurements of bed height is estimated to be between 1 to 6%. The errors are higher at high flow rates.

3.3 Type of Particles and Size Reduction

Type 13X zeolites and alumina doped with cobaltum - molybdenum were used as the fluidised photocatalysts These particles had been used as photocatalysts or catalyst supports for promoting photoassisted reactions The solids were reduced to different sizes and the grounded materials were sieved and separated into five size ranges by using six sieves of 150, 120, 100, 85, 72 and 60 mesh, with the assistance of a vibrator.

Because of the narrow size ranges, the arithmetic mean of two successive cuts was taken as the mean particle diameter of a size range. The mean particle diameters, d_p and other fluidisation parameters are given in Table 3.2.

Type of Particles	Reactor	Mean Particle Diameter dp (μm)	Minimum Fluidising Velocity Umf (mm/sec)
Zeolites 13X	A	116	9.03
	B	138	13.40
	C	165	17.30
	D	196	23.32
		231	27.54
Cobalt — Molibdenum Allumima $Co-Mo-Al_2O_3$	A	116	14.00
	B	165	24.22
	D	231	47.50

TABLE 3.2 Particle Sizes and Fluidisation Properties

3.4 Optical Techniques for Light Absorption Measurements

The study of light energy distribution within a photoreactor is an important problem because it is the light energy, which promotes photochemical reactions. The amount of light absorbed in a liquid or gas-liquid photoreactor can be determined by performing a test reaction such as the photoreduction of potassium ferrioxalate, [38,108-110], the kinetics of which are well known. However there is no standard test reaction which can be easily performed in a gas solid photoreactor. Thus, no direct light absorption measurements for gas solid systems are feasible at present.

In this research new optical techniques have been developed for measuring the fraction of light transmitted through (transmittance) and the fraction which is reflected from (reflectance) a gas solid photoreactor. From these measurements light absorption can be evaluated by performing a radiation balance. The new methods are described in detail in sections 3.5 - 3.9.

3.5 Process Equipment for Transmittance and Reflectance Experiments

Figure 3.5.1 shows the equipment used for measuring transmittance and reflectance. The equipment consisted (Table 3.3) of gas supply, control valves and rotameters, a fluidised photoreactor, a light source with its associated optical accessories, and transmittance and reflectance detection systems, and computer hardware for data acquisition and analysis.

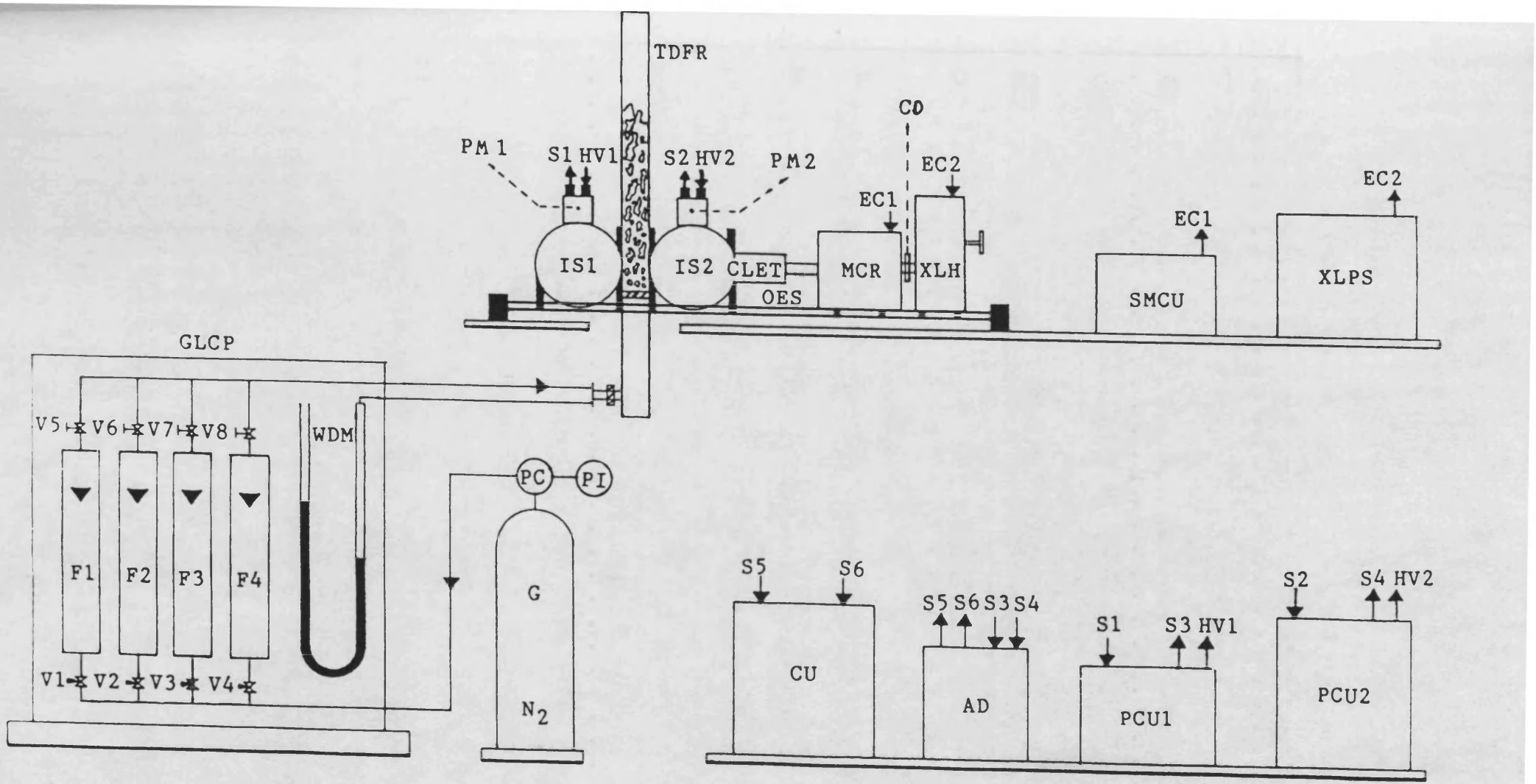

Figure 3.5.1. Schematic diagram of experimental equipment

Symbol	Description
AD	Two-Channel analog digitizer
CLET	Colimated lenses and extention tube
CD	Cut-off diaphragm
CU	Computer including monitor, keyboard and disk drive
EC1, EC2	Electrical Connections
F1 - F4	Gas flow rotameters
G	Nitrogen cylinder
GLCP	Gas-line control panel
IS1, IS2	Transmittance and reflectance integrating spheres
MCR	Monochromator
OES	Optical equipment support
PC	Pressure gauge

TABLE 3.3 Explanation of symbols in Figure 3.5.1

Symbol	Description
PM1, PM2	Transmittance and reflectance photomultipliers
PI	Pressure indicator
S1-S6	Directed electrical signals
SMCU	Stepping motor control unit
TDFR	Two-dimentional fluidised bed reactor
V1-V4	Needle valves
V5-V8	Shut-off valves
WDM	Water differential manometer
XLH	Xenon lamp housing
XLPS	Xenon lamp power supply

TABLE 3.3 (First page of continuation)

The gas flow rate was measured by four calibrated rotameters of different scales connected in parallel. This arrangement made it possible to use a wide range of flow rates according to the degree of fluidisation required. High purity nitrogen was used as the fluidising gas. The pressure drop across the bed was measured by a differential manometer connected with one end to the inlet line of reactor and the other end open to atmosphere.

Fluidisation parameters such as minimum fluidising velocities, bed heights at U_{mf} and at different flow rates were carefully determined in independent experiments. The data obtained have been compared with the results of others[105-107].

The light source was a 150 Watt two-electrode Xenon lamp powered by a DC power supply. A stepping motor control unit coupled with a monochromator, provides the means to select a fixed wavelength of the light beam. The high brightness Xenon source was housed in a metal case equipped with back reflectors and an exit aperture. The selection of wavelength and light bandpass adjustments of both entrance and exit apertures was achieved by a grating monochromator.

The coupling of the lamp housing with the monochromator is critical as the exit and entrance slits must be matched to give the proper alignment. The light beam, at a preselected wavelength, exit the monochromator and passed through an extension tube which held further lenses to establish good light collimation. The collimated light beam was directed to an area of the photoreactor chosen for irradiation. The area of the irradiation was kept at 3mm x 6mm ensuring that the total light transmitted and reflected from the photoreactor is collected by the detection devices.

The ratio of apertures between the incident light on the focal plane, i.e. the area of 3mm x 6mm, and that of entrances of integrating spheres, was selected at 20. This high value of 20 ensured that all reflected and transmitted light was collected by the respective integrating spheres. The wavelength selected was 560nm.

For measurements of reflectance, the incident light passed through an integrating sphere before irradiating the front wall of the reactor. Light energy transmitted through the reactor was collected by a second integrating sphere placed behind the reactor. The inside of the integrating spheres was coated with barium sulphate which collected the total transmittance or reflectance integrally.

Two high-gain photomultipliers with independent power supplies were used to modulate the transmittance and reflectance signals. The analogue signals were digitised and processed by an on-line BBC microcomputer by using an assembler programme written to obtain time-averaged values.

The photomultipliers were calibrated against a photometer. The calibration procedures will be described in detail in sections 3.6 and 3.7. The light energy input to the reactor front wall was kept at 25 $\mu W/cm^2$ for all the experiments performed. This value was the maximum of the lamp irradiance output that could be obtained at the selected conditions such as wavelength, distance between light source-reactor, monochromator apertures, etc.

3.6 Calibration of Equipment for Transmittance Measurements

Figure 3.6.1 shows the light path during experimental collection of transmittance data. For the transmittance experiments

the following method was used to calibrate the output signals.

The light beam was allowed to pass through an adjustable and precisely graduated exit slit of the monochromator. A light beam of rectangular shape was obtained at a distance of 35 cm from the monochromator after collimation by lenses held in an extension tube. The calibration measurements were taken at the focal plane of the light beam. At this plane a photocell was placed against the light path and its output signals were measured by a photometer for their conversion into irradiance readings in ($\mu W/cm^2$). Irradiance data were collected by the photometer over a wide range of known light bandpasses, i.e. known apertures of the exit slit of monochromator and precisely graduated slit widths in nanometers. Thus it was able to obtain a correlation between irradiance and light energy bandpasses.

Next the photocell was replaced by an integrating sphere[112] with two ports i.e. A and B, (see Figure 3.6.1). A suitable high voltage was selected to maximise the sensitivity of the photomultiplier. A correlation was obtained between the output signals of the photomultiplier in voltage and light bandpasses. The analogue signals were converted to digital signals by an analogue-to-digital converter. The analogue digitiser was calibrated by using a precision voltage calibrator. The digitized signals were sampled and recorded by a microcomputer where a time-averaged analysis was performed. The time-averaged values were stored on disc for further analysis which will be described in section 3.8. The high voltage used for transmittance experiments was 230 Volts and the gain of output signal was set to five times.

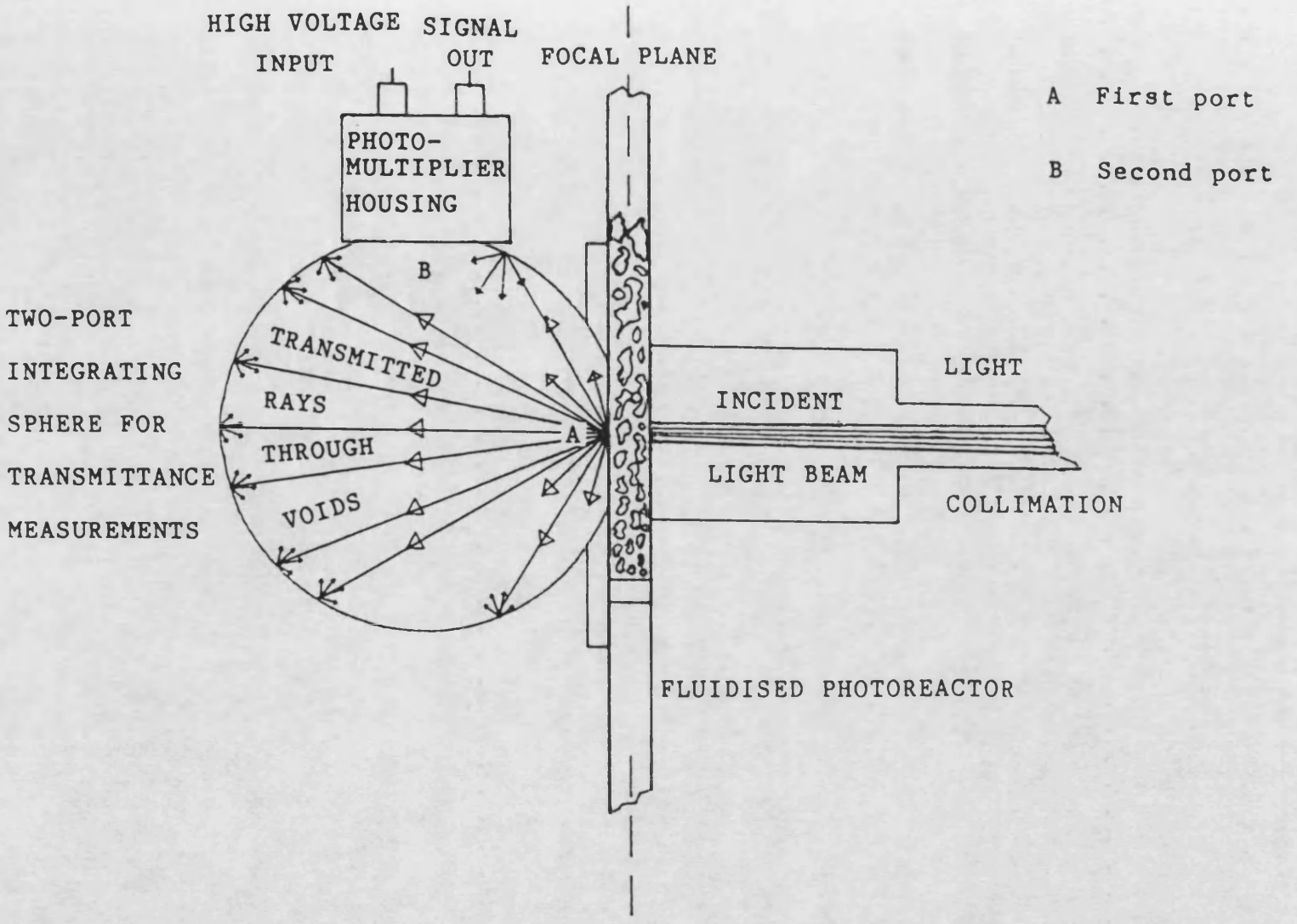

Figure 3.6.1. Schematic diagram of light path for transmittance measurments

3.7 Calibration of Equipment for Reflectance Measurements

The equipment was calibrated for reflectance measurements. The procedure used for establishing the correlation between irradiance and light bandpasses was identical to that described for transmittance calibration in section 3.6. The only difference was the selection of the scale of light bandpasses. This was necessary because the amount of light transmitted differed very much from that reflected from the reactor.

An integrating sphere[112] with three ports i.e. A, B and C (see Figure 3.7.1) was placed with its second port (B) directly opposite to the light path, which coincided with the focal plane of the light beam. A sphere coated with barium sulphate, (its reflectivity[111] given by Kodak Ltd was 99.9%), was placed against the second port.

The light beam struck this $BaSO_4$ surface, producing diffuse reflectance within the integrating sphere. Reflectance was measured by the photomultiplier detector, again giving output signals which were measured by a voltmeter. These voltages corresponded to known light bandpasses. Statistical analysis was applied to the data collected and another collection was obtained. Combining the two correlations obtained between irradiance, known apertures of light bandpasses and voltages, the relation between irradiance and voltages was obtained. This relation enabled light reflected by the diffuse reflecting surface of the integrating sphere to be quantified. The light path travelled during reflectance measurements is shown in Fig. 3.7.1.

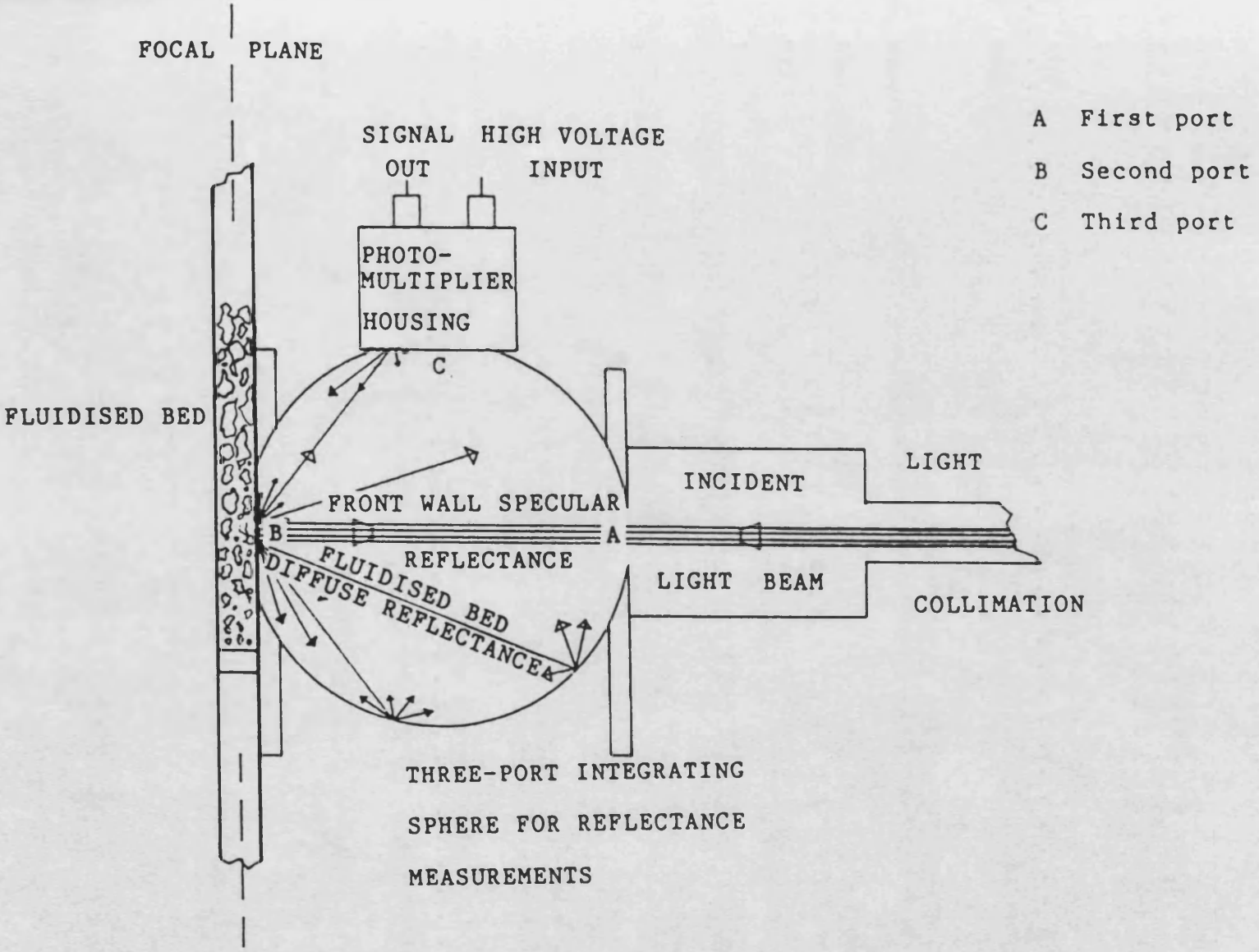

Figure 3.7.1. Schematic diagram of light path for reflectance measurements

The assumptions which were made in this procedure was that the incident light energy was conserved before and after its reflection on the surface of barium sulphate. In fact, the absorption of this powder was practically zero. The same assumption was valid within the integrator sphere because it was internally coated by the same powder.

A high voltage of 700 Volts provided by a photometric unit was used to increase the sensitivity of photomultiplier, and the gain of the photomultiplier was set to one. A least-square analysis was applied to all the calibration correlations obtained in order to find the best fit of data.

3.8. Time-Averaged Analysis

As the output signals of light transmittance and reflectance were fed into two different channels of an analogue to digital convector. Provisions were made for the selection of the most appropriate voltage scale to maintain a high degree of accuracy of measurements as the signals fluctuated over a range of values. An assembler programme was written to obtain time-averaged values of the output signals. The time-averaged measurements were stored on disc for further analysis.

Before each run, which consisted of the collection and processing of individual values of the fluctuating signals through time, the sampling frequency, i.e. the number of collected samples per second, was selected. The total number of samples for all runs was constant. As frequency was increased the time of sampling

decreased for the time-averaged analysis. An increase in frequency minimises the analysis time required. This was especially applicable in the cases where the intensity of fluctuations was low giving a smooth output signal corresponding to the case of static bed or low flowrates. In the cases when the intensity of fluctuations was high, the frequency was kept at 50. This frequency gave reproducible time-averaged value even for the largest fluctuated signals observed throughout all the experiments performed.

3.9 Local Light Transmittance and Reflectance at a Given Bed Height

The mean light reflectance ($\hat{E}_r$) and transmittance ($\hat{E}_t$) through a two dimensional fluidised photoreactor were evaluated by integrating the local reflectance (E_r) and tranmittance (E_t) with bed height above the distributor.

The local values of E_r and E_t, i.e. the light reflected and that transmitted at a given height above the distributor, were obtained by taking the arithmetic mean of values at three irradiated locations at the same height. It should be noted that the ratio between the width of incident light beam and that of the reactor was ten.

The locations of the points selected for measurement were determined by finding those points which gave an average measurement closest to that obtained when a large number of locations was used. This procedure was necessary in order to keep the total number of measurements down but still ensure representative spatial averages be obtained. Thus, light transmittance and reflectance

measurements were performed in three locations for a given height. These, were situated, one on the geometrical axis of the bed and the other two at 15 and 20 mm from the axis. Their arithmetic mean gave the local light transmittance (E_t) and reflectance (E_r) accordingly.

3.10 Summary

Fluidisation and optical equipment have been constructed, suitably arranged and carefully calibrated for the experimental measurement of light transmittance and reflectance of a gas solid fluidised bed.

The degree of fluidisation required was selected to cover a wide range of flow rates.

Independent experiments were performed for the determination of fluidisation parameters experimentally i.e. minimum fluidising velocity, bed heights at u_{mf} and at different flow rates, visual observation of bed behaviour etc.

The optical equipment and the calibration techniques devised were used for the first time in the study of light absorption in a heterogeneous medium.

CHAPTER 4

LIGHT TRANSMITTANCE IN 2-D FLUIDISED BED REACTORS

4.1 Introduction

Recently photocatalytic or photoassisted reactions have been performed in flat plate and cylindrical shape heterogeneous photoreators giving relatively high yields [e.g. 25, 100]. Before these reactions can be conducted in large scale reactors, reliable models for reactor analysis and design are required.

For the modelling and design of photoreactors, quantitative information on light absorption and reaction kinetics are needed. The absorption of light in a gas solid reactor[113] can be determined by an energy balance once light transmittance (E_t) and reflectance (E_r) are known.

In this chapter the relationship between the light lost through the fluidised photoreactor ($\hat{E}_t$) and fluidisation parameters will be examined. The experimental programme covered the following variables: gas flow rate, particles diameter, reactor internal thickness and bed expansion.

The particles used belong to the Group A classification according to Geldart[92].

The correlation found by Rizzuti and Yue [77] of this type of photoreactor using Group B particles was tested. Possible experimental and theoretical difficulties in such studies will be pointed out with recommendations for further improvement.

4.2 Procedure of Analysis of Experimental Results

The method of time-averaged analysis described in Section 3.8 was applied to all irradiated locations. The local values of light transmittance (E_t), as described in Section 3.9, represent the time-averaged amount of light lost through the photoreactor at selected heights. The E_t values were used for the evaluation of mean light transmittance ($\hat{E}_t$) through the whole photoreactor as follows.

A sufficient number of locations at different heights was chosen for irradiation. The collected data, after normalisation with respect to the input energy, were plotted against the corresponding bed heights. The plots were tested with different equations including the linear, polynomial and exponential equations to identify the best fit for data. For each set of data, the equation with the highest r-squared value observed was chosen. Then the mean light transmitted through the whole reactor at given flow rates was evaluated by the integration of $E_t(h)$ curves according to

$$\hat{E}_t = \frac{1}{H}\int_0^H E_t(h)dh \qquad 4.1$$

The values of the upper limit (H) were taken to be as close to the top bed as possible. Large fluctuations at the top of the bed caused high light scattering and made measurements very difficult.

It should be noted that the reactor width was not included in the evaluation of $\hat{E}_t$ because it was constant with height.

4.3 Selection of Design Variables

The configuration of a fluidised bed with flat walls separated by a small gap is more advantageous with respect to light absorption than a packed bed or a cylindrical one under identical conditions of mixing and irradiation. Such reactors have been used recently to test photoassisted heterogeneous reactions[100]. The light lost through the bed is a function of many reactor parameters.

A number of preliminary experiments were performed to find the fluidisation parameters which might affect light transmittance. Once these parameters were established, attempts were made to correlate $\hat{E}_t$ with these parameters. The significant variables were found to be d_p, d_r and $(H-H_{mf})/H_{mf}$.

The reactor thickness (d_r) was one of the parameters chosen because increased bed thickness decreased light penetration through the bed. The particle diameter was another variable which affected light transmittance because of the effect of photon-scattering. As

gas flow was increased bed expansion increased, creating larger voids and hence affecting light penetration through the bed. Thus bed expansion was the third variable considered. The effect of flow rate itself was also examined. Finally two different colours of particles were used to study the effect of varying the absorption of the medium.

4.4 Local Light Transmittance as a Function of Bed Height

When a bed of solids was fluidised, small bubbles formed near the distributor, and the detected local light transmittance was low. As the bubbles rose up the bed they coalesced, decreasing in number but increasing in size. Subsequently local light transmittance increased with bed height.

In the present section some typical graphs of the variation of local light transmittance $E_t(h)$ with bed height (h) for different reactor thicknesses, particle diameters and flow rates using 13X zeolites are reported in Figs. 4.4.1 - 4.4.9.

Figures 4.4.1-4.4.3 and 4.4.5 show the variation of $E_t(h)$ curves at different flow rates for reactors A, B, and C. Initially, E_t increases quite linearly with bed height. At a bed height of about 60 to 80mm above the distributor the $E_t(h)$ curves approach some asymptotic values. The height at which this transition on the $E_t(h)$ curves is observed can probably be regarded as that height at which the bubbles reached their maximum stable size. From a comparison of Figs 4.4.2, 4.4.5 and 4.4.8, it can be seen that the shape of the graphs becomes more linear as reactor thickness is increased.

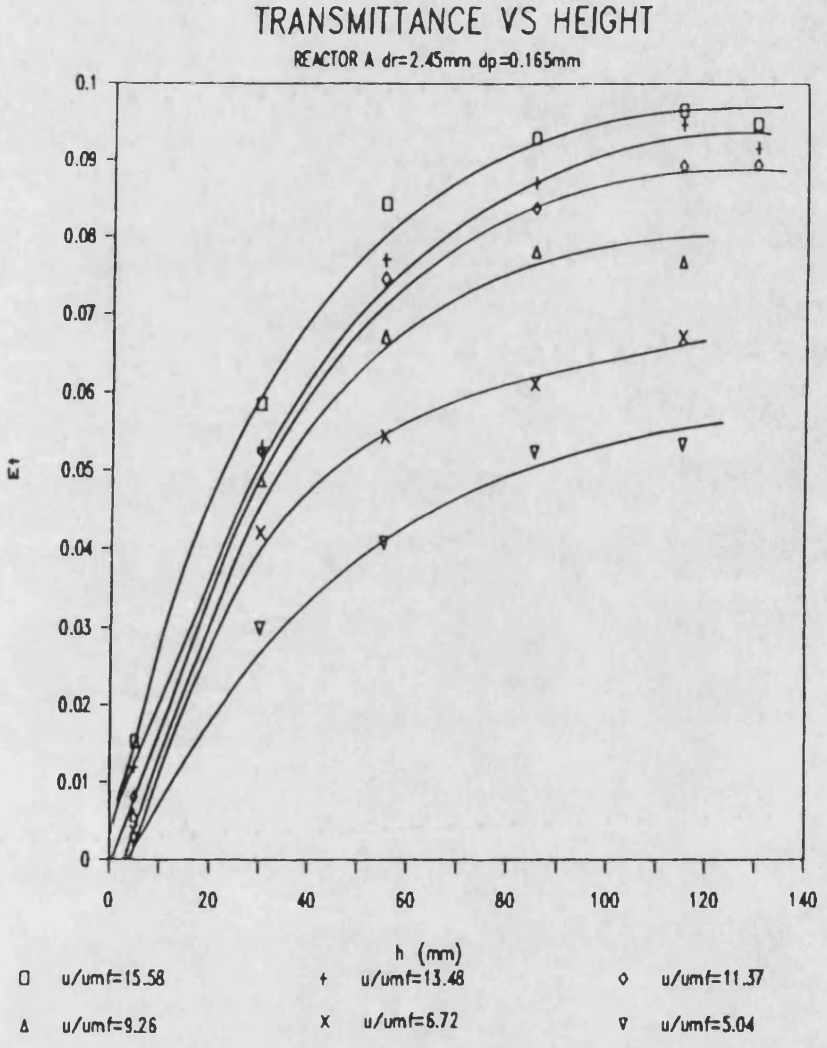

Figure 4.4.1. Local light transmittance as a function of bed height. Reactor A, dp=0.165mm, 13X zeolites

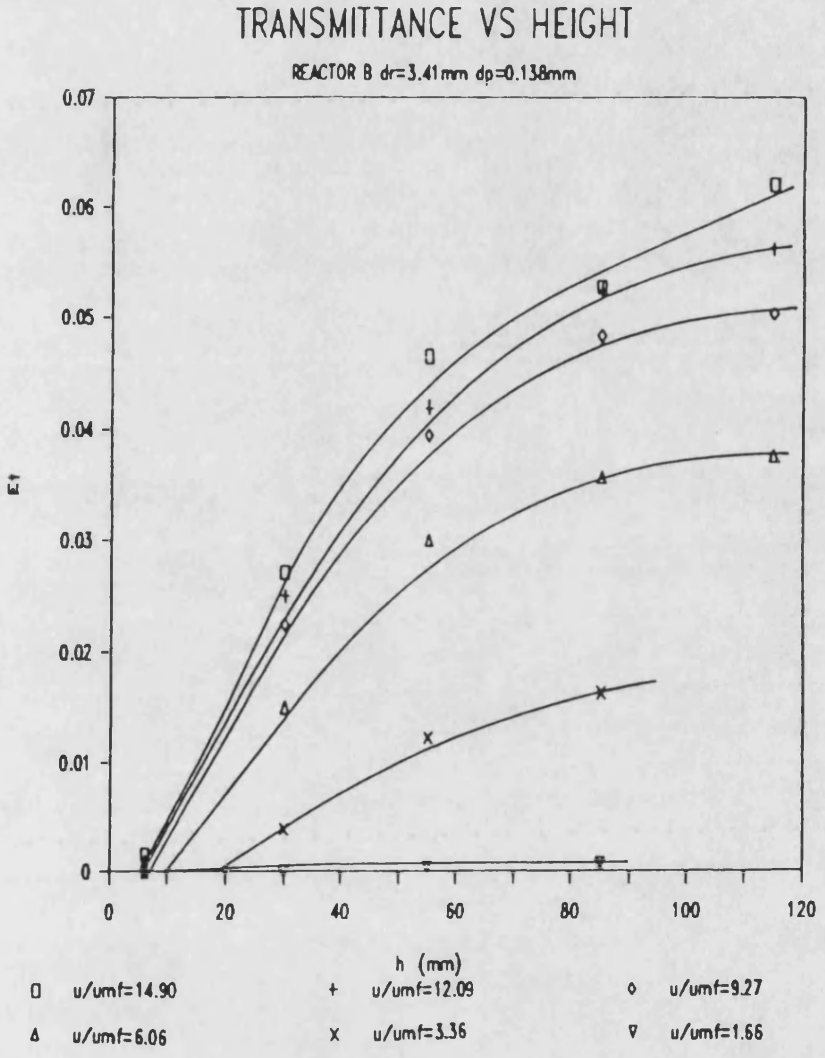

Figure 4.4.2. Local light transmittance as a function of bed height. Reactor B, dp=0.138mm, 13X zeolites

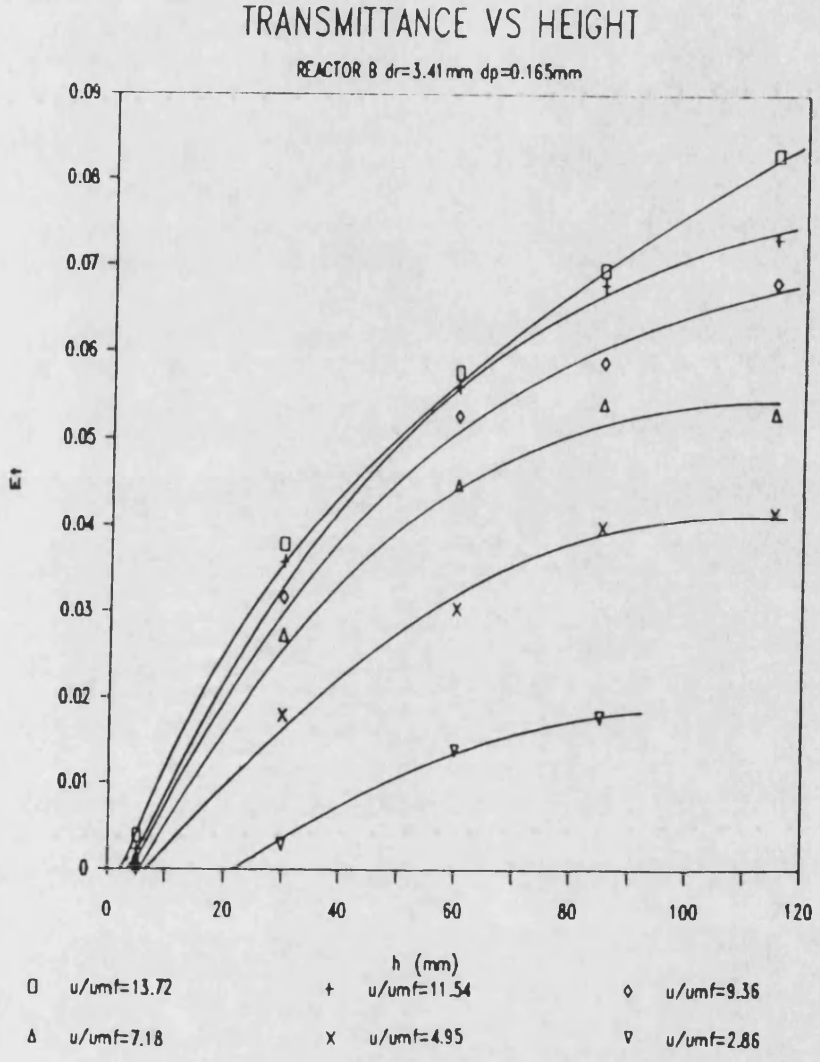

Figure 4.4.3. Local light transmittance as a function of bed height. Reactor B, dp=0.165mm, 13X zeolites

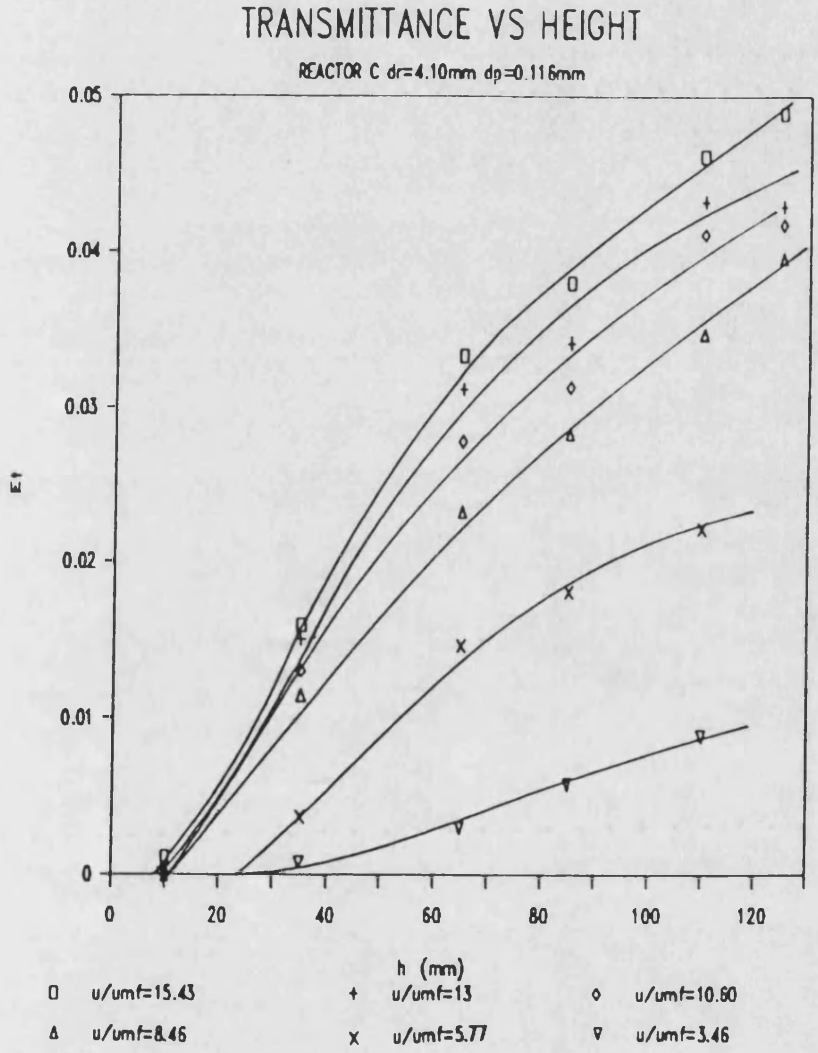

Figure 4.4.4. Local light transmittance as a function of bed height. Reactor C, dp=0.116mm, 13X zeolites

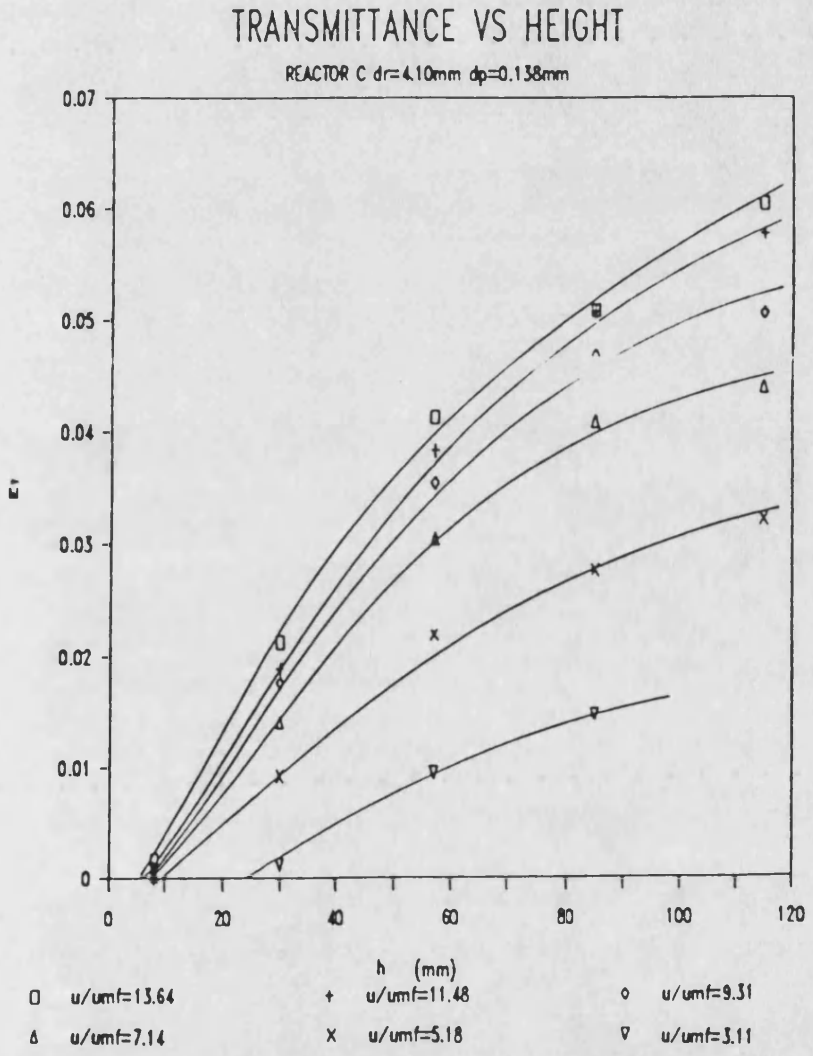

Figure 4.4.5. Local light transmittance as a function of bed height. Reactor C, dp=0.138mm, 13X zeolites

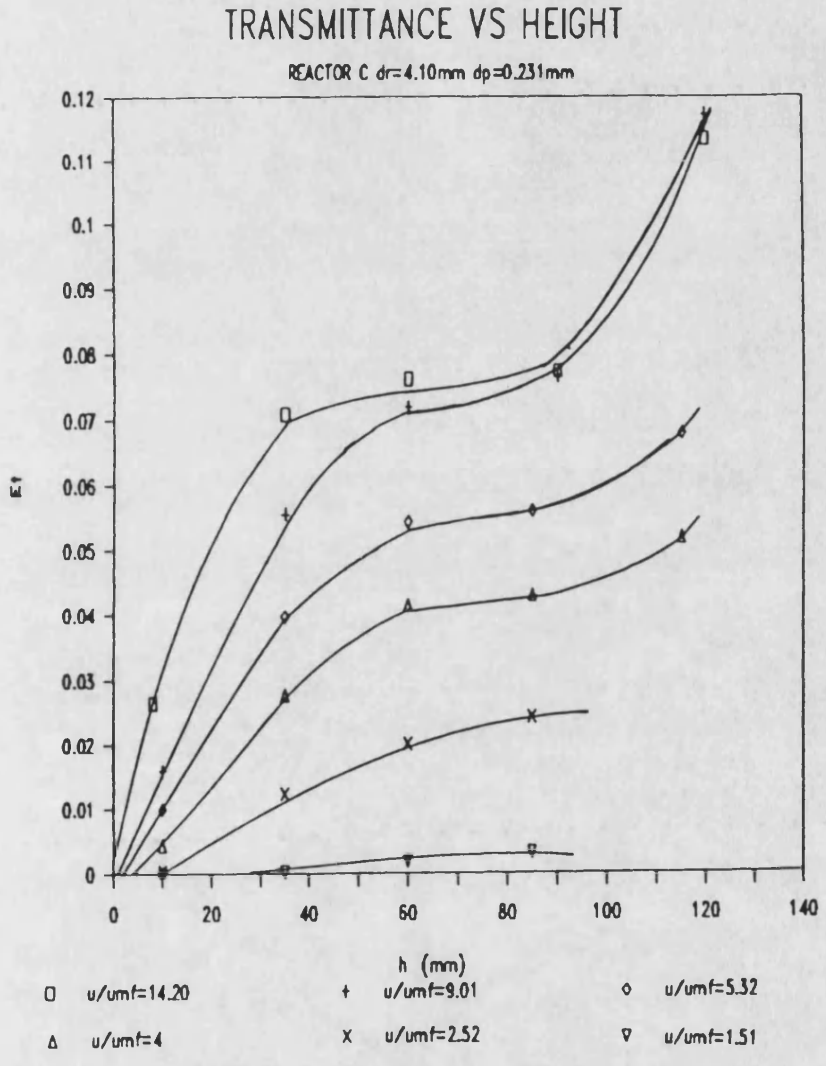

Figure 4.4.6. Local light transmittance as a function of bed height. Reactor C, dp=0.231mm, 13X zeolites

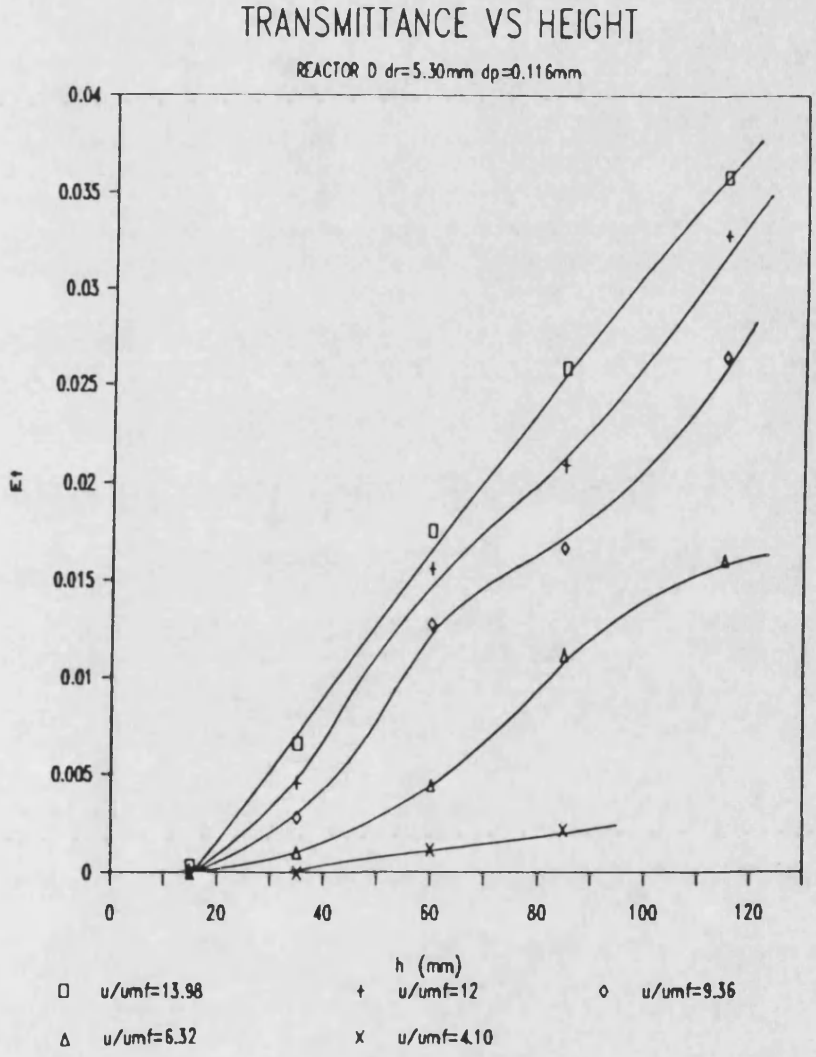

Figure 4.4.7. Local light transmittance as a function of bed height. Reactor D, dp=0.116mm, 13X zeolites

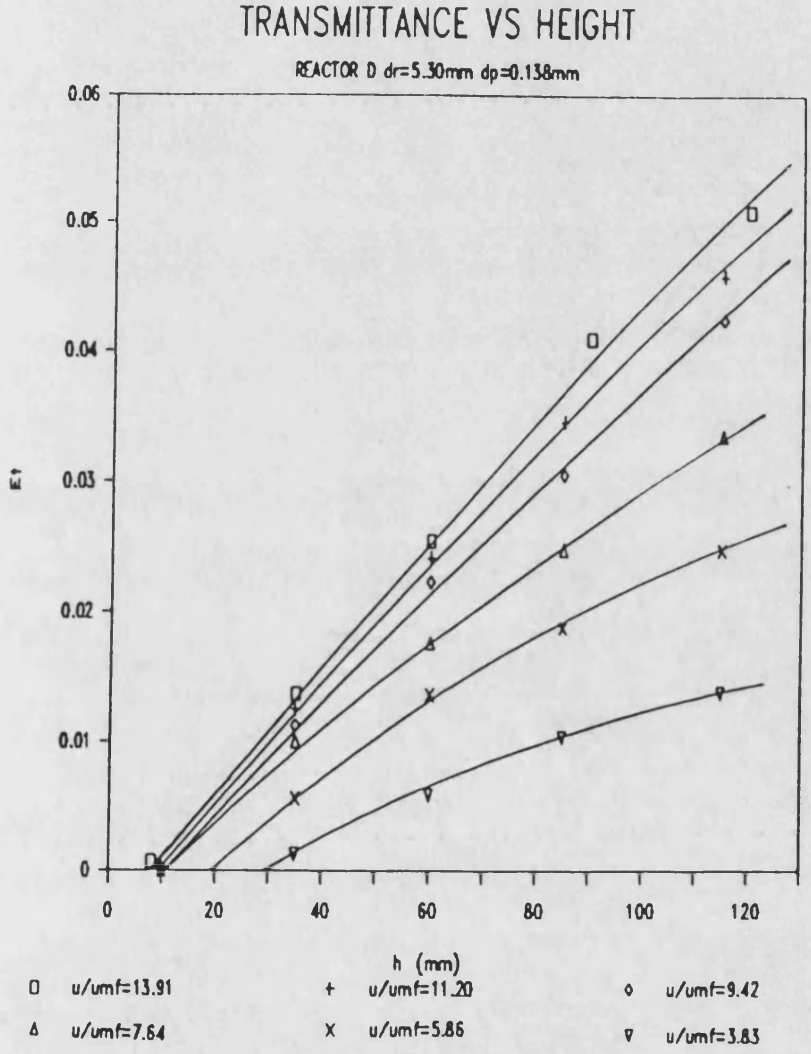

Figure 4.4.8. Local light transmittance as a function of bed height. Reactor D, dp=0.138mm, 13X zeolites

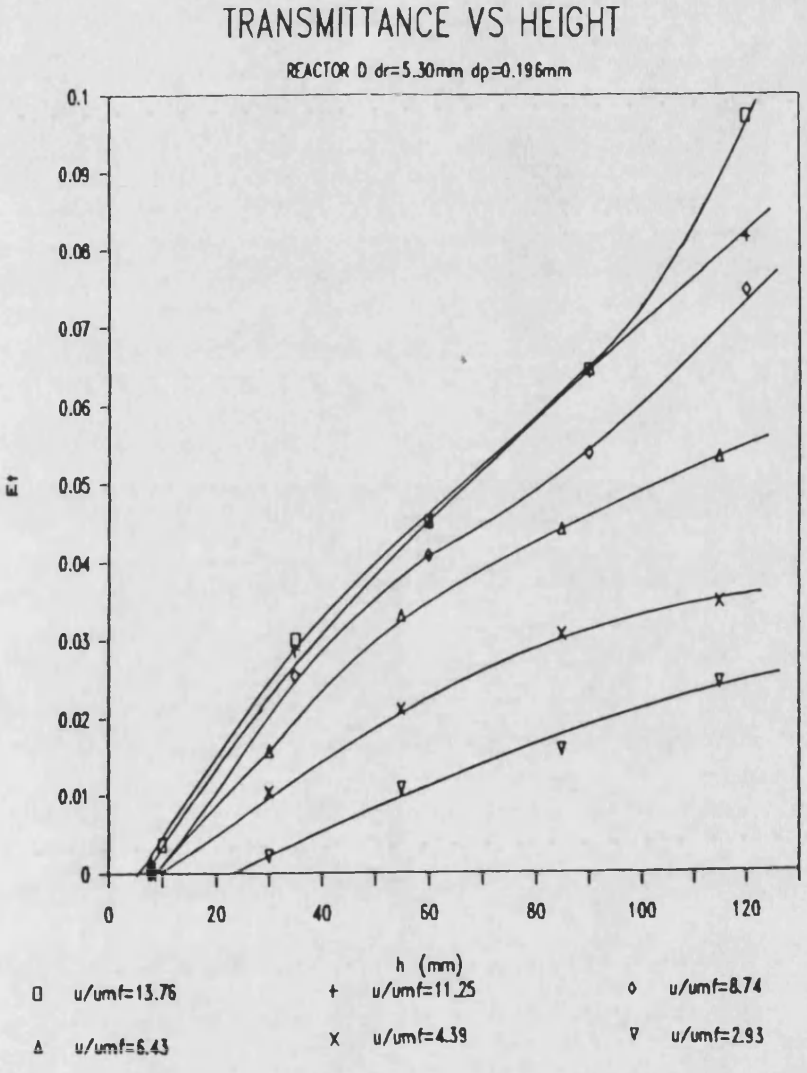

Figure 4.4.9. Local light transmittance as a function of bed height. Reactor D, dp=0.196mm, 13X zeolites

4.5 The Effect of Gas Flow Rate on Light Transmittance

An important fluidisation parameter which directly affects the light transmitted through the bed is the flow rate of fluidising gas. It is responsible for the bed expansion starting from fixed bed conditions. Light transmittance occurs for all beds used at a gas velocity greater than that required for minimum fluidisation.

For example, Fig. 4.5.1 shows how $\hat{E}_t$ varies with flow rate for reactor A for different sizes of 13X zeolite particles. It can be seen that light transmittance begins to occur at flow rates just above that at incipient fluidisation. The onset of light transmittance is closer to the point of incipient fluidisation (u_{mf}) as particle size increases and seems to coincide with the appearance of bubbles in the bed, a point usually referred as minimum bubbling point u_{mb}.

A linear dependence of $\hat{E}_t$ (u/umf) curves can be observed as u/u_{mf} increases. The rate of rise of $\hat{E}_t$ with u/u_{mf} drops at further increases in gas flow rate for all particle sizes. The point of transition from a linear increase of light transmittance with flow rate to a much lower rate of $\hat{E}_t$ occurs between a flow rate of 7 to 10 u/u_{mf}. It should be noted that the transition corresponds approximately to the onset of slugging at high flow rates. Similar behaviour can be observed for different reactors and different particle sizes as shown in Figs 4.5.2 - 4.5.4.

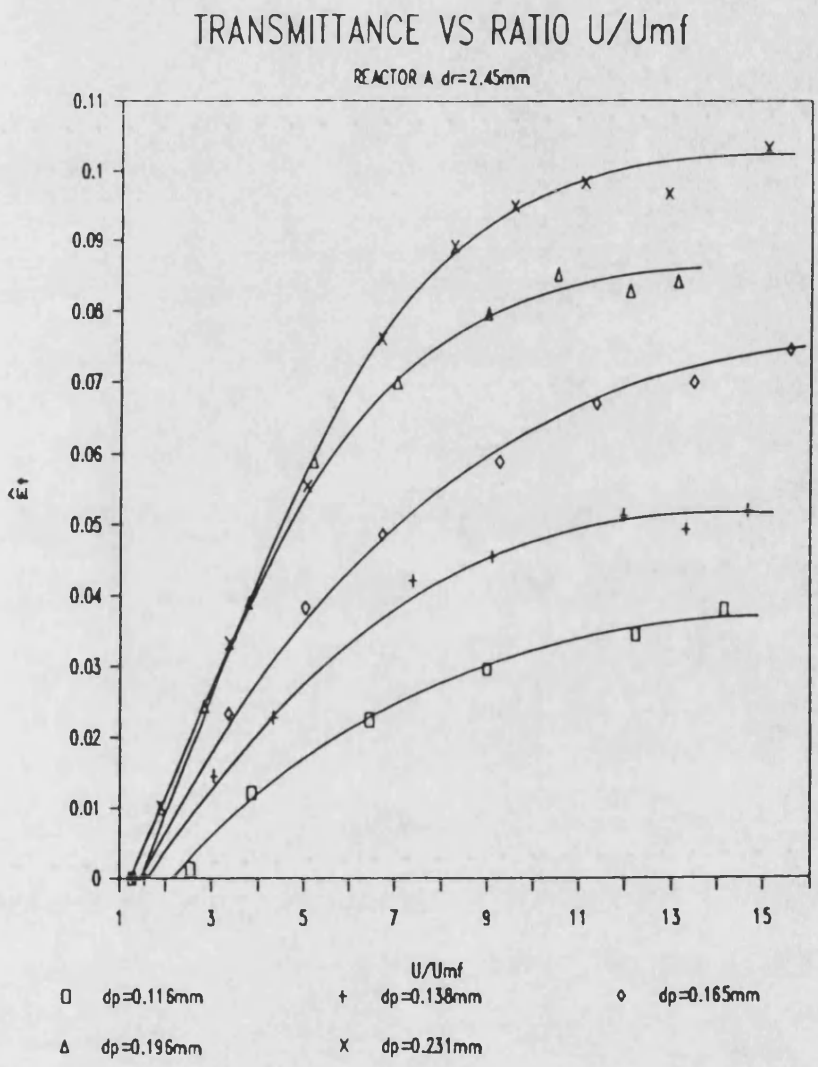

Figure 4.5.1. Variation of light transmittance with flow rate for reactor A and 13X zeolite particles

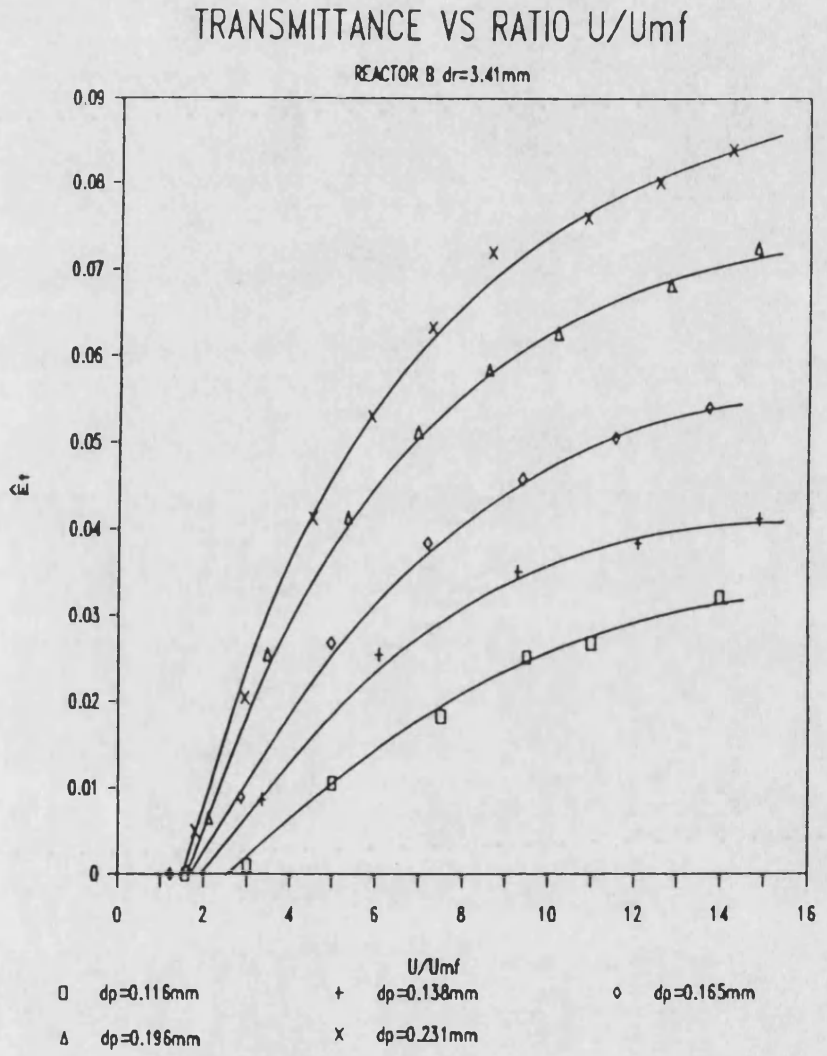

Figure 4.5.2. Variation of light transmittance with flow rate for reactor B and 13X zeolite particles

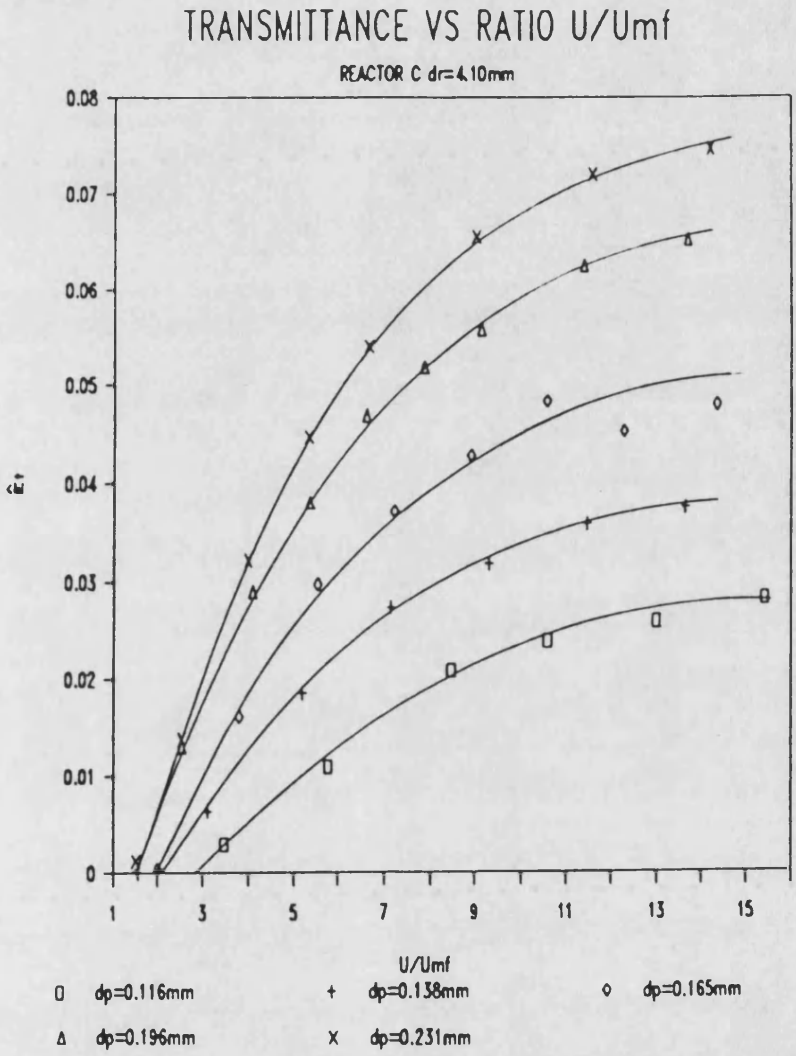

Figure 4.5.3. Variation of light transmittance with flow rate for reactor C and 13X zeolite particles

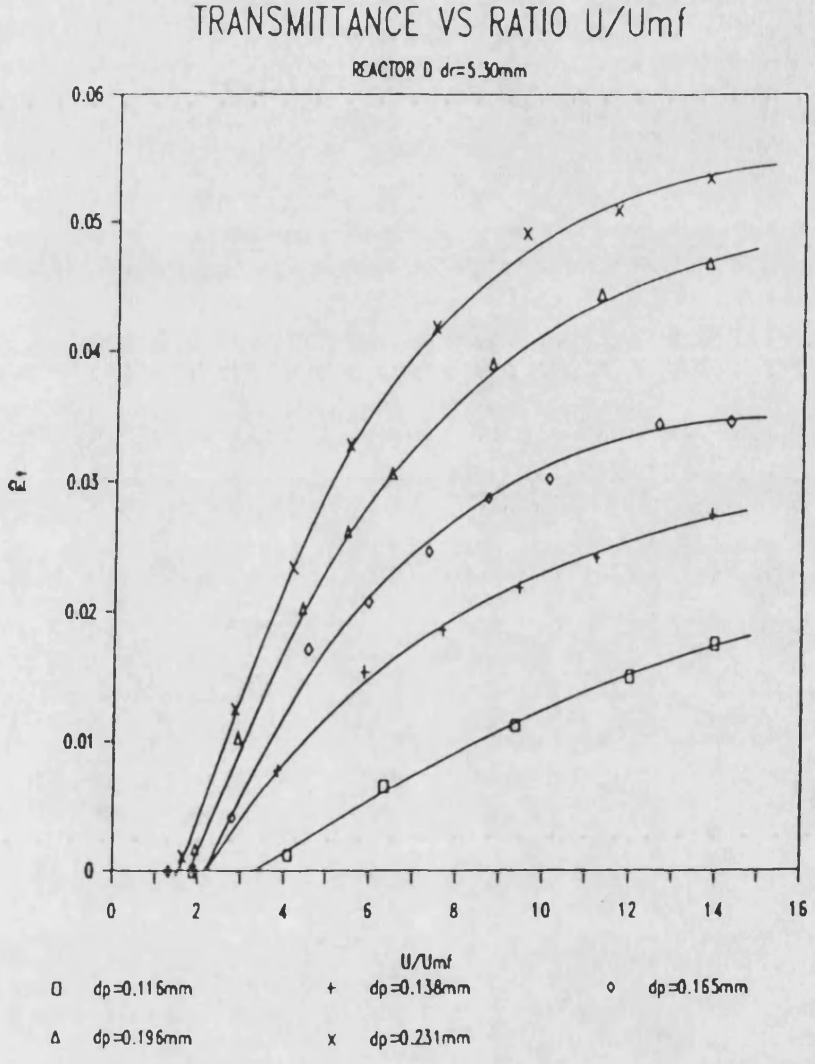

Figure 4.5.4. Variation of light transmittance with flow rate for reactor D and 13X zeolite particles

4.6 Effects of Particle Size, Reactor Thickness and Bed Expansion on Light Transmittance

The behaviour of a fluidised bed depends upon the physical properties of the system. A gas-solid system such as Nitrogen-13X zeolites of the size range used in the present experiments has the fluidisation characteristics of group A particles according to Geldart's[92] classification. When the behaviour of such a system is observed in a two-dimensional reactor, the bubbles within the bed can be seen to split and recoalesce very frequently resulting in a restricted bubble size. This bubble size is a function of the mean particle diameter hence the fraction of light transmitted through the bed will in turn be affected by particle diameter.

The dependence of $\hat{E}_t$ on mean particle diameter is shown in figs 4.6.1 and 4.6.2. A linear increase of $\hat{E}_t$ with d_p for reactor B (fig 4.6.1) and reactor D (fig 4.6.2) can be observed. This increase can be explained as follows.

As particle diameter increases, the void fraction within the bed increases and hence light transmitted through the bed for a given flow rate is increased. Similar dependence of E_t on d_p was observed for all other reactors.

The effect of reactor thickness of light transmittance has also been examined. The semilogarithmic correlation between $\hat{E}_t$ and

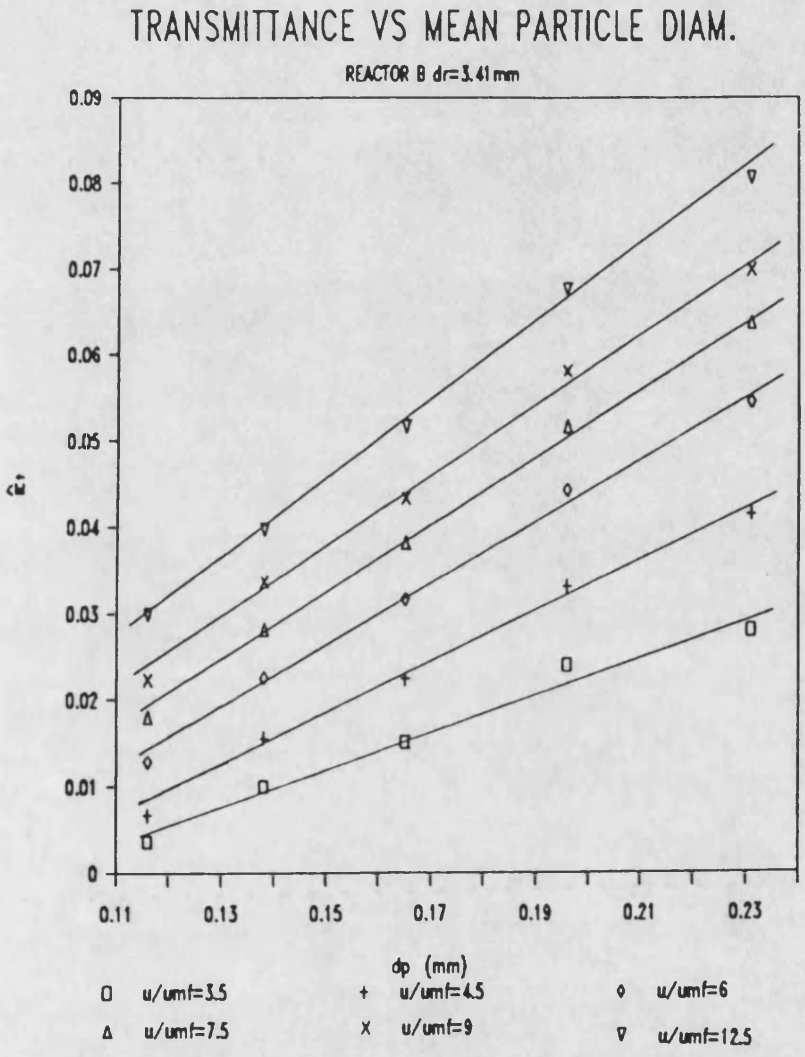

Figure 4.6.1. Linear function of light transmittance with mean particle diameter for reactor B and 13X zeolites

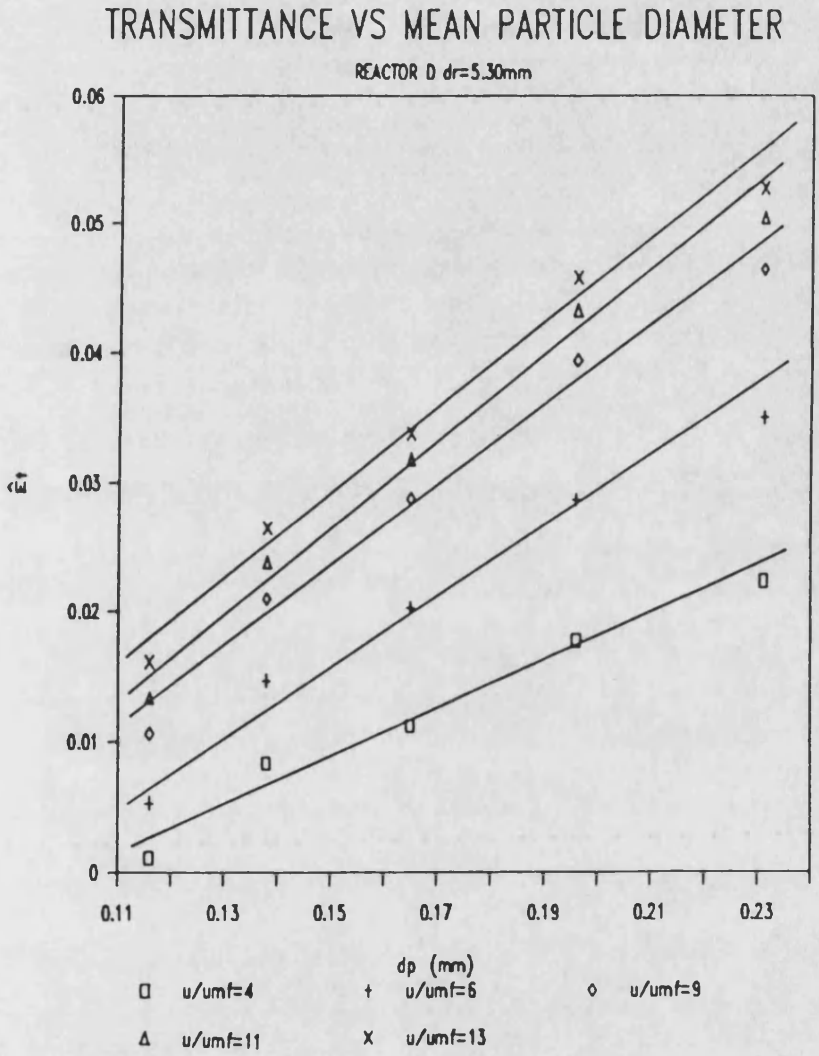

Figure 4.6.2. Linear function of light transmittance with mean particle diameter for reactor D and 13X zeolites

d_r found by Yue et al[78] for group B particles was shown to be valid in the present reasearch for particles belonging to group A. The results of the semilogarithmic equations obtained were characterised by r-squared values even higher than that reported by Yue et al[78]. The semilogarithmic dependence of $\hat{E}_t$ on d_r is shown in figs 4.6.3 - 4.6.5 for different flow rates.

$\hat{E}_t$ was plotted as a function of bed expansion $(H-H_{mf})/H_{mf}$ in figs 4.6.6 and 4.6.7 for three size of particles of 13X zeolites fluidised in reactors A and B respectively. Below a bed expansion of about 0.05 hardly any detection of light transmittance was observed. As bed expansion increased, light transmittance increased for all particle sizes and reactor thicknesses. From these plots it can be seen that there is approximate linearity between light transmittance and bed expansion.

4.7 Correlation of Light Transmittance with Design Variables

In the earlier sections, the effects of three reactor parameters individually on the fraction of light lost through an irradiated fluidised bed have been reported. A single correlation which describes the combined effects of these characteristic reactor parameters is presented here.

The basic correlating variables which were considered to have an effect on light transmittance are particle diameter d_p, reactor internal thickness d_r, superficial gas velocity u, bed height H, and bed expansion $(H-H_{mf})/H_{mf}$. All possible combinations between these parameters were considered for the test correlations. The

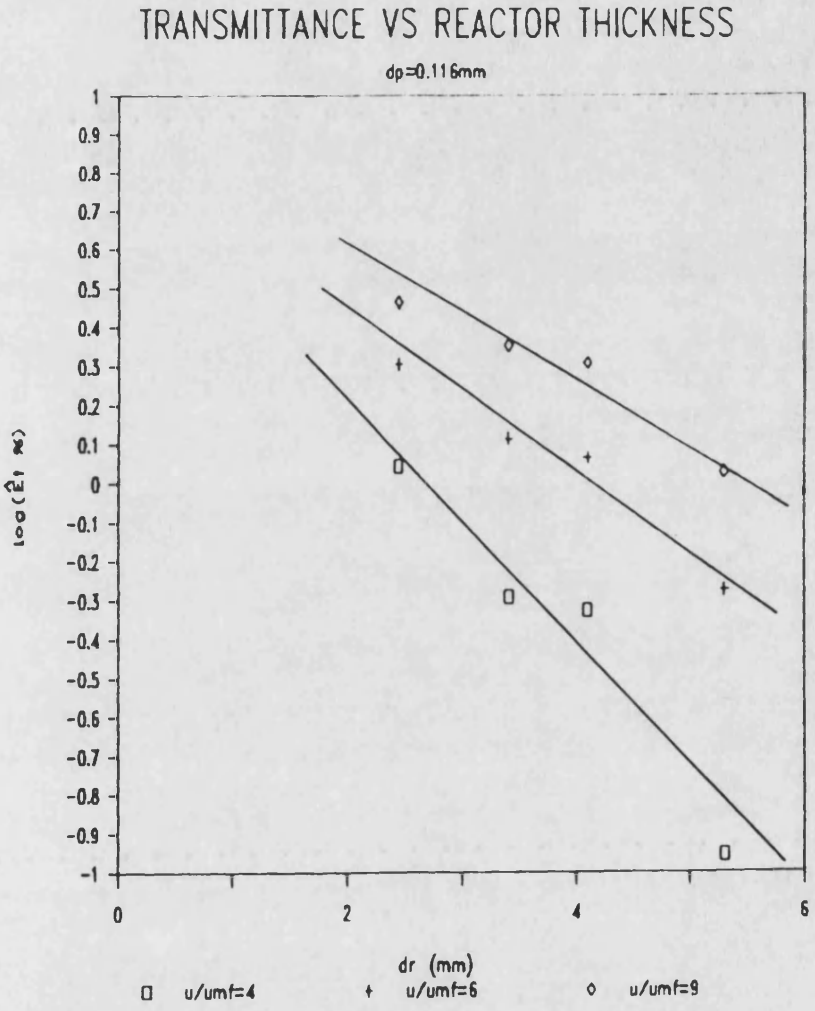

Figure 4.6.3. Semilogarithmic function of light transmittance (%) with reactor thickness. 13X zeolites, dp=0.116mm

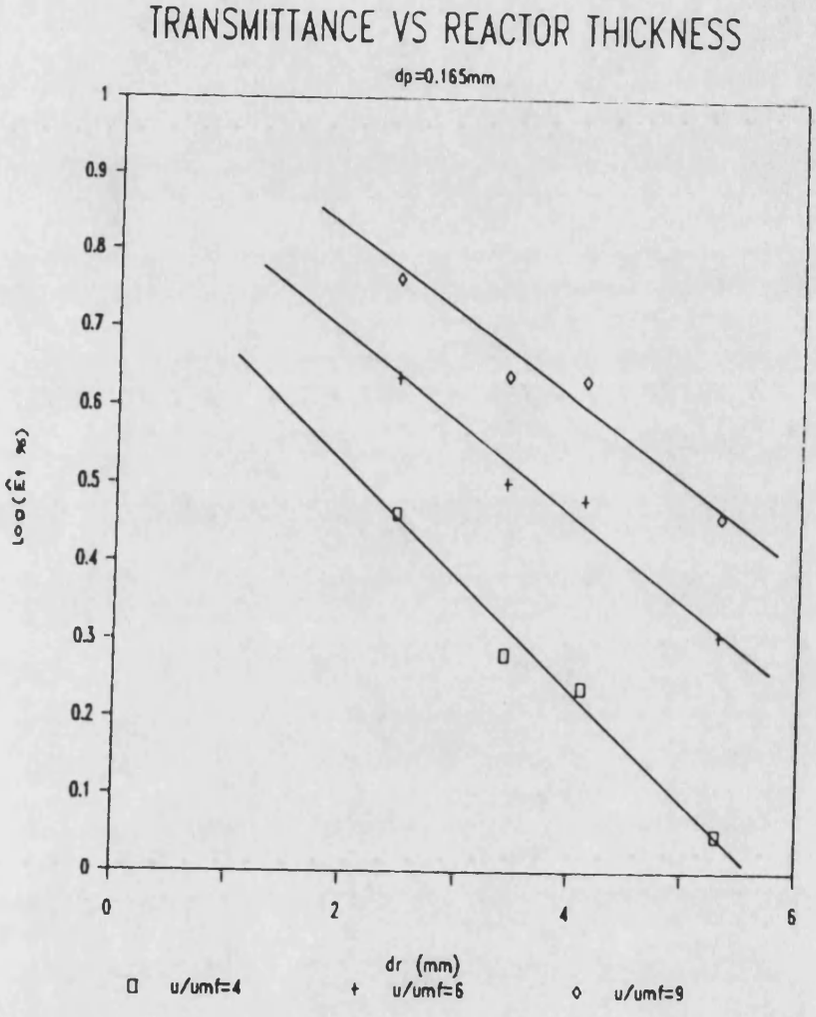

Figure 4.6.4. Semilogarithmic function of light transmittance (%) with reactor thickness. 13X zeolites, dp=0.165mm

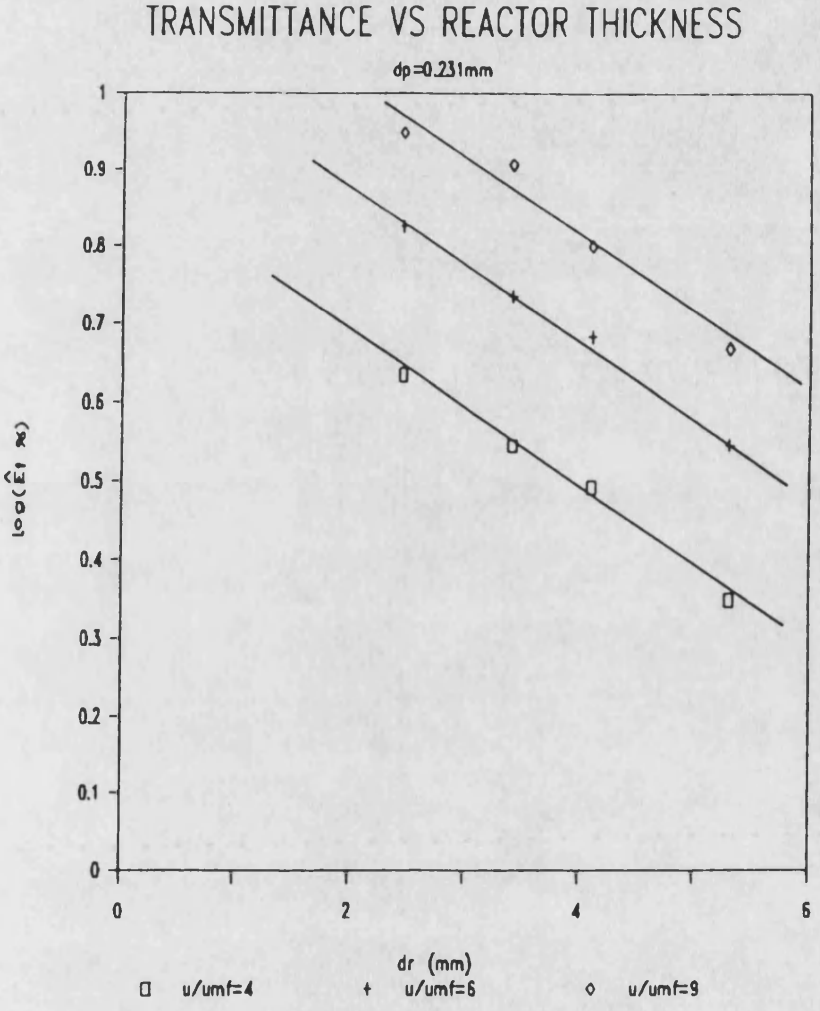

Figure 4.6.5. Semilogarithmic function of light transmittance (%) with reactor thickness. 13X zeolites, dp=0.231mm

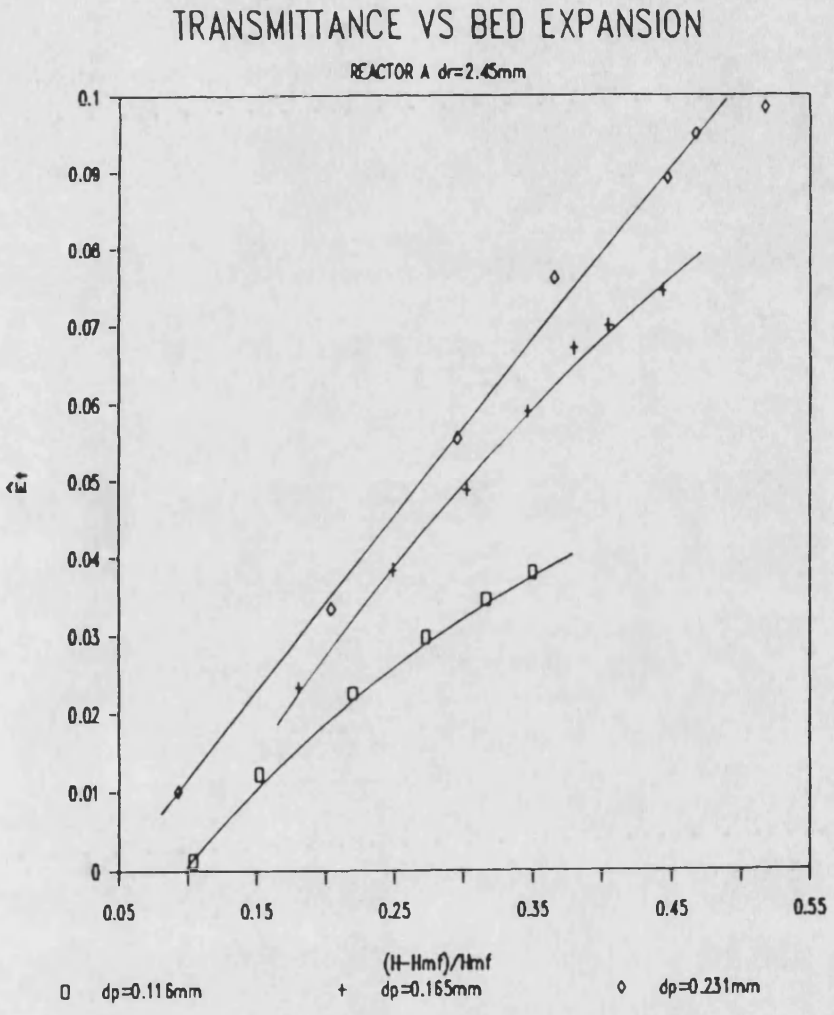

Figure 4.6.6. Light transmittance with bed expansion for reactor A and 13X zeolites

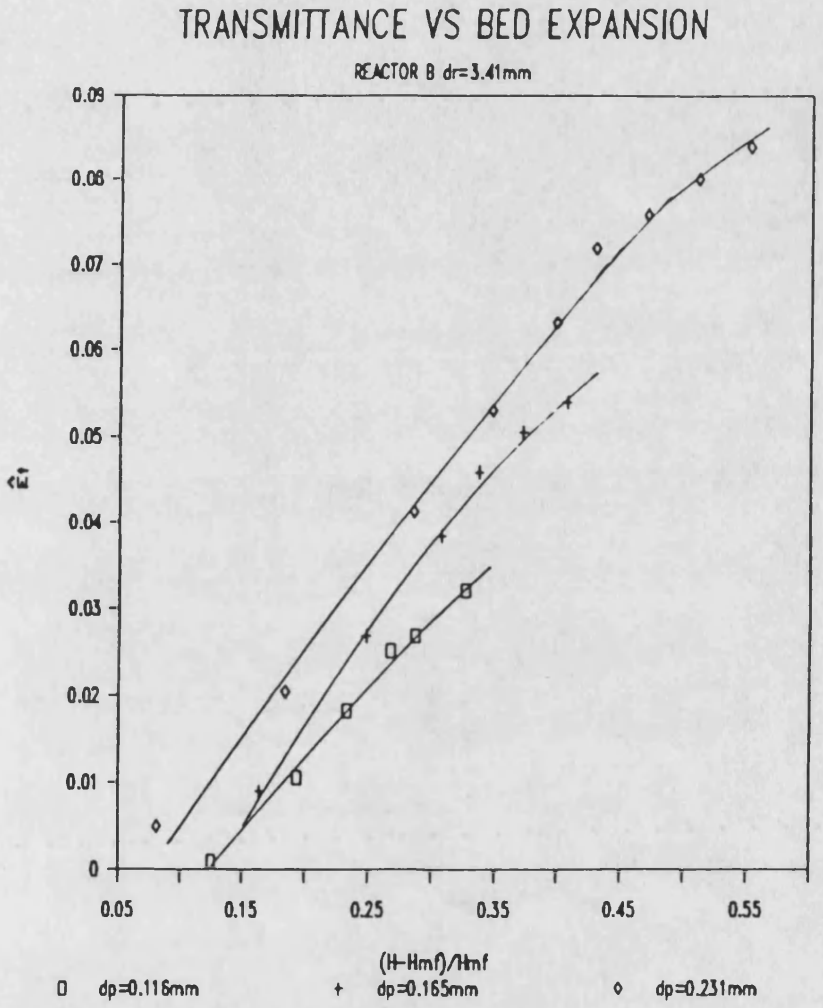

Figure 4.6.7. Light transmittance with bed expansion for reactor B and 13X zeolites

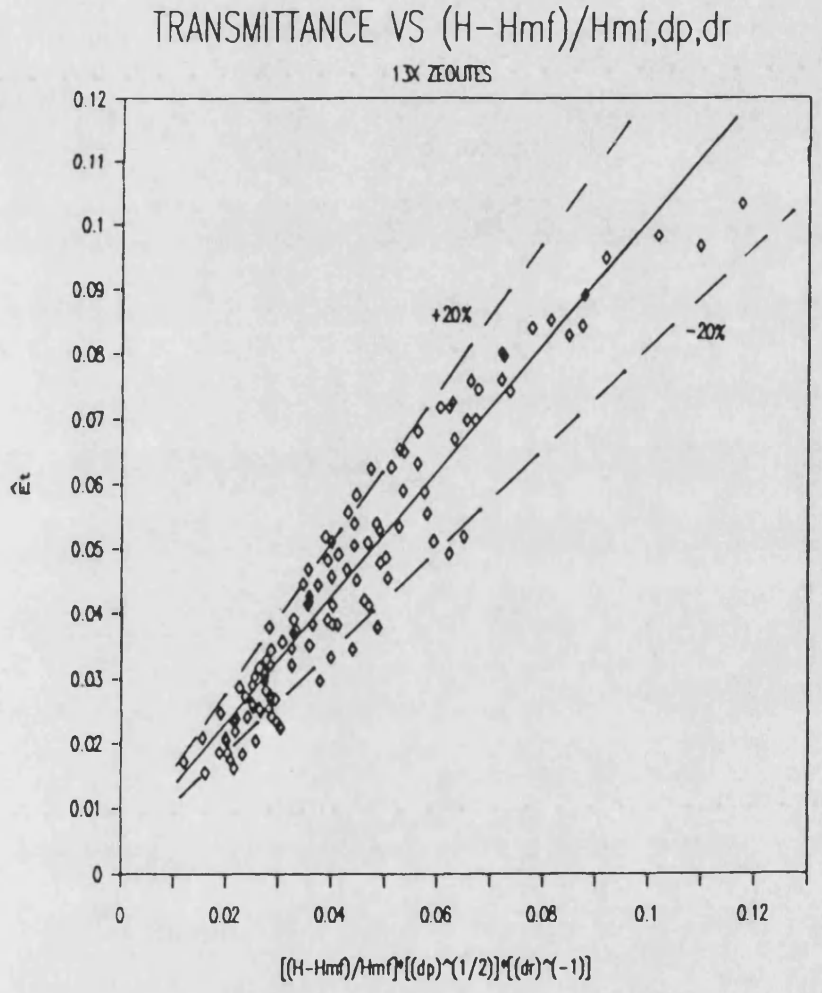

Figure 4.7.1. Correlation between light transmittance and fluidisation parameters for 13X zeolites

functional dependence of light transmittance on these fluidisation parameters was determined empirically by performing linear regression analyses. The best correlation, i.e. the one with the highest r-squared value, was chosen.

A total number of 115 experimental points were regressed. The resulting correlation showed that the mean light transmittance was a function of bed expansion, particle diameter and the reactor thickness. Statistical analysis gave r-squared value of 0.91, with approximate scatter of $\pm$ 20%. The equation was of the following form

$$\hat{E}_t = a'_t + b'_t \left[\frac{(H-H_{mf})}{H_{mf}}\right]\left[d_p^{1/2}\right]\left[d_r^{-1}\right] \qquad 4.2$$

The correlation shows that average light transmittance is directly proportional to bed expansion, the square root of particle diameter and inversely to reactor thickness.

On the whole, transmittance was low, being no more that 11% at the highest flow rates examined. Figure 4.7.1 shows the 115 experimental points used for the regression, the linear equation obtained. The dotted lines in the figure show the boundaries of data-scatter of $\pm$20%. The values of a'_t and b'_t were 0.0031 and 0.976 respectively. It should be noted that this equation should not be used for values of $\hat{E}_t$ less than 0.015, as deviation of up to $\pm$50% from the regression equation at low $\hat{E}_t$'s were observed.

Instead of the bed expansion used in the 4.2 equation, bubble voidage was used in Rizzuti and Yue's[77] correlation. The values

of bed expansion and bubble voidage have the same order of magnitude and the two variables are obviously related, the two correlations are therefore very similar. It can be concluded that a linear correlation between E_t and $(H-H_{mf})/H_{mf}$, $d_p^{1/2}$, and d_r^{-1}, is valid for group A and group B particles.

Once the linearity has been established for 13X zeolites, an investigation was carried out to examine the influence of type of particle on the correlation coefficients. Blue Co-Mo-Al_2O_3 particles were tested. The experimental equipment and techniques used were the same as described in Chapter 3.

A total number of 42 experimental data were obtained. The linear dependence of $\hat{E}_t$ on $(H-H_{mf})/H_{mf}$, $d_p^{1/2}$ and d_r^{-1} was again found. The r-squared coefficent obtained was 0.93. The equation assumed the following form:

$$\hat{E}_t = c'_t + d'_t \left[\frac{(H-H_{mf})}{H_{mf}}\right]\left[d_p^{1/2}\right]\left[d_r^{-1}\right] \qquad 4.3$$

The coefficients of the equation obtained, c'_t and d'_t were -0.003 and 1.01 respectively. In fig 4.7.2 mean light transmittance through fluidised Co-Mo-Al_2O_3 particles was plotted against the fluidisation parameters in correlation 4.3. The coefficients c'_t and d'_t in equation 4.3 differ from a'_t, b'_t, thus showing that the values of the coefficients of the equations are slightly affected by the type of particles used. It should also be noted that 13X zeolites and Co-Mo-Al_2O_3 belong to group A and B respectively.

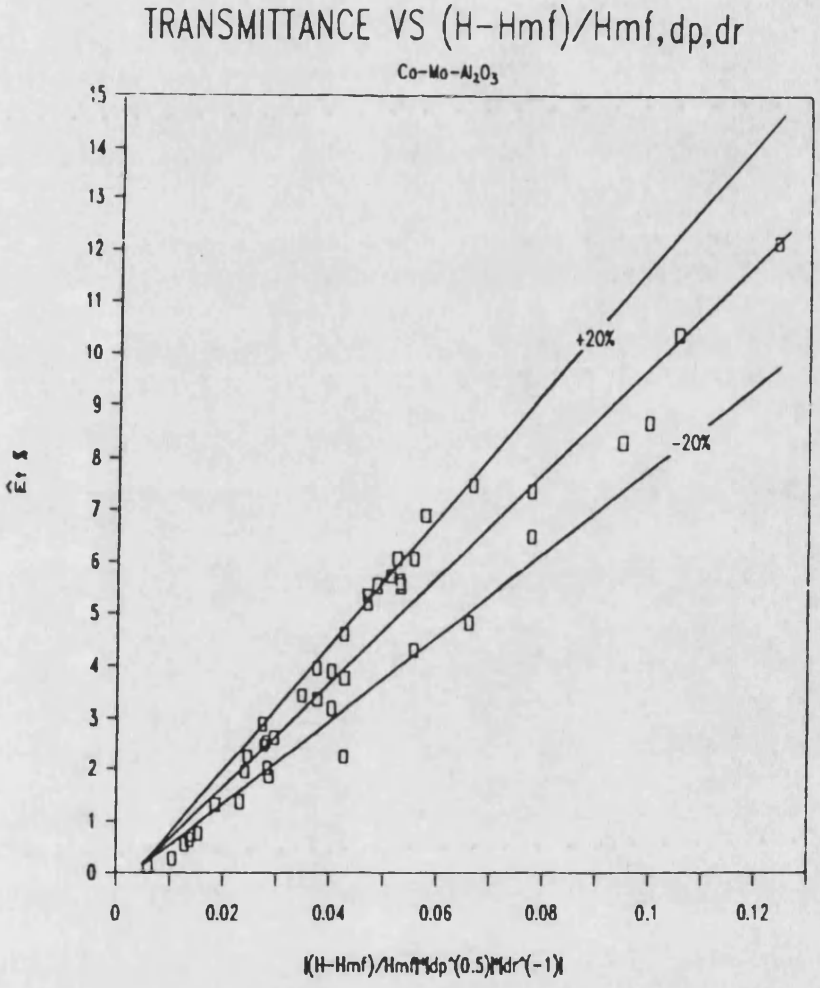

Figure 4.7.2. Correlation between light transmittance (%) and fluidisation parameters for Co-Mo-Al_2O_3

4.8 Conclusions

The light transmittance through a series of two-dimensional fluidised beds, has been studied. The important conclusions drawn, are summarised as follows.

When a thin fluidised bed reactor is irradiated by a light source with the reactor containing a heterogeneous medium such as a gas-solid fluidised bed, the local light transmittance increases with bed height above the distributor. The increase is reduced to some asymptotic value when the gas flow rate exceeds 10 times that at incipient fluidisation. For high reactor thicknesses (5.30 mm) the rate of increase of E_t with height is linear.

The mean light transmittance through the whole irradiated area of the reactors increases linearly with flow rate at low flow rates.

Mean light transmittance increases linearly with particle diameter.

A semilogarithmic form of $\hat{E}_t$ versus reactor thickness (d_r) curves was observed.

Two important equations 4.2 and 4.3 have been obtained between irradiation and fluidisation parameters, i.e. $\hat{E}_t$, $(H-H_{mf})H_{mf}$, d_p and d_r. The values of the coefficients a'_t, b'_t, c'_t and d'_t were dependent on the type of particles used. These equations may be used for $\hat{E}_t$ predictions as well as for scale-up studies.

CHAPTER 5

LIGHT REFLECTANCE IN 2-D FLUIDISED BED REACTORS

5.1 Introduction

It has already been pointed out that quantitative information of light transmittance (E_t) and reflectance (E_r) are required for the evaluation of light absorption by the contents of a fluidised photoreactor. The methods and techniques used for the evaluation of $\hat{E}_t$ have been described in chapter 4. In this chapter light reflectance ($\hat{E}_r$) from fluidised reactors is evaluated and a new technique for such studies is reported.

As yet, there is no systematic study on the evaluation of E_r in an heterogeneous and continuously mixed system, such as a fluidised photoreactor reported in open literature. Rizzuti and Yue[77] in 1983 estimated light reflectance ($\hat{E}_r$) from a two-dimensional fluidised photoreactor. They irradiated a 2-D fluidised bed with an incident light beam held at an angle of 45° to the reactor walls. The reflected light was detected by a photodiode positioned at a right angle (according to the specular reflectivity law) to the incident beam.

The results reported only provided an estimate of light reflectance. The authors suggested that light reflectance measurements should follow a somewhat different technique. Indeed, the combined phenomena of specular and diffuse reflectance from a

reactor wall and a heterogeneous medium within, imposed considerable difficulties on the collection of reflected light.

Later Rizzuti et al[104] investigated the influence of the catalyst reflectance on light transmittance through an irradiated fluidised bed. In the same study values of light reflectance for static beds rather than fluidised beds were reported.

In the present study light reflectance from a fluidised photoreactor, $\hat{E}_r$ was succesfully measured with the aid of a three-port integrating sphere. These measurements led to a useful correlation between light reflectance with the fluidisation parameters. Details of the methods followed for the determination of $\hat{E}_r$ and of the correlations obtained are given in the following sections.

5.2 Experimental Methods

The diffuse reflectance of the heterogeneous medium within reactors was measured by using a three port integrating sphere. An incident light beam of a fixed wavelength of 560 nm was allowed to pass through the integrating sphere.

The reactor was placed at the focal plane of the incident light beam which coincided with the exit port (B) of the sphere, as shown in the schematic diagram for reflectance measurements in Fig. 3.7.1. With such an arrangement, as the incident light beam struck the fluidised bed, the diffuse reflectance of the heterogeneous medium was collected by the sphere and measured by the photomultiplier at the third port (C) of the integrating sphere.

Specular reflectance was however, measured in a second stage. It was not possible to simultaneously measure both diffuse and specular reflectance of the heterogeneous medium and the reactor front wall. Two different arrangements of the reactor-detection system were required.

The specular reflectance of the front wall of the reactor was evaluated by means of a sheet-glass which was identical to the ones which made up the reactor walls. The glass was placed at the focal plane of light beam at an angle of 45° to the incident beam. Then a photocell was placed at the correct angle for the reception of the specularly reflected light. The schematic arrangement for the specular reflectivity measurements is shown in Fig. 5.2.1.

5.3 RESULTS AND DISCUSSION

5.3.1. Average Light Reflectance over the Entire Reactor

The measurements of light reflectance at selected irradiated locations, in the form of photomultiplier output signals, were subjected to a time-averaging analysis. The values of local light reflectance was measured using the procedures as in section 3.9 described. The average light reflectance from the reactor was evaluated from the E_r versus h plots according to

$$\hat{E}_r = \frac{1}{H}\int_{H_o}^{H} E_r(h)dh \qquad 5.1$$

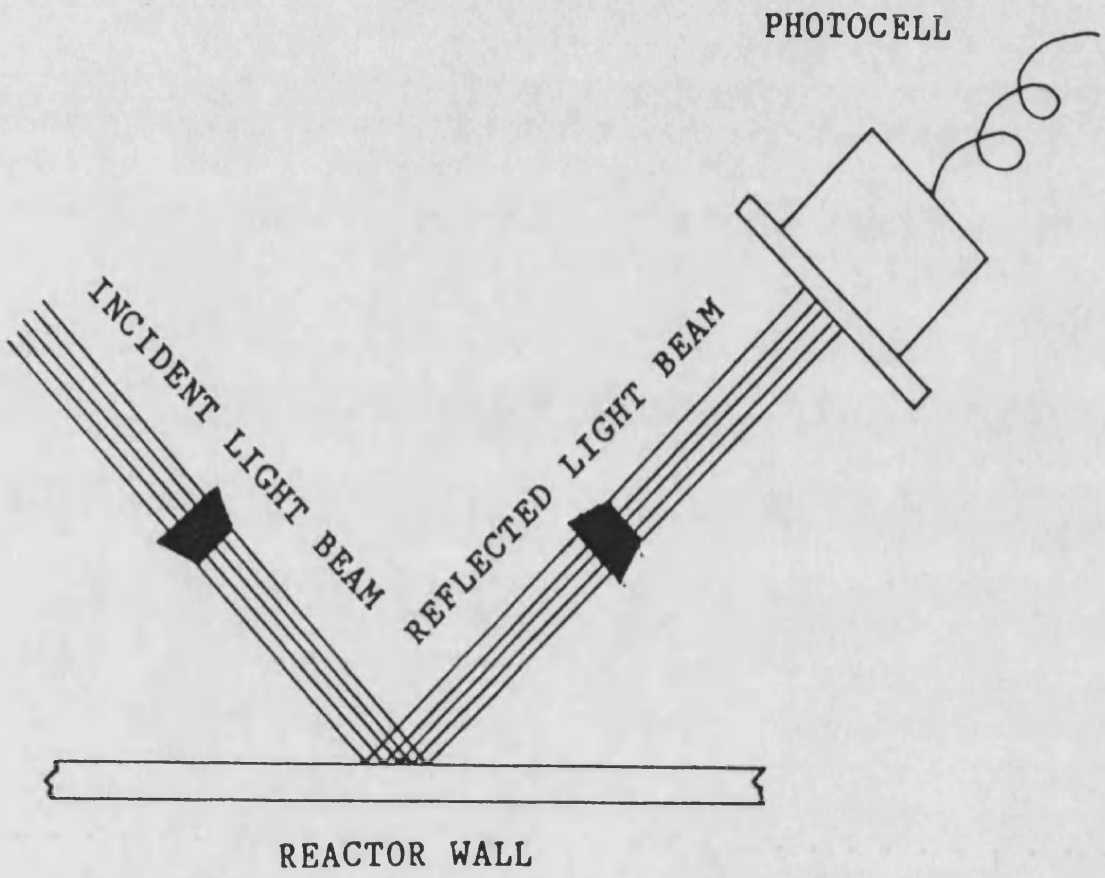

Figure 5.2.1. Schematic diagram for reactor wall specular reflectance measurements

The selection of upper limit (H) was obtained in the same way as in the transmittance experiments reported in section 4.4. The lower limit was defined as that height at distributor, i.e. Ho = 0mm. This selection brought up some implications due to the impossibility of reflectance measurements at zero height. In fact, due to the presence of distributor, the reflected signals were distorted for measurements at zero height. For this reason the distributor was masked and measurements took place at heights 7 mm and upwards.

The assumption of the local light reflectance at zero height, equal to that measured at a height nearest the distributor might introduce errors of 0 to 1.5% on the $\hat{E}_r$ values by using 5.1 equation. Thus, for a selected reactor, a particular type and size of particles, and a chosen flow rate, the integral of each $E_r(h)$ graph would yield the mean light reflectance ($\hat{E}r$).

Figs. 5.3.1, 5.3.2 and 5.3.3 show the variation of local light reflectance $E_r(h)$ with bed height for reactor A at different flow rates and particle sizes. Generally, local reflectance declined with bed height above the distributor. In some instances, especially at conditions of static bed or low flow rates, a slight increase on local reflectance with bed height was observed. This can be explained as follows.

Since the mean particle diameter represents a range of two successive cuts and because successively experiments were run at decreasing flow rates, the larger particles according to Baeyens and Geldart[92] are preferentially settled to the bottom of the bed due to size segregation. Thus smaller particles occupying the

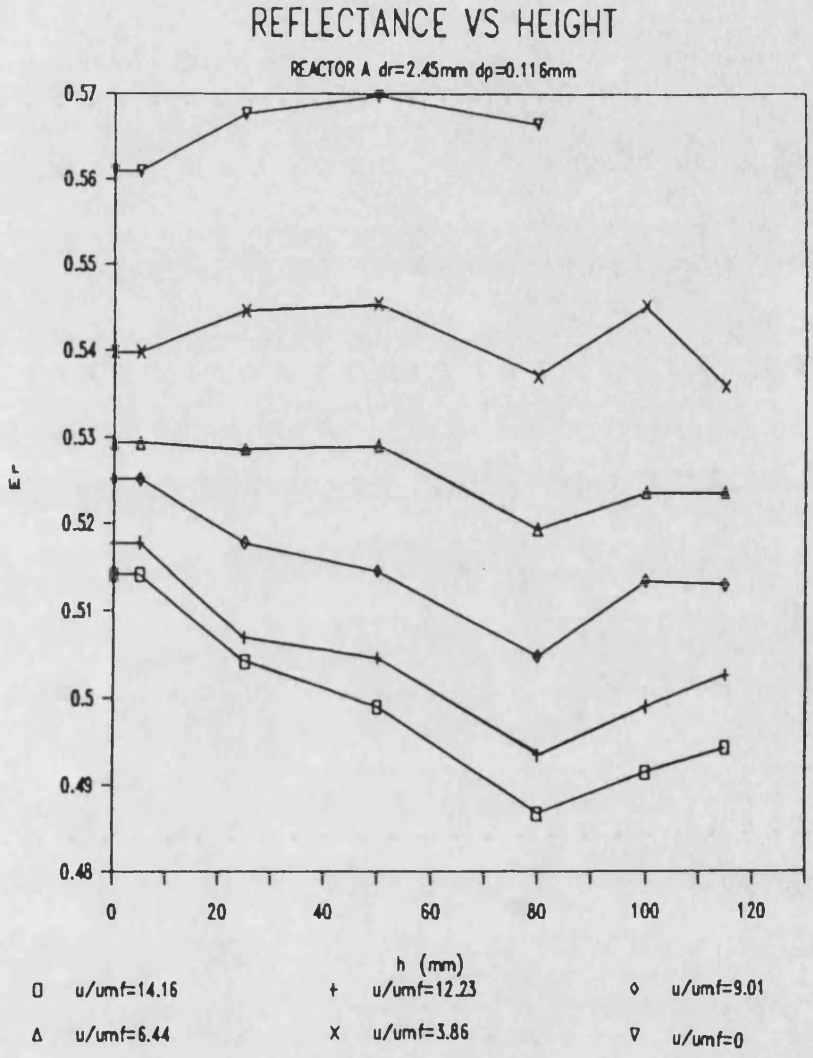

Figure 5.3.1. Local light reflectance as a function of bed height. Reactor A, dp=0.116mm, 13X zeolites

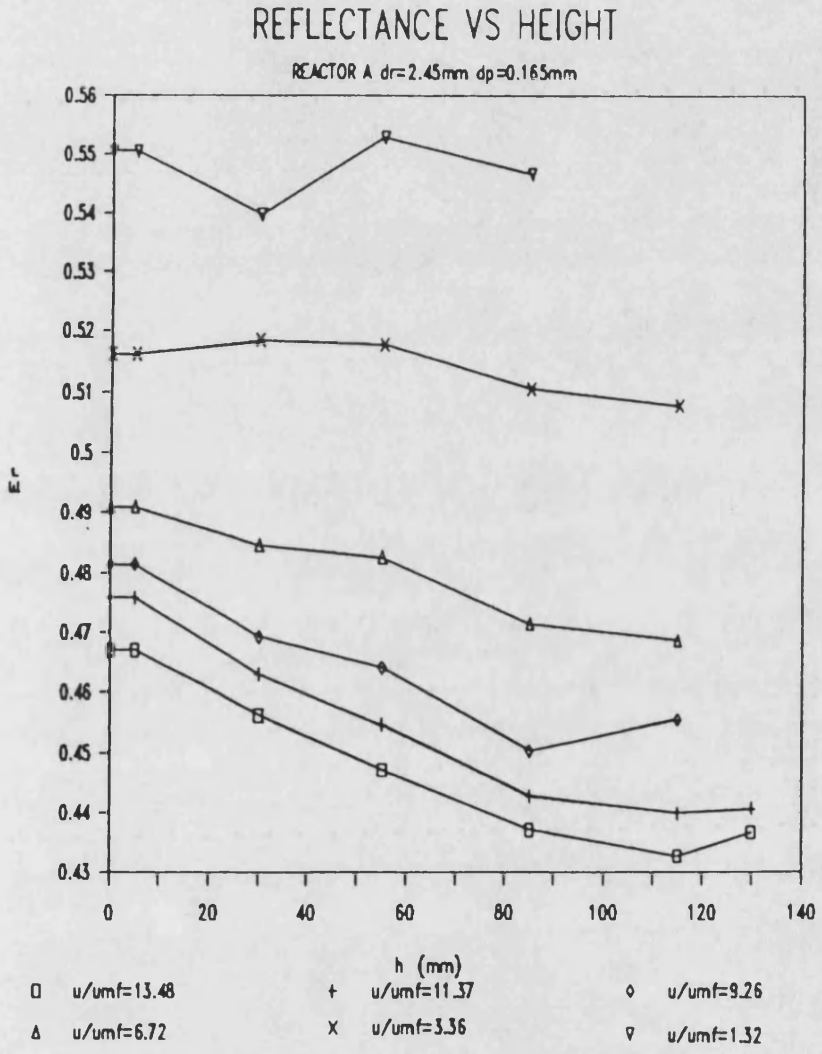

Figure 5.3.2. Local light reflectance as a function of bed height. Reactor A, dp=0.165mm, 13X zeolites

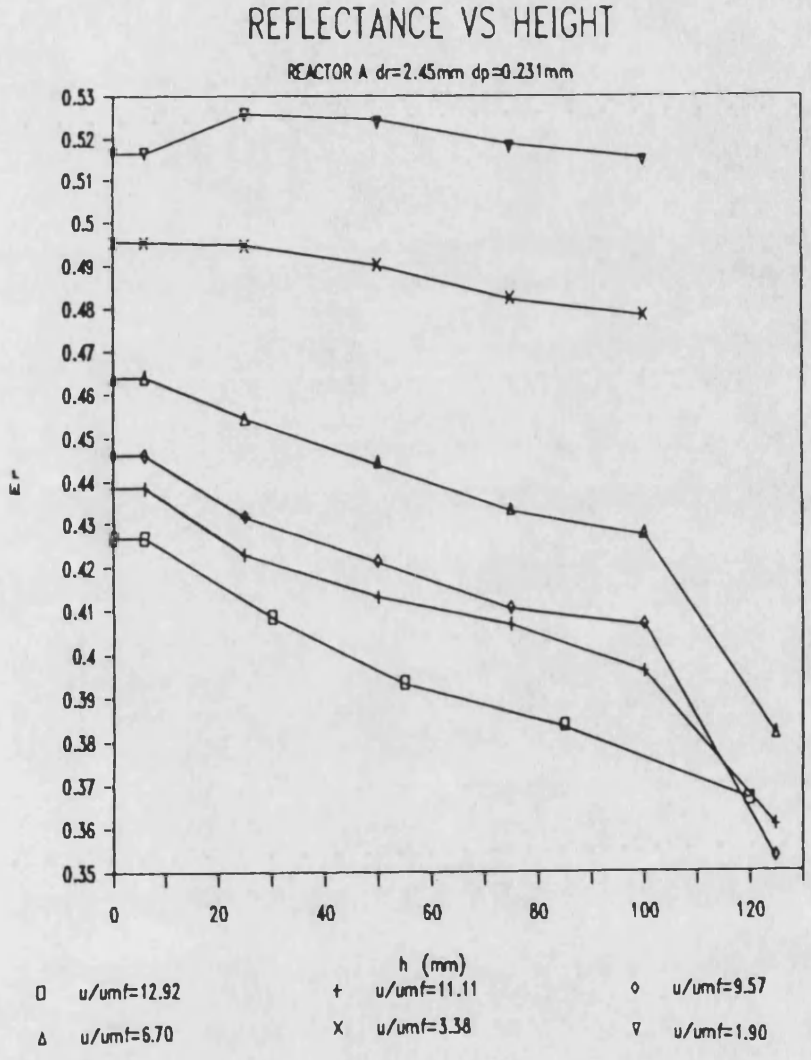

Figure 5.3.3. Local light reflectance as a function of bed height. Reactor A, dp=0.231mm, 13X zeolites

top part of bed has lower porosity than the bottom part and hence a higher light reflectance.

Figs 5.3.4 and 5.3.5 represent the variation of E_r with h for reactor B. Similar plots were obtained for reactors C and D. It should be noted that the E_r has been expressed as fraction of input energy.

5.3.2. Effect of Flow Rate on Reflectance

For all four reactors and all particle sizes used an increase in flow rate led to a decrease in $\hat{E}_r$. Light reflectance has been normalised with respect to input energy according to:

$$\hat{E}_r = \frac{\text{Irradiance of diffuse light reflectance } (\mu W/cm^2)}{\text{Irradiance of incident light beam } (\mu W/cm^2)} \qquad 5.2$$

Figs 5.3.6 and 5.3.7 show the variation of $\hat{E}_r$ with flow rates for reactor A and C for five different particle diameters of 13X zeolites respectively. From these plots, it can be seen that the slope of the $\hat{E}r$ versus u/u_{mf} graphs increases as particle diameter is increased. The rate of reduction of $\hat{E}_r$ with u/u_{mf} is high at low flow rates. For further increases in flow rate a smoother decrease of $\hat{E}_r$ with u/u_{mf} is observed. For particles with mean diameter of 0.116 mm, $\hat{E}_r$ varies approximately linearly with u/u_{mf}.

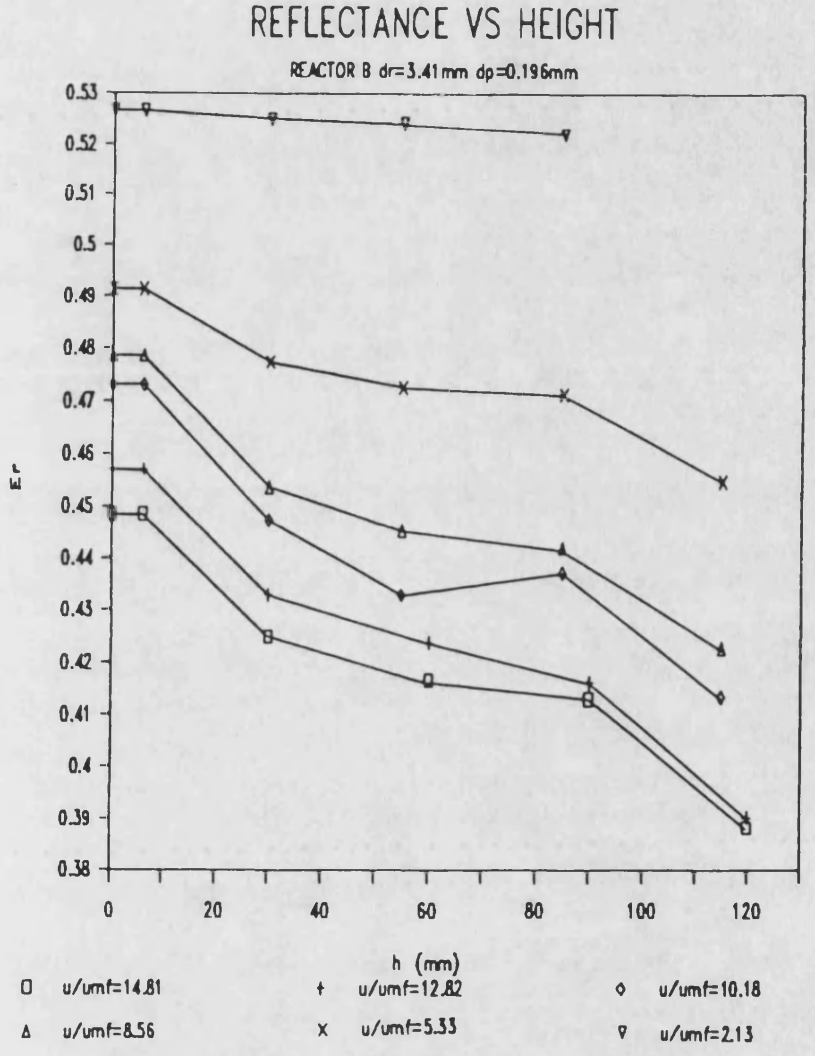

Figure 5.3.4. Local light reflectance as a function of bed height. Reactor B, dp=0.196mm, 13X zeolites

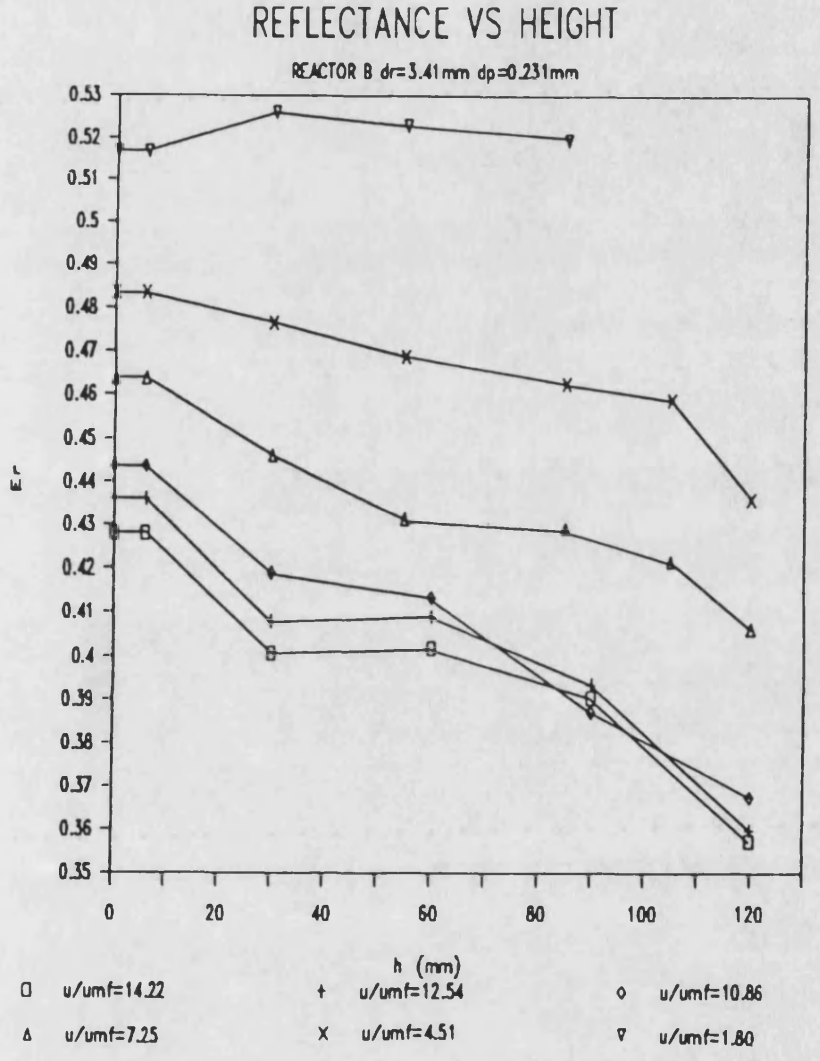

Figure 5.3.5. Local light reflectance as a function of bed height. Reactor B, dp=0.231mm, 13X zeolites

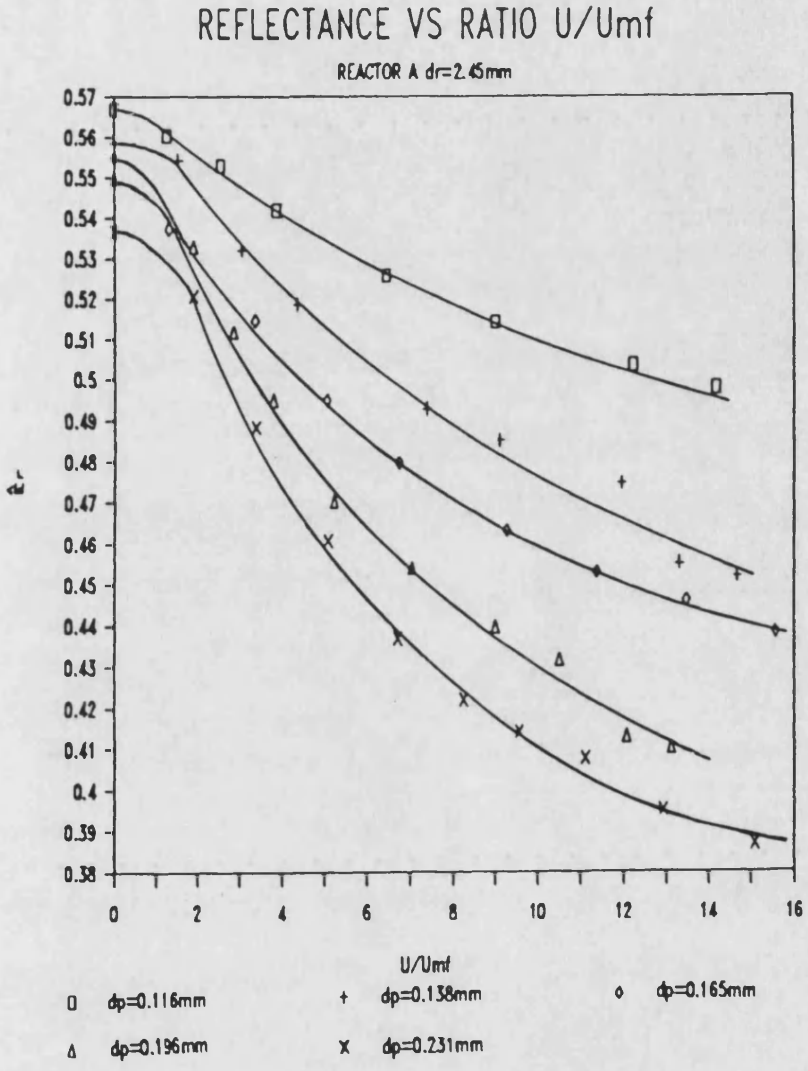

Figure 5.3.6. Variation of light reflectance with flow rate for reactor A and 13X zeolite particles

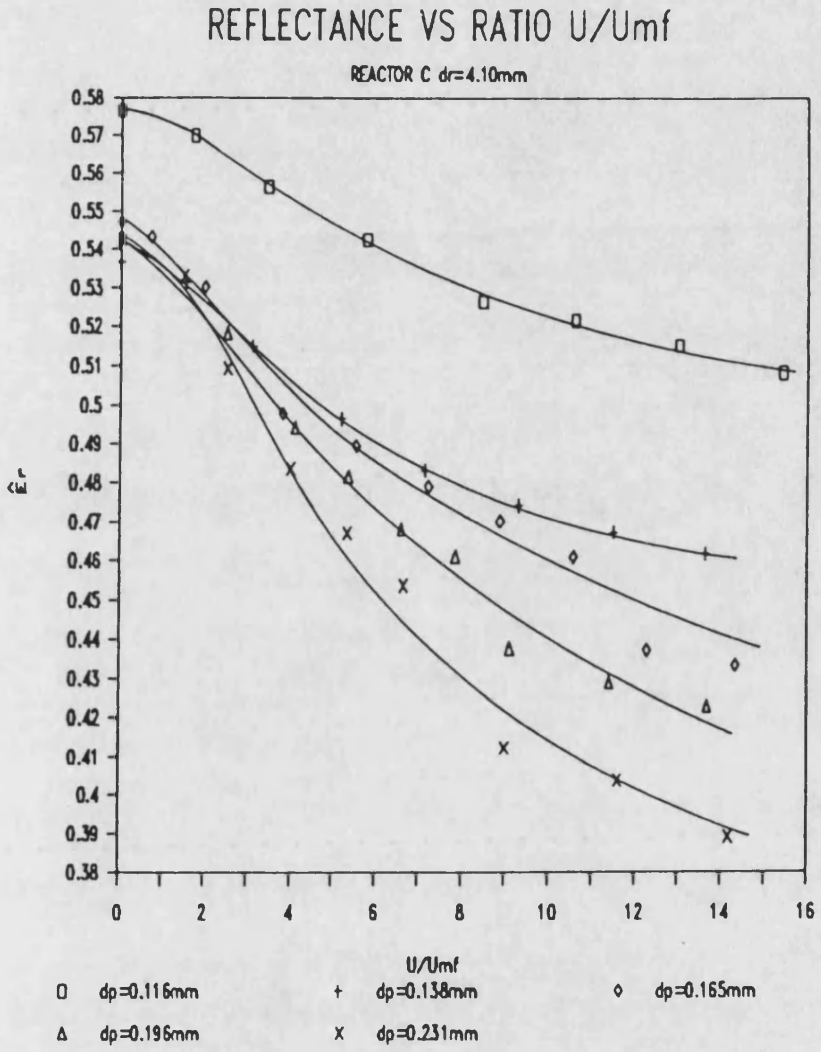

Figure 5.3.7. Variation of light reflectance with flow rate for reactor C and 13X zeolite particles

The reduction of light reflectance with increasing flow rate can be explained as follows. As flow rate is increased, light reflectance ($\hat{E}_r$) drops because the bed porosity increases. A higher bed porosity leads to higher light penetration into the bed. Thus the scattering of photons by the particles increases. More photons are transmitted through the bed and less light is reflected resulting in a reduction in $\hat{E}_r$.

Finally, it should be noted that the values of light reflectance obtained for the conditions of static bed and low flow rates ($u<u_{mb}$) are reproducible to with $\pm$1.5%, because the $\hat{E}_r$ is dependent on the porosity of bed offered to incident light which is affected by the particles settlement in the bed.

5.3.3 Effects of Particle Diameter, Reactor Thickness and Bed Expansion on Light Reflectance

In sections 4.6 and 4.7 light transmittance ($\hat{E}_t$) has been successfully correlated with the fluidisation variable (d_p) and the optical variable (d_r). The same variables were investigated to find their effect on light reflectance.

Figures 5.3.8 and 5.3.9 illustrate the variation of $\hat{E}_r$ with d_p for reactors B and D. For reactor B, it can be seen that for low flow rates the $\hat{E}_r$ versus d_p curves assume an asymptotic form as particle diameter is increased. A possible explanation is that the ratio of bubble/dense phase is low and light penetration or transmittance increases with particle diameter. Thus, light absorption is increased and light reflectance is decreased. For

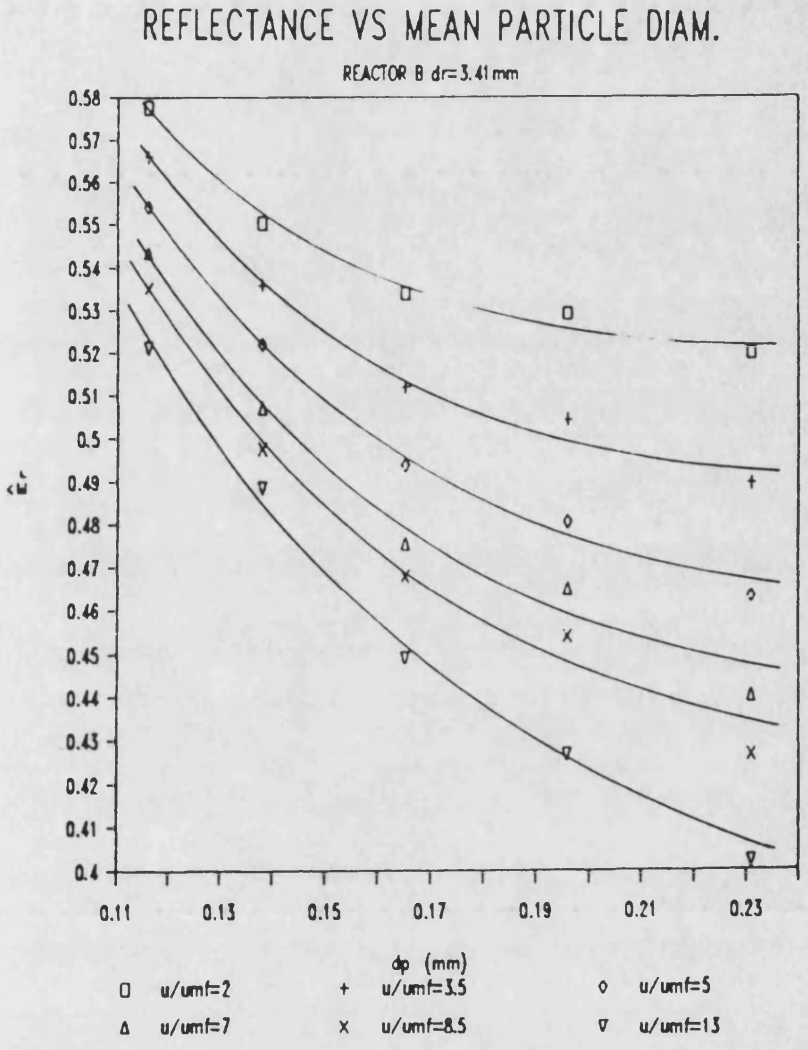

Figure 5.3.8. Light reflectance with particle diameter for reactor B and 13X zeolites

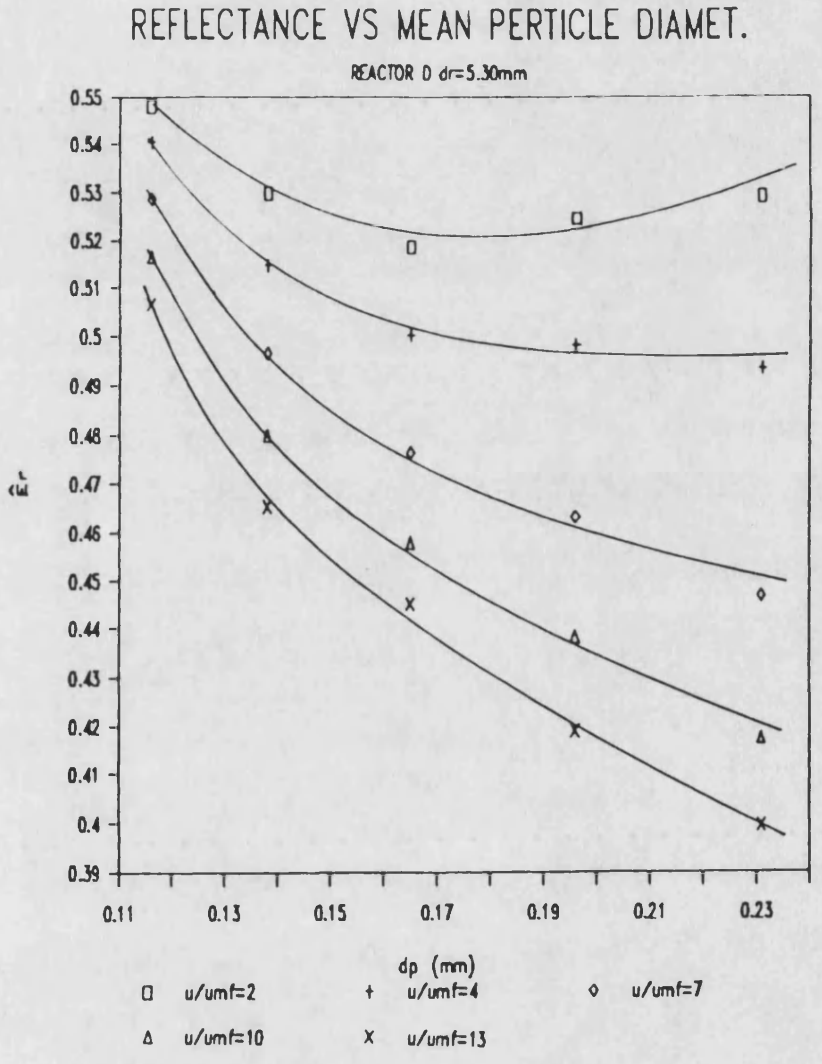

Figure 5.3.9. Light reflectance with particle diameter for reactor D and 13X zeolites

high flow rates, it can be seen that light reflectance drops rapidly with increasing particle size. The same phenomena were observed when reactor D was used.

In section 4.6, the reactor thickness (d_r) has been shown to have a very significant effect on light transmittance. This is however, not true with light reflectance. Figure 5.3.10 shows a $\hat{E}_r$ versus d_r plot for particles of mean diameter 0.165 mm.

Since bed expansion affected light transmittance, $(H-H_{mf})/H_{mf}$ was plotted against light reflectance for three different sizes of particles of 13X zeolites. Figure 5.3.11 shows the linear dependence obtained between E_r and $(H-H_{mf})/H_{mf}$ for particles with mean particle diameters of 0.116, 0.165 and 0.231 mm when reactor A was used. From these plots it can be seen that as bed expansion increases, light reflectance ($\hat{E}_r$) is reduced.

5.3.4 Correlation of Average Light Reflectance with Design Variables

The experimental data reported in the previous sections reveal that light reflectance is a very significant parameter. Its contribution to the light lost by the whole system is high, especially when particles characterised by high light reflectance are used. Up to nearly 60% of light energy irradiating the reactor may be reflected from 13X zeolite particles

For photoreactor modelling and design it would be useful to obtain an equation which correlates light reflectance with reactor design variables.

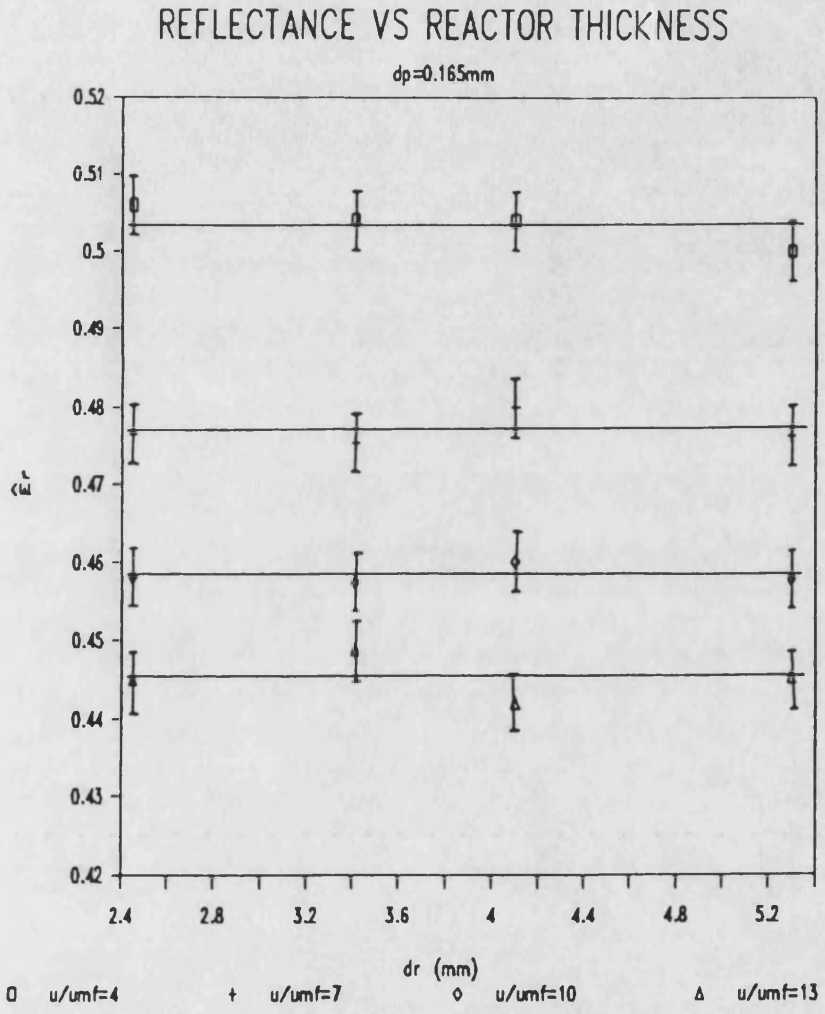

Figure 5.3.10. Light reflectance with reactor thickness for particle diameter of 0.165mm and 13X zeolites

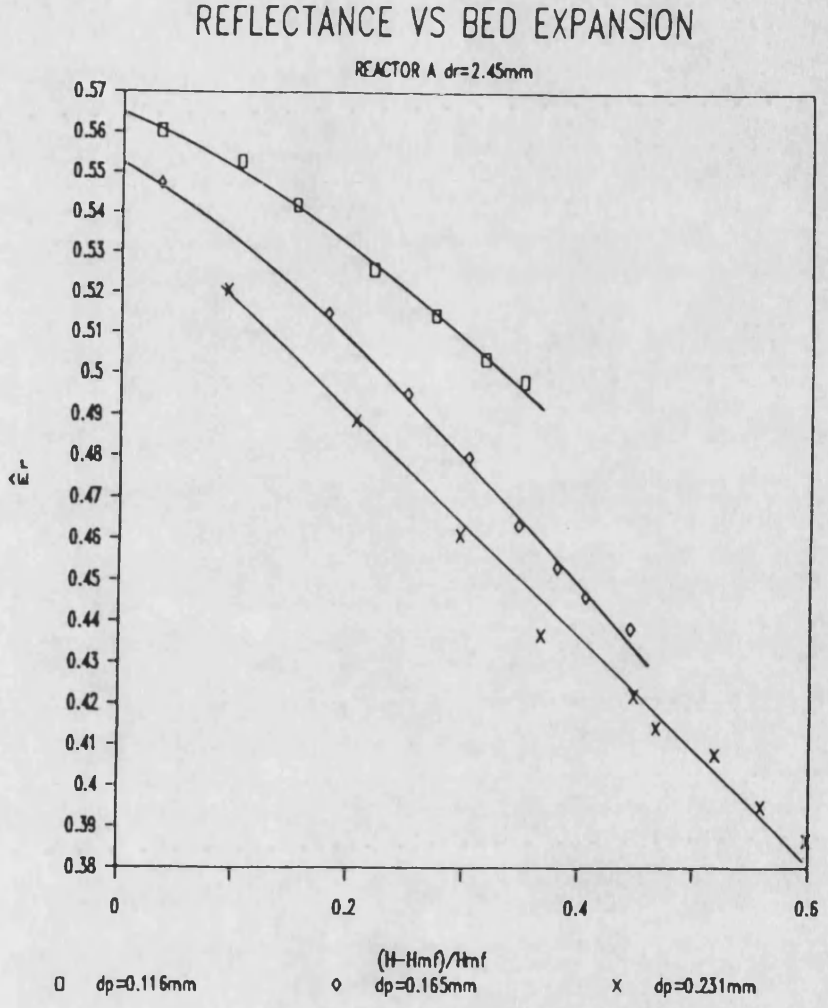

Figure 5.3.11. Light reflectance with bed expansion for reactor A and 13X zeolites

A statistically representative equation correlating $\hat{E}_r$ with important design variables was sought for. The parameters considered were similar to those presented in section 4.7.

For 13X zeolites the equation which gave the best statistical representation is as follows:

$$\hat{E}_r = a'_r + b'_r \left(\frac{H}{H_{mf}}\right)^{-1/2} \left(d_p\right)^{-1/8} \qquad 5.3$$

A total of 169 data points were included and the regression coefficient was found to be 0.93. The scattering of experimental points was within $\pm 5\%$ of the regression equation. The values of a'_r and b'_r were -0.0827 and 0.509 respectively. These experimental points together with the regression equation are illustrated in Figure 5.3.12.

Equation 5.3 suggests that reflectance is inversely proportional to the square root of expanded bed height (H/H_{mf}) and to the $1/8^{th}$ power of particle diameter. Reactor thickness did not seem to have any significant effect on light reflectance. This was shown by the fact that the same value of the regression coefficient was obtained, when the reactor thickness was included in equation 5.3.

Once equation 5.3 was established for 13X zeolites a further study was conducted to test if a similar equation could be applied to Co-Mo-Al_2O_3 particles. Regression analysis of 39 data points yielded a coefficient of 0.75 using equation 5.4 which has the same form as equation 5.3:

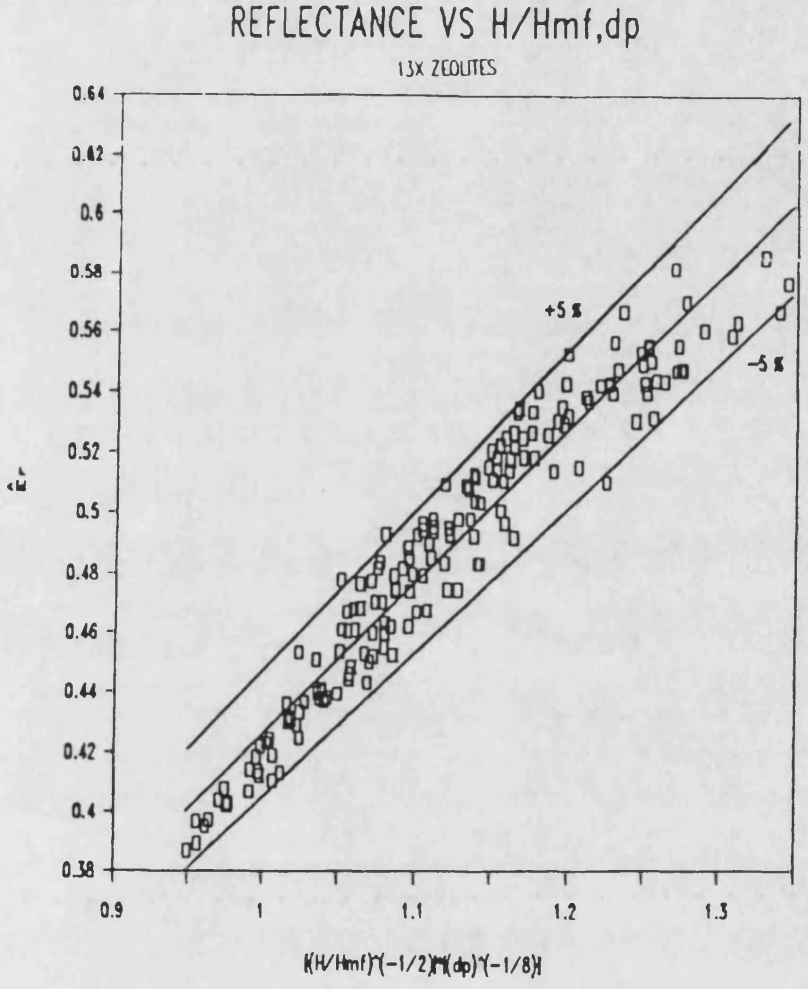

Figure 5.3.12. Correlation between light reflectance and fluidisation parameters for 13X zeolites

$$\hat{E}_r = c'_r + d'_r \left(\frac{H}{H_{mf}}\right)^{-1/2} \left(d_p\right)^{-1/8} \qquad 5.4$$

The experimental points were scattered within ±15% of the equation, as seen in Figure 5.3.13. Due to the lower reflectance of the Co-Mo-Al_2O_3 particles, the values of two coefficients in equation 5.4 were different from that of 13X zeolite particles. These values c'_r and d'_r were found to be -0.05361 and 0.1096 respectively.

It should be pointed out that the equations obtained were dimensional and that the reflectance value of Co-Mo-Al_2O_3 particles was of the same order of magnitude as that obtained by Rizzuti and Yue[77] in 1983.

5.4. Conclusions

The most important conclusions about reflectance measurements are as follows:

1) The mean light reflectance from the particles decreases with increasing flow rate.

2) $\hat{E}_r$ decreases with increasing particle size. At low flow rates mean light reflectance approaches some asymptotic values.

3) Light reflectance does not vary significantly with reactor thickness. $\hat{E}_r$ is approximately constant when particles of the same diameter fluidised at the same flow rate in different reactors.

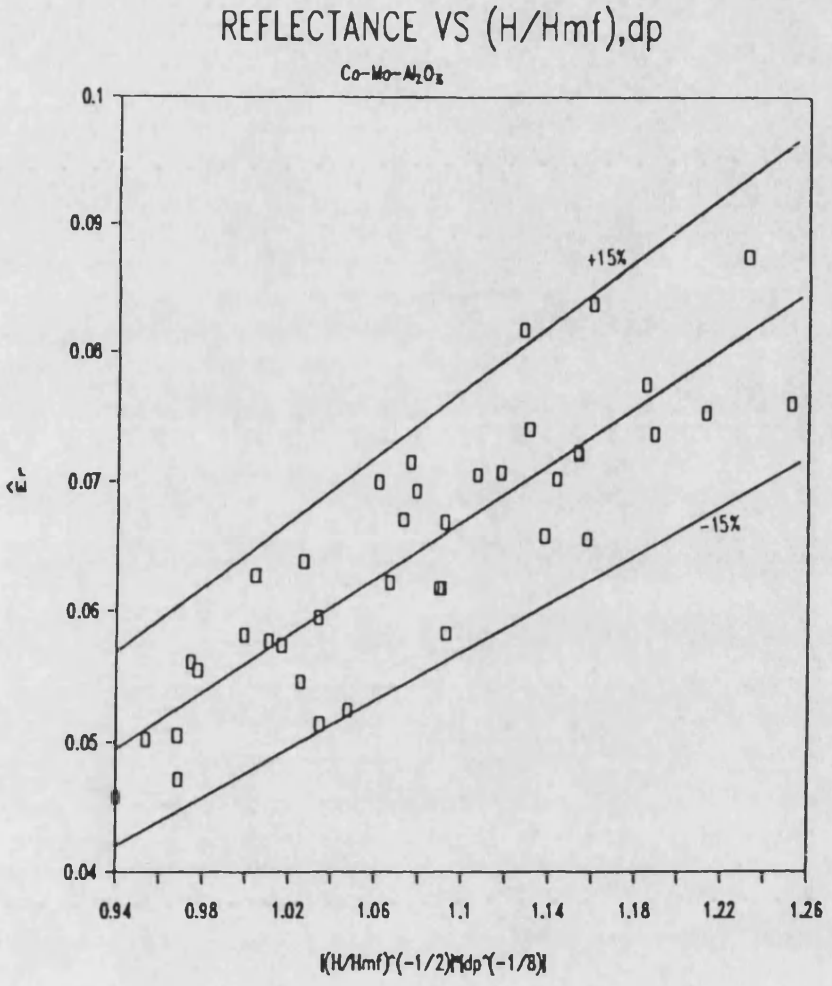

Figure 5.3.13. Correlation between light reflectance and fluidisation parameters for $Co-Mo-Al_2O_3$

4) Equations 5.3 and 5.4 have been found to give a satisfactory correlation between light reflectance from a gas-solid fluidised photoreactor and reactor design variables. The values of the constants in equations 5.3 and 5.4 are dependent on the type of particles used. Such equations may be used for modelling and design studies.

CHAPTER 6

LIGHT ABSORPTION IN 2-D FLUIDISED BED REACTORS

6.1. Radiation Balance in a Two-Dimensional Photoreactor

In order to evaluate the light absorption in a fluidised photoreactor, a radiation balance should be applied to the whole reactor system. The method devised in this study may be applied to any heterogeneous system when a direct method of absorption measurement is not possible. This method[113] is based on the optical measurements of two key variables: (a) light transmittance and (b) light reflectance. These variables are involved in the light energy balance equation as shown below:

$$\text{Absorption} = \text{Incidence} - \text{Transmittance} - \text{Reflectance} \qquad 6.1$$

$$E_a = E_i - E_t - E_r \qquad 6.1a$$

Since equation 6.1a represents a general formulation of light absorption, the amount of light absorbed by the particles in a fluidised or static bed is given by the following equation:

$$\hat{E}_a^P = \hat{E}_a^{E+P} - \hat{E}_a^E \qquad 6.2$$

Light absorbed by the particles = Light absorbed by empty reactor and particles − Light absorbed by empty reactor

Light "absorbed" by particles as defined by equation 6.2 is the maximum amount of light energy available for photocatalytic reactions in the reactor. However, the amount of light energy actually utilised for photocatalytic reactions is determined by the absorption characteristics of the particles and specific to the reactions to be conducted. This actual amount utilised is usually less than this maximum because of photon-scattering and decay. However, for the purposes of the present study, the light "absorbed" by particles as defined by equation 6.2 is the variable of interest.

From equation 6.2 it can be seen that the light absorbed by the particles is obtained by taking the difference between that absorbed by the whole system, i.e. empty reactor and particles, and that absorbed by the empty reactor.

For the evaluation of light absorption by the empty reactor and particles ($\hat{E}_a^{E+P}$), equation 6.1a is applied to the whole reactor system giving the following equation:

$$\hat{E}_a^{E+P} = \hat{E}_i - \hat{E}_r^{E+P} - \hat{E}_t^{E+P} \qquad 6.3$$

where

$\hat{E}_i$ = fraction of mean incident light energy to the whole reactor system.

$\hat{E}_r^{E+P}$ = fraction of mean light reflectance, i.e. specular and diffuse reflectance from the whole reactor system with respect to incident light.

$\hat{E}_t^{E+P}$ = fraction of mean light transmittance through the whole reactor system with respect to incident light.

The evaluation of light absorption by the empty reactor ($\hat{E}_a^E$) is obtained by applying again equation 6.1a to the front wall of the reactor and to the rear wall of the reactor, and then, by taking the sum of these two sets of light measurements according to:

$$\hat{E}_a^E = (\hat{E}_i - \hat{E}_r^{fw} - \hat{E}_t^{fw})_I + (\hat{E}_i' - \hat{E}_r' - \hat{E}_t^{E+P})_{II} \qquad 6.4$$

where

$\hat{E}_r^{fw}$ = fraction of mean light reflectance of front wall only with respect to incident light.

$\hat{E}_t^{fw}$ = fraction of mean light transmittance of front wall only with respect to incident light.

$\hat{E}_r'$ = fraction of mean light reflectance of rear wall with respect to incident light.

The first term (I) of equation 6.4 represents the light absorption by the front wall of the reactor.

The second term (II) of equation 6.4 represents the light absorption by the rear wall of the reactor. Since the flow rate, particle size, and reactor thickness affected the light penetration through the bed, the rear wall was subjected to different light irradiation at different reactor conditions. Thus the only way to evaluate the light absorption by the rear wall was to simulate the

incident light at the rear wall ($\hat{E}_i'$) making use of the measured values of light transmittance through the whole system ($\hat{E}_t^{E+P}$) in independent experiments.

In these experiments a glass plate identical to that which made up the reactor walls was irradiated. The incident light of irradiation to the glass was adjusted in order that light transmitted through it coincided with the $\hat{E}_t^{E+P}$. Thus $\hat{E}_i'$ was selected and $\hat{E}_r'$ of the glass was measured by applying the specular reflectivity law. Hence the second term (II) of equation 6.4 was evaluated.

It should be noted that the light absorbed by the front wall of the reactor was 2.4% of the input light energy and that the light absorbed by the rear wall could hardly reach a maximum value of 30% of that absorbed by the front wall. Thus the highest light absorbed by the empty reactor was low and equal to 3.12% of that of the incident light. Since in the present study the light absorption by the rear wall is too low, the second term (II) of the equation 6.4 could be ignored. However, the above procedure for $\hat{E}_a^E$ evaluation is indispensible when reactor walls of higher optical density are used.

6.2. Variation of Light Reflectance Relative to Transmittamce with Flow Rate

In an irradiated 2-D fluidised bed reactor the variation of light transmittance with flow rate is different from the variation of light reflectance with flow rate.

For this reason their relative influence on the fluidisation parameters has been investigated.

The influence of flow rate on reflectance relative to transmittance can be shown by examining the plots of $\hat{E}_r/\hat{E}_t$ versus u/u_{mf}. Figure 6.2.1 shows the variation of $\hat{E}_r/\hat{E}_t$ with flow rate for reactor A and five sizes of 13X zeolite particles. For all five particle diameters, it can be seen that reflectance relative to transmittance drops rapidly with increasing flow rate. A transition on the $\hat{E}_r/\hat{E}_t$ versus u/u_{mf} curves is observed at flow rates of about 4 to 7 times u_{mf}. Further increases of flow rate cause the $\hat{E}_r/\hat{E}_t$ curves to approach some asymptotic values. The transition on the $\hat{E}_r/\hat{E}_t$ versus u/u_{mf} curves was due to the rapid drop of light transmittance as flow rates were decreased.

Each curve on the $\hat{E}_r/\hat{E}_t$ versus u/u_{mf} plots assumes two asymptotes. For example, the curve for particles of diameter 0.231 mm assumes the asymptotes PQ and MN. The intersection of PQ with u/u_{mf} axis defines the minimum flow rate in which light transmittance through the bed starts to occur.

On the other hand, the intersection N of MN with $\hat{E}_r/\hat{E}_t$ axis determines the minimum value of $\hat{E}_r/\hat{E}_t$ which can be obtained for the particular reactor and particle size used. The same form of graphs has been obtained when reactor B, C and D were used. It can be concluded that the asymptotes of these curves provide the bounds within which the fluidised photoreactor should operate.

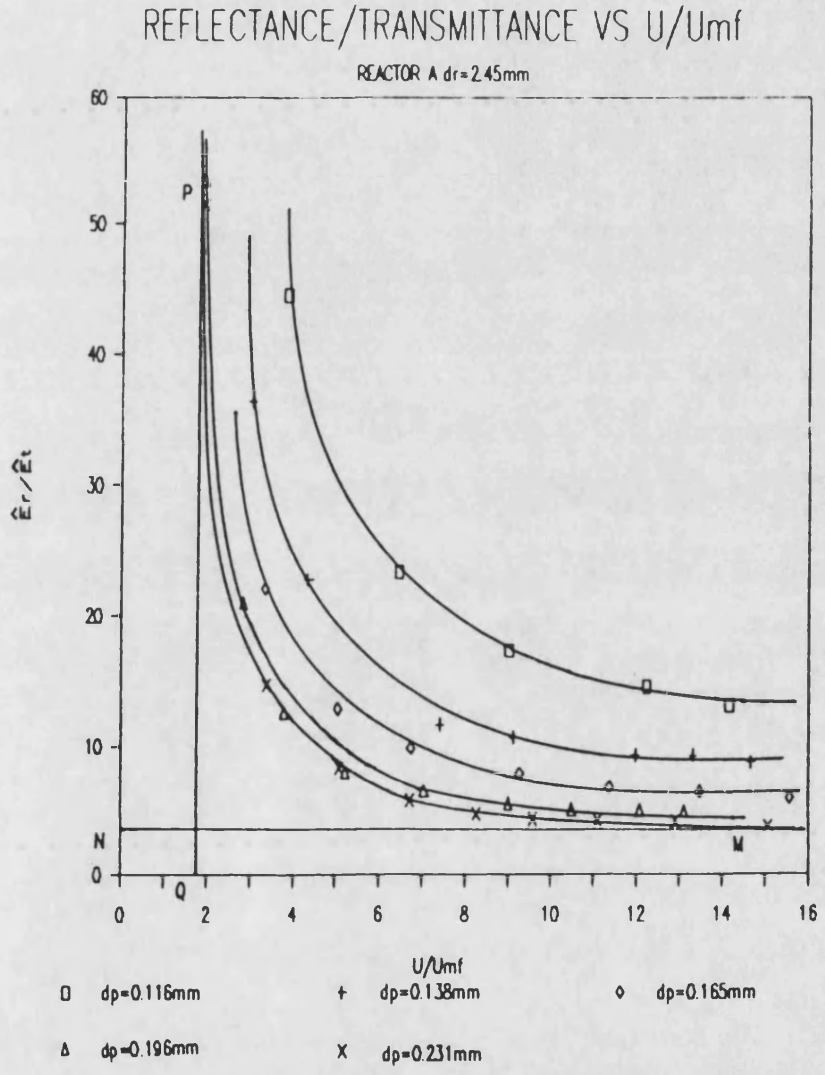

Figure 6.2.1. The ratio of light reflectance to transmittance as a function of flow rate for reactor A and 13X zeolites

It should be noted that these plots are very useful for calculating transmittance or reflectance when the other parameter is known.

6.3. Influence of Reactor Thickness on the Ratio of Reflectance to Transmittance

It has been shown by Yue et al[78] that light transmittance followed a semilogarithmic form with reactor thickness. The same behaviour was found in the present research, (see section 4.6). On the other hand, the present study showed that light reflectance was approximately independent of the reactor thickness as shown in section 5.3.3.

Figures 6.3.1 and 6.3.2 show the dependence of the ratio of reflectance to transmittance ($\hat{E}_r/\hat{E}_t$) on reactor thickness (d_r). From these plots, it can be seen that there is a linear dependence of $\hat{E}_r/\hat{E}_t$ on reactor thickness at flow rates higher than 7 times u_{mf}. For lower flow rates the rate of increase of $\hat{E}_r/\hat{E}_t$ with reactor thickness increases rapidly beyond a thickness of 4 mm. This sharp increase is due to the low transmittance of light at low flow rates.

6.4 Effect of Flow Rate on Light Absorption

The average light absorbed ($\hat{E}_a$) by the fluidised particles was found to increase as flow rate was increased. The same behaviour was observed for all four reactors and all five particle sizes used.

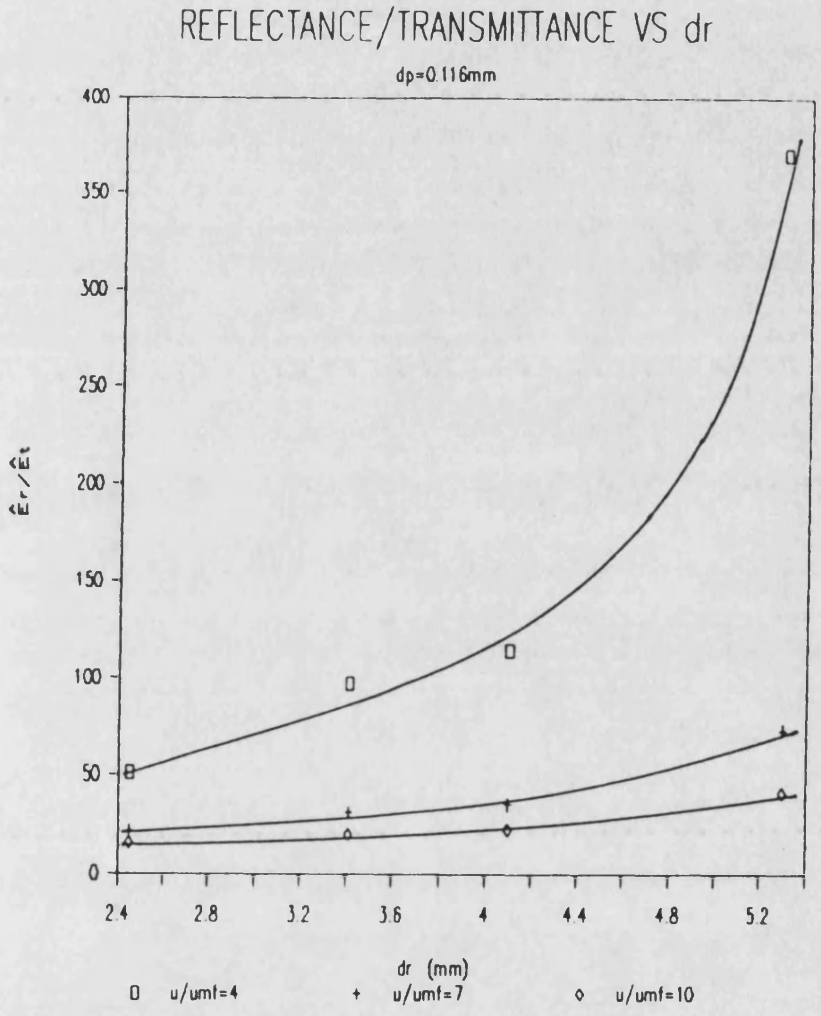

Figure 6.3.1. Variation of the ratio of light reflectance to transmittance with reactor thickness. 13X zeolites, dp=0.116mm

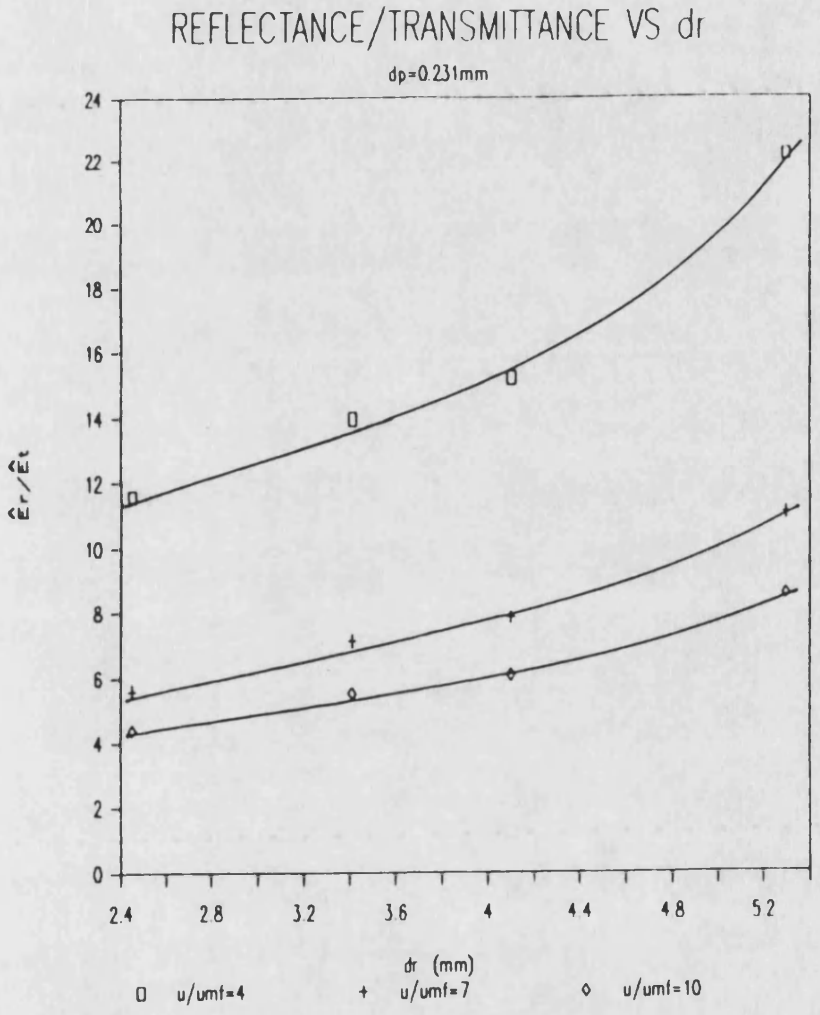

Figure 6.3.2. Variation of the ratio of light reflectance to transmittance with reactor thickness. 13X zeolites, dp=0.231mm

Figure 6.4.1 and 6.4.2 show the variation of light absorption with flow rate for reactors B and D using 13X zeolite particles. From the $\hat{E}_a$ versus u/u_{mf} plots, it can be seen that light absorption increases with flow rate. This increase on light absorption is explained as follows.

When the bed is static and because the reactor system is irradiated on one side, only a small fraction of the particles is exposed to light energy as light penetration into the bed is very limited. Thus light absorption is small. As gas flow rate increases, the particles become fluidised, allowing more light to penetrate further into the bed. Thus a higher fraction of particles is subjected to light irradiation leading to a higher light absorption. The intersection of the $\hat{E}_a$ versus u/u_{mf} curves in figure 6.4.2 coincide approximately with the simultaneous appearance of bubbles in fluidised bed observed visually.

It should be noted that small fluctuations in measurements on $\hat{E}_t$ and $\hat{E}_r$ may cause much larger fluctuations in light absorption, especially at high flow rates, hence there is a higher degree of scatter of results.

6.5 Effects of Particle Diameter on Light Absorption

The irradiation of fluidised beds containing different sizes of particles showed that the light absorption varies with the particle diameter. This variation of $\hat{E}_a$ with d_p is shown in figures 6.5.1 and 6.5.2. For small particle diameters of up to about 0.200 mm an increase of light absorption with increasing particle diameter was observed.

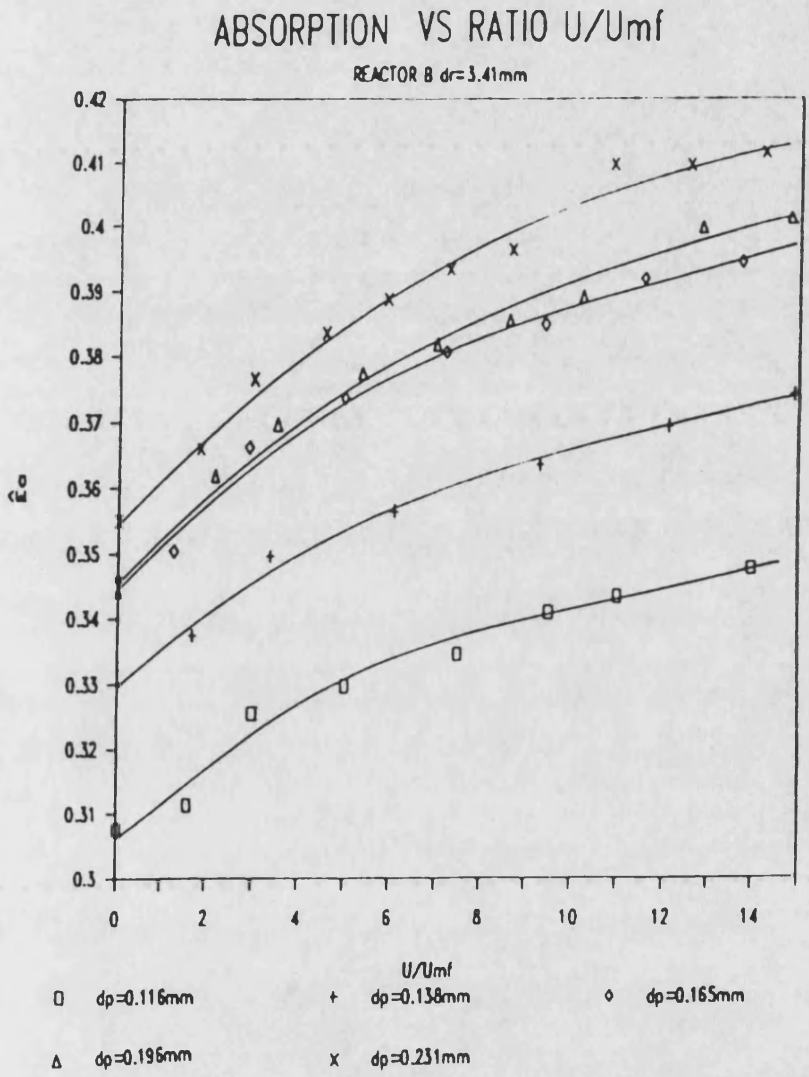

Figure 6.4.1. Light absorption as a function of flow rate for reactor B and 13X zeolites

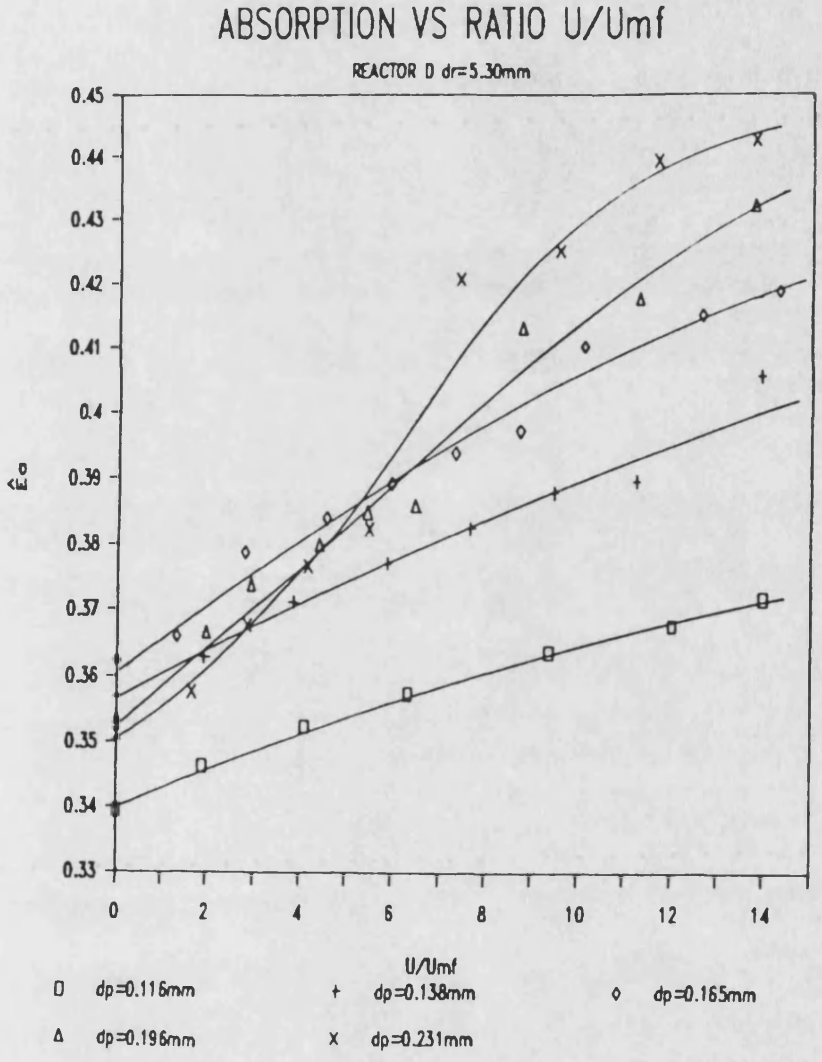

Figure 6.4.2. Light absorption as a function of flow rate for reactor D and 13X zeolites

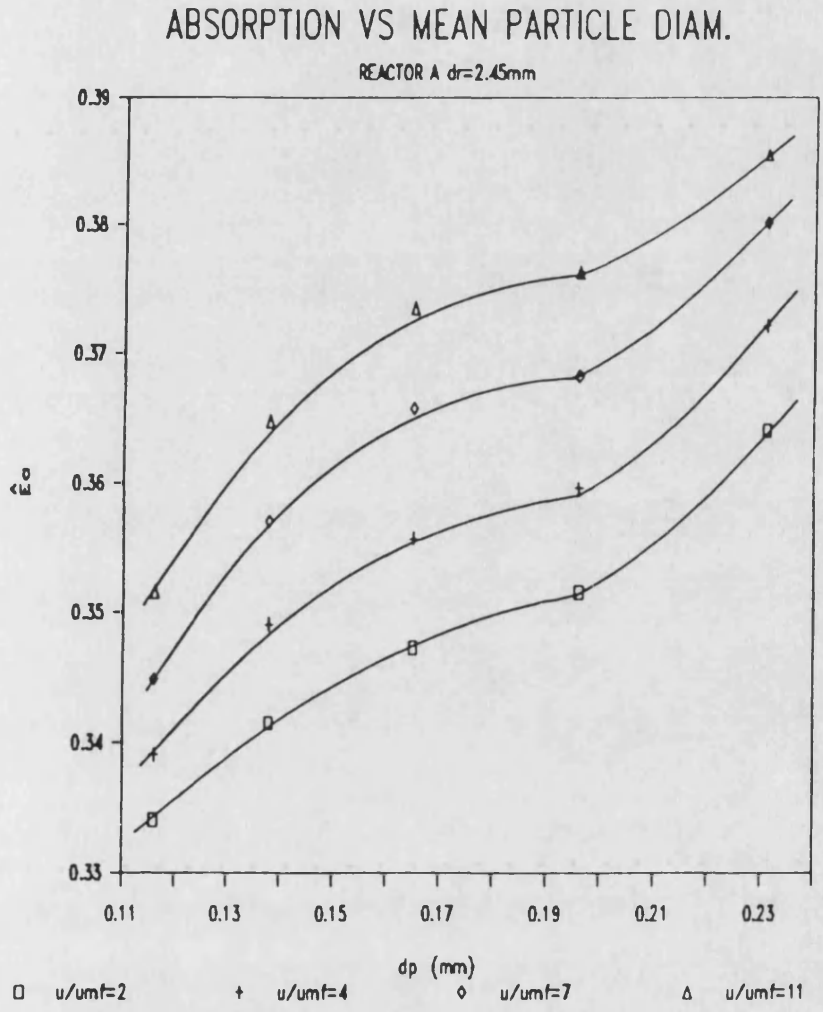

Figure 6.5.1. Variation of light absorption with particle diameter for reactor A and 13X zeolites

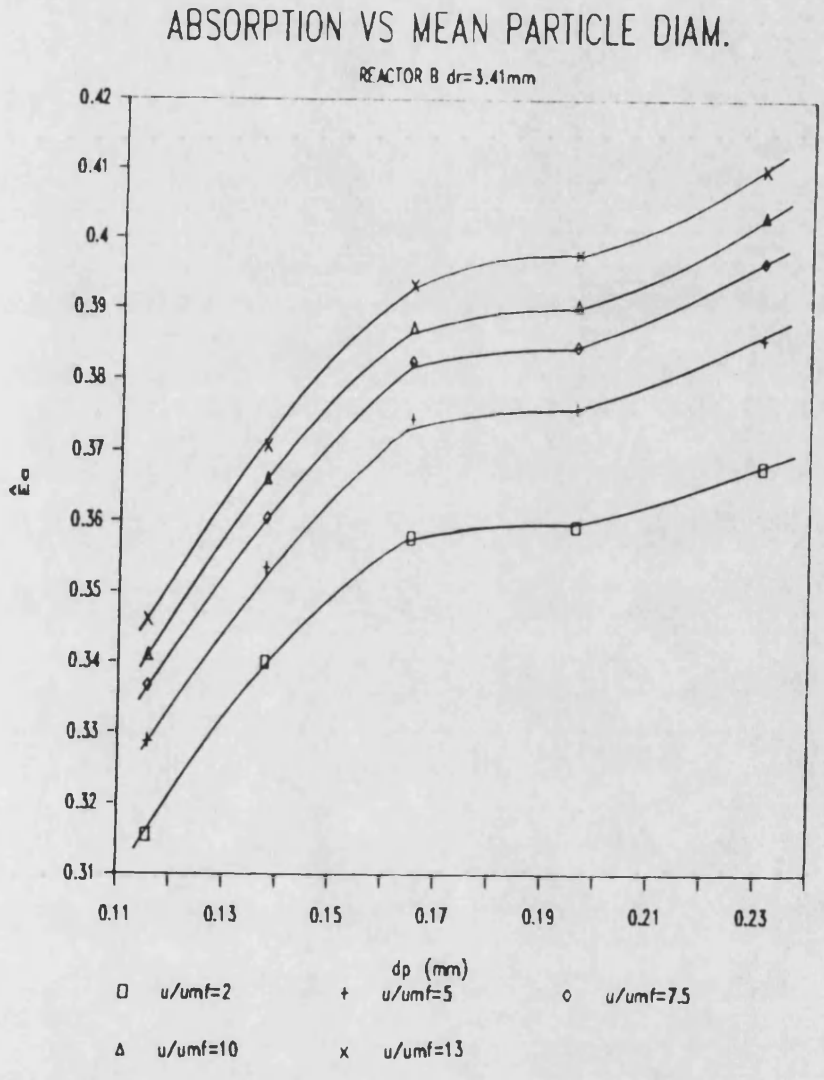

Figure 6.5.2. Variation of light absorption with particle diameter for reactor B and 13X zeolites

This is due to a decrease of $\hat{E}_r$ with d_p which has only a slightly greater effect on the light absorption ($\hat{E}_a$) than that of the increase of $\hat{E}_t$ with d_p on $\hat{E}_a$.

A sharper increase in $\hat{E}_a$ was observed for particles of diameters greater than about 0.200 mm because the increase of $\hat{E}_r$ with d_p was much more prominent than that of the reduction of $\hat{E}_t$ with d_p on light absorption ($\hat{E}_a$).

Finally, it can be concluded that for a fixed flow rate and reactor thickness the shape of the $\hat{E}_a$ versus d_p curves is determined by the simultaneous effect of light transmittance ($\hat{E}_t$) and light reflectance ($\hat{E}_r$) on light absorption ($\hat{E}_a$) as particle diameter is varied.

6.6. Effect of Reactor Thickness and Bed Expansion on Light Absorption

The influence of reactor thickness (d_r) on light absorption ($\hat{E}_a$) was examined. Figure 6.6.1 shows the $\hat{E}_a$ versus d_r plots for 13X zeolite particles of 0.165 mm diameter. From these graphs it can be seen that the dependence of $\hat{E}_a$ with d_r is different at different flow rates. In fact for low flow rates $\hat{E}_a$ increases with d_r up to about a reactor thickness of 3.5 mm, then the rate of increase decreases at higher reactor thicknesses. This is because the fraction of particles exposed to light irradiation is reduced and hence the light absorption.

At higher flow rates ($u/u_{mf} > 7$) and for reactor thickness greater than 4.10 mm, there is a sharp increase of $\hat{E}_a$ with

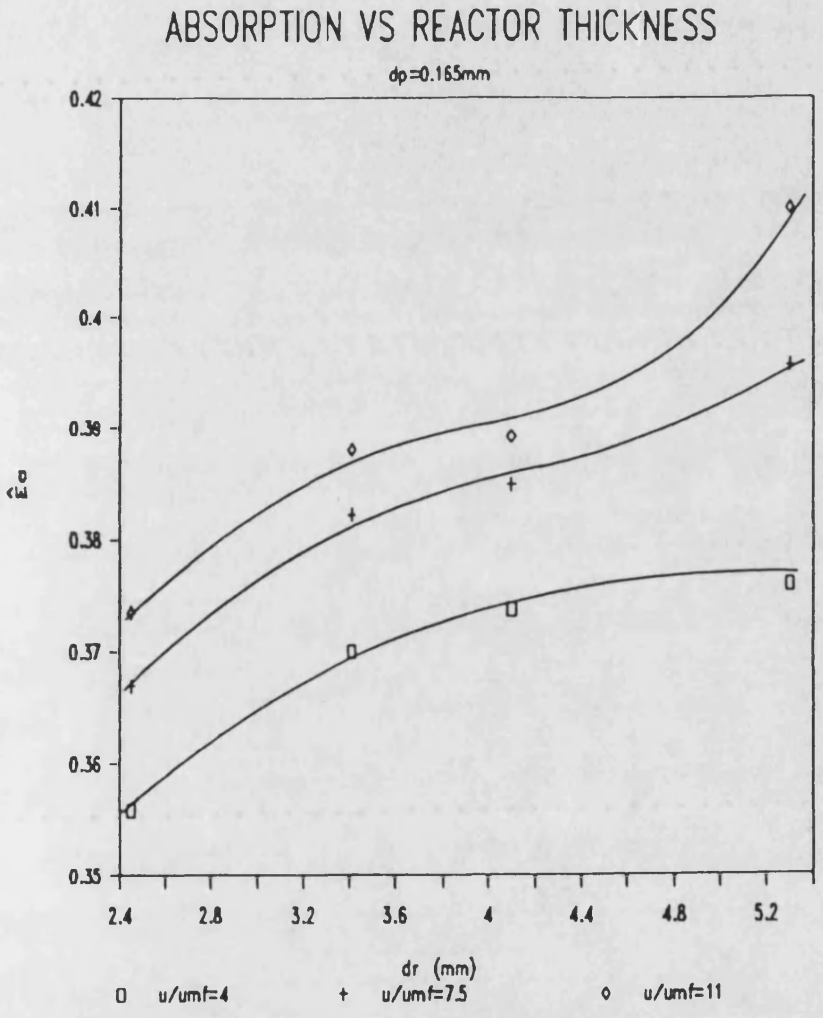

Figure 6.6.1. Variation of light absorption with reactor thickness for particle diameter of 0.165mm and 13X zeolites

increasing d_r. This is due to the scattering of photons within the fluidised bed leading to a higher fraction of particles exposed to light irradiation and hence to light absorption.

The variation of light absorption with bed expansion was also examined. Figure 6.6.2 shows the dependence of $\hat{E}_a$ versus $(H-H_{mf})/H_{mf}$. As has been explained in section 4.6, due to the effect of particle size on bed expansion, light absorption approaches higher values as bigger particle sizes are used. The linear variation of $\hat{E}_a$ with $(H-H_{mf})H_{mf}$ is observed similar to that observed for $\hat{E}_t$ and $\hat{E}_r$.

6.7. Modelling of Light Absorption in a Fluidised Photoreactor

For the purpose of modelling and design of photoreactors, reliable models for reactor analysis and design are required. Quantitative information on light absorption by the reactor contents is needed in the radiation and kinetics equations.

It is possible to combine the correlations obtained for light transmittance and reflectance and use an energy balance to obtain a correlation for light absorption. However, the resulting equation is quite unwieldy to use because the correlations for $\hat{E}_t$ and $\hat{E}_r$ are of different forms. Hence the data on light absorption were regressed to find if there might be a simpler correlation that could be used more easily for the purpose of reactor design.

An empirical model correlating light absorption in a fluidised photoreactor with a number of fluidisation variables was attempted. A total number of 175 experimental data on zeolite 13X

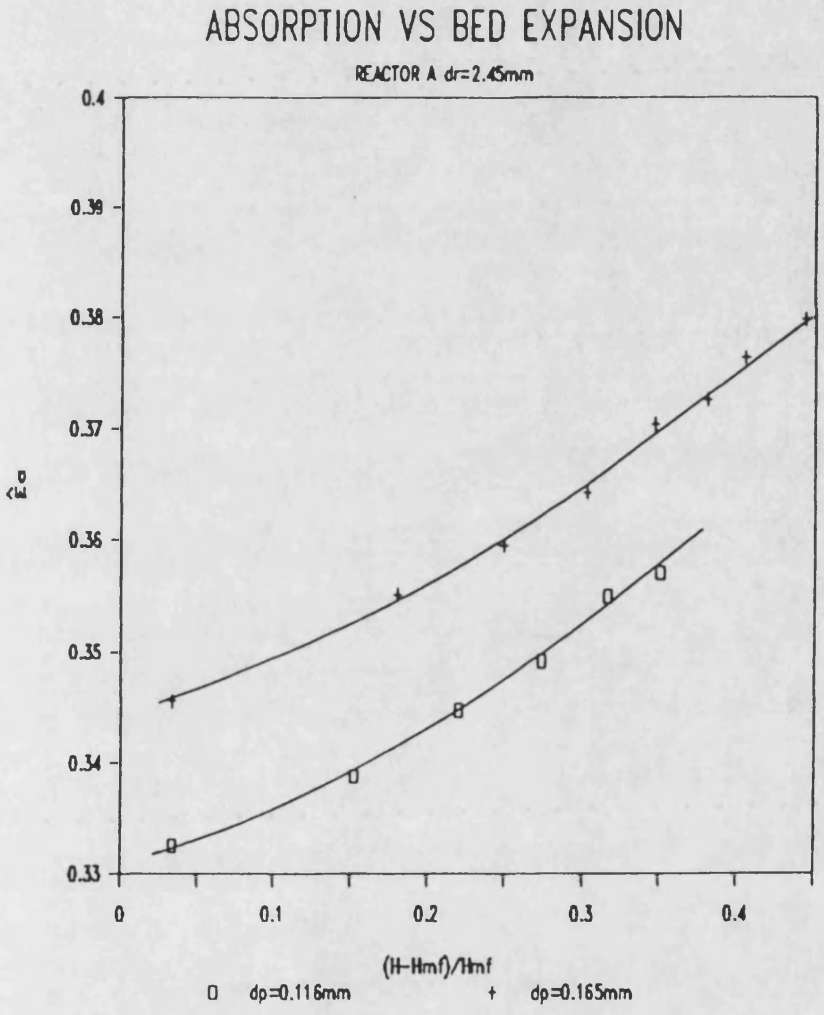

Figure 6.6.2. Variation of light absorption with bed expansion for reactor A and 13X zeolites

were subjected to data regression. The equation which gave the most satisfactory correlation was of the following form:

$$\hat{E}_a = a'_a + b'_a \left(\frac{H}{H_{mf}} \right)^2 \left(d_p \, d_r \right)^{1/2} \qquad 6.7.1$$

The regression coefficient is 0.85 and the degree of scatter is within ±5% of the regression equation. The values of a'_a and b'_a are 0.3045 and 0.0527 respectively.

Equation 6.7.1 suggests that absorbance is proportional to the second power of bed height and to the square root of particle diameter and reactor thickness.

The validity of equation 6.7.1 was tested for different type of particles. Unfortunately, the above equation did not give satisfactory correlation of the 42 data points of Co-Mo-Al_2O_3. Instead the following correlation was found to be better:

$$\hat{E}_a = c'_a + d'_a \left(\frac{H}{H_{mf}} \right)^{-1/2} \left(d_r \right)^{1/8} \qquad 6.7.2$$

The degree of scatter was within ±2% of the regression equation. The r-squared value is 0.80 and the coefficients c'_a and d'_a are 0.5115 and 0.2728 respectively.

Figs 6.7.1 and 6.7.2 show the experimental points of light absorption correlations for 13X zeolites and Co-Mo-Al_2O_3 respectively.

Equation 6.7.2 shows that $\hat{E}_a$ is proportional to the $1/8^{th}$ power of reactor thickness and inversely proportional to the square root of bed height. Particle diameter did not seem to have any significant effect on light absorption according to equation 6.7.2.

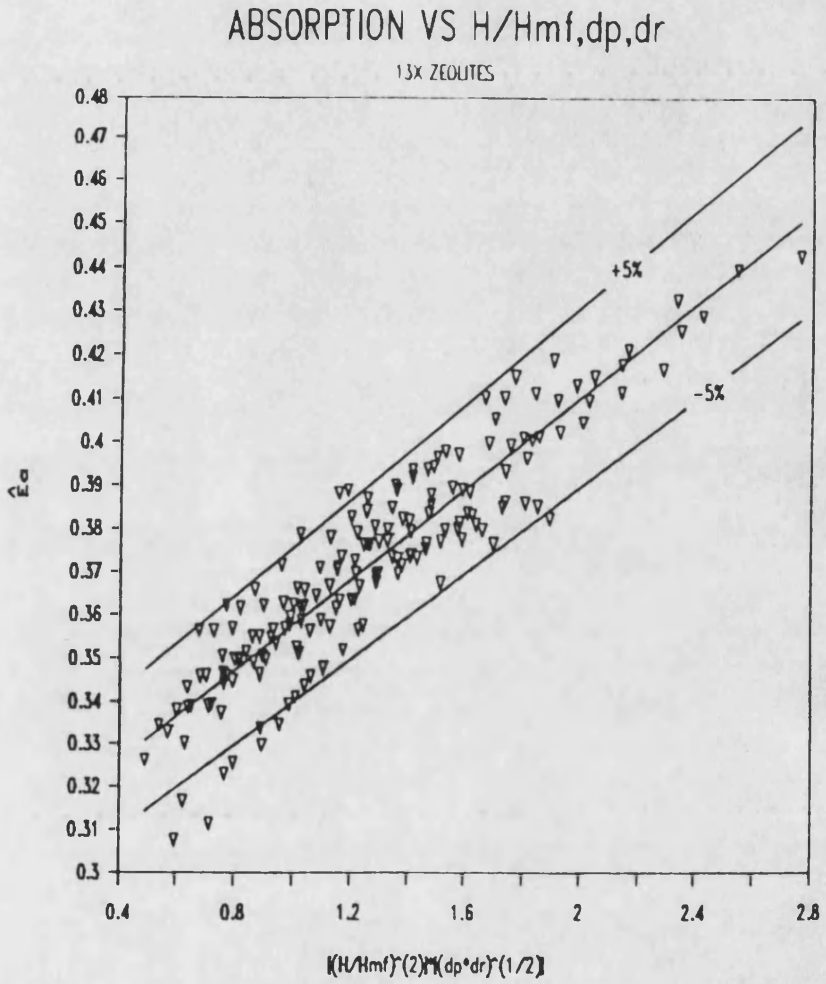

Figure 6.7.1. Correlation between light absorption and fluidisation parameters for 13X zeolites

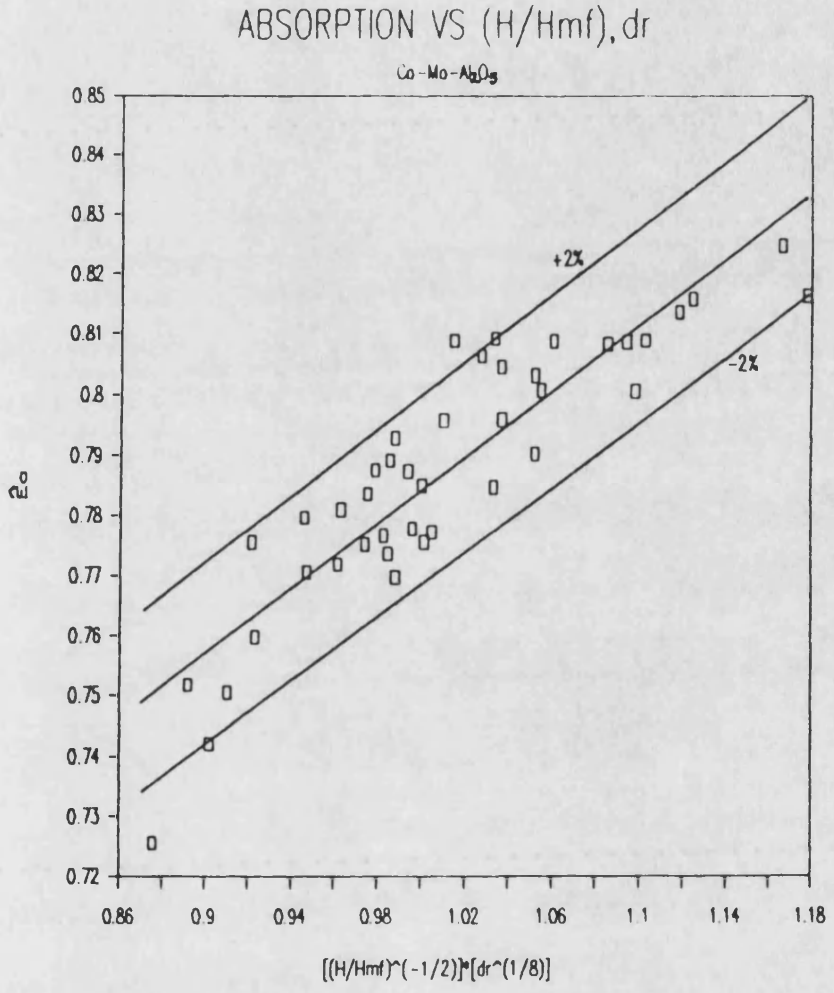

Figure 6.7.2. Correlation between light absorption and fluidisation parameters for $Co-Mo-Al_2O_3$

The reason for the differences between 13X zeolites Co-Mo-Al_2O_3 can be seen by examining the $\hat{E}_r/\hat{E}_t$ versus u/u_{mf} plots. Figures 6.7.3 and 6.7.4 show the bounded zones (as explained in section 6.2.) of $\hat{E}_r/\hat{E}_t$ vs u/u_{mf} plots of 13X zeolite and Co-Mo-Al_2O_3 particles for reactors A and D. From these plots it can be seen that the bounded zones for the two types of particles are in different regions on the plot.

Since light transmittance is of the same order of magnitude for both types of particles, the higher zone occupied by the 13X zeolites on the $\hat{E}_r/\hat{E}_t$ vs u/u_{mf} plots means that their reflectance is higher than that on Co-Mo-Al_2O_3. This behaviour implies that light absorption must be higher for Co-Mo-Al_2O_3 than that of 13X zeolites. In fact, on the whole light absorption by zeolites 13X particles is 30 to 44% of the input energy, while light absorption by Co-Mo-Al_2O_3 particles is 72 to 82%.

Finally, it can be concluded that these correlations can be used for the specific types of particles used. A more general equation for modelling light absorption was not found.

6.8 Conclusions

The experimental results of the present chapter led to the following conclusions:

1) Light absorption by fluidised particles in a two-dimensional fluidised photoreactor can be evaluated by using a radiation balance of light energy.

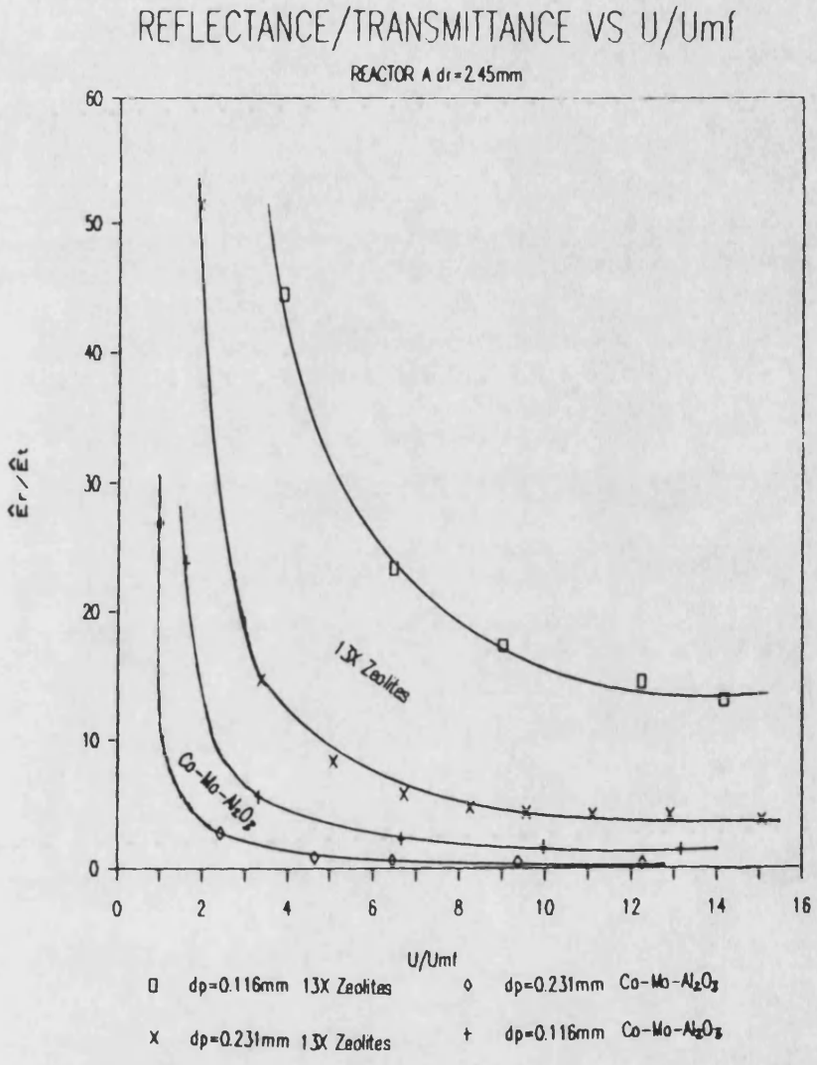

Figure 6.7.3. The ratio of light reflectance to transmittance as a function of flow rate for reactor A. 13X zeolite and Co-Mo-Al_2O_3 particles

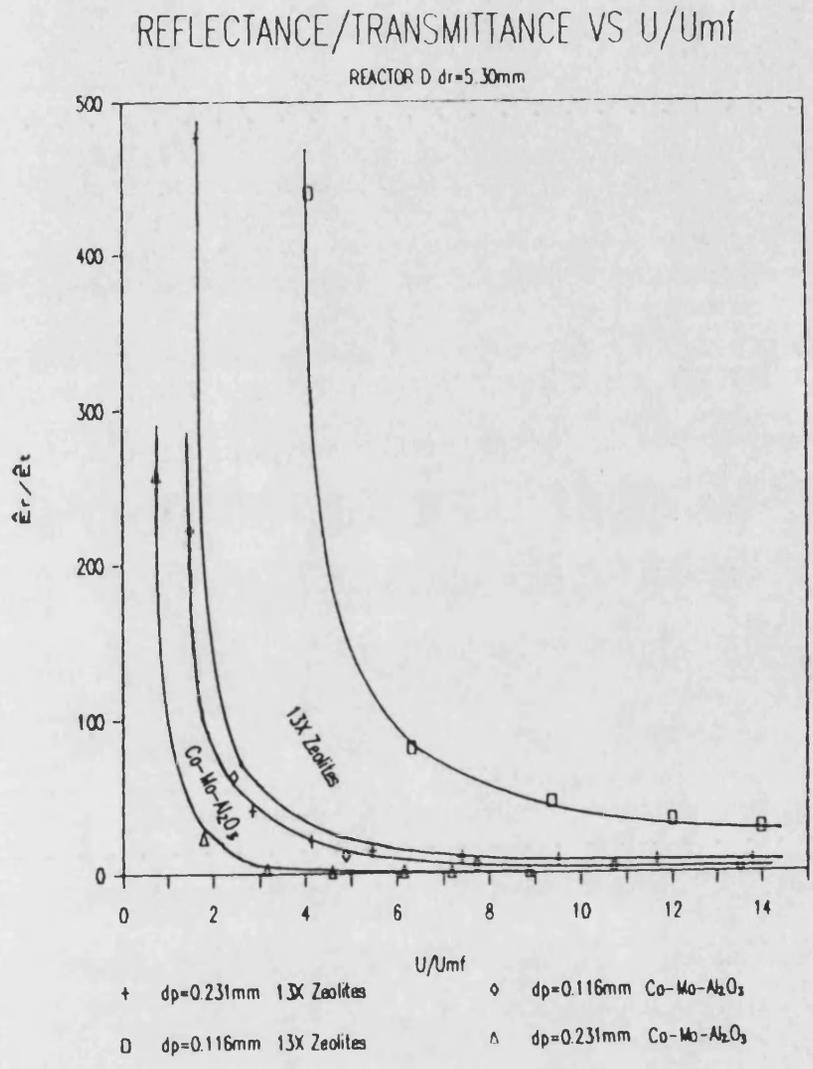

Figure 6.7.4. The ratio of light reflectance to transmittance as a function of flow rate for reactor D. 13X zeolite and Co-Mo-Al_2O_3 particles

2) The $\hat{E}_r/\hat{E}_t$ versus u/u_{mf} plots provide the means for defining the domain of the operating conditions of the reactor for a given range of particle diameters.

3) The ratio $\hat{E}_r/\hat{E}_t$ increases with reactor thickness.

4) Light absorption increases with flow rate as well as with particle diameter.

5) Equations 6.7.1 and 6.7.2 have been found to correlate light absorption in two-dimensional fluidised photoreactors. Although these equations are dependent on the type of particles used, it should be worth to examine their validity in larger scale systems.

CHAPTER 7

7. THE MODELLING OF A HYPOTHETICAL REACTION IN A FLAT FLUIDISED PHOTOREACTOR

7.1 Introduction

The performance and the behaviour of a chemical reactor can be predicted if a reactor model exists which can describe the successive states of a physical or chemical process.

For a conventional chemical reactor model, the stoichiometry, thermodynamics and energetics of the reaction must be known, the transport processes and reaction kinetics must be correctly represented.

For a photochemical reactor-model, it has been pointed out[93] that not only the photochemistry of the reaction, the transport processes and reaction kinetics are needed, it is also necessary to include a radiation energy absorption equation.

The following sections describe the representation of reaction kinetics, flow characteristics and the application of the radiation energy absorption equation.

7.2 Selection of Hypothetical Photoassisted Reaction

Usually, simple reactions with well established kinetic equations were used as test-reactions in photochemical reactor

studies. These reactions generally were performed in homogeneous or pseudohomogeneous systems with the purpose of evaluating the light distribution within the systems or when a photoreactor design analysis was performed. Among the test-reactions used by many author's[81,82,86-89] involved in photoreaction engineering studies, were the oxalic acid decomposition, the photodecomposition of chloroplatinic acid and the photoreduction of potassium ferrioxalate.

There is not as yet any suitable test-reaction with known kinetics that can be easily performed in a gas solid fluidised system. A hypothetical photochemical reaction is considered here. To simplify the mathematical model and its solution, the reaction chosen was assumed to be first order with respect to light intensity and reactant concentration. Thus, the reaction can be represented as follows :

$$A \xrightarrow{h'\nu} B \qquad 7.1$$

with a kinetics equation of

$$r_A = k\hat{E}'_a C_A \qquad 7.2$$

where

A	=	reactant in equation 7.1	
B	=	product in equation 7.1	
h'	=	Planck's constant	ergs.sec/molecule
ν	=	frequency of radiation	sec^{-1}
r_A	=	consumption rate of reactant A	gr-mole/cm^3 sec
k	=	kinetic constant	$cm^3/\mu J$

$\hat{E}a'$	=	volumetric rate of light absorption	$\mu J/cm^3 sec$
C_A	=	concentration of reactant A	$gr\text{-}mole/cm^3$

A similar kinetic equation has been used in the past by Schechter and Wissler,[46] for photoreactor design analysis. Cassano et al[29] have used equation 7.2 to show the performance of photoreactors of different geometry.

7.3 Treatment of a Fluidised Photoreactor as a Single Phase Continuous Stirred Tank Reactor (CSTR)

A variety of models[96] describing the behaviour of gas solid fluidised bed reactors have been developed. These are classified as single, two and three phase models. Since the gas fluidised reactor catalysed by the bed particles is treated for the first time as a photochemical reactor, and the light absorbed by the bed has been integrally evaluated, the single phase model, i.e., the simplest of the existing fluidised bed models, for the present seems to be an appropriate choice for the treatment of a fluidised photoreactor.

If the volume change due to photochemical reaction is negligible, the mass balance for reactant A of equation 7.1 in a single constant flow stirred tank i.e. the total irradiated fluidised bed volume is treated as only one compartment can be written as follows :

$$r_A = \frac{(C_{Ao} - C_A)F_{Ao}}{VC_{Ao}} \qquad 7.3$$

where

r_A	=	consumption rate of reactant A	$gr\text{-}mole/cm^3 sec$
C_{Ao}	=	initial concentration of reactant A	$gr\text{-}mole/cm^3$
C_A	=	final concentration of reactant A	$gr\text{-}mole/cm^3$
F_{Ao}	=	mass flow rate of reactant A	gr-mole/sec
V	=	total volume of the fluidised bed.	cm^3

7.4 Modelling of a Fluidised Photoreactor

In chapter 6, the light absorption by a gas-solid fluidised bed without any photoreaction take place within bed has been considered. An irradiated fluidised bed is now treated as a photoreactor by considering a hypothetical pseudohomogeneous photoreaction.

The modelling of the photoreactor requires the combined treatment of radiation energy absorption, reaction kinetics and the transport phenomena in the reactor. Equations 6.6.1, 7.2 and 7.3 are solved simultaneously with the following assumptions.

* Monochromatic light
* Isothermal operation
* Constant gas physical properties
* Steady state operation
* Reaction rate is first order with respect to light absorption and the exit concentration of reactant A

The fluidised bed photoreactor is assumed to be a single phase well-mixed reactor (CSTR).

If the reactor is treated as a single compartment CSTR and the maximum available light energy is utilised for reaction, the expression for r_A given by equation 7.2 can be substituted into equation 7.3 and rearranged so that the conversion of reactant A (X_A) is obtained by the following equation.

$$x_A = \frac{k\hat{E}'_a\tau}{1 + k\hat{E}'_a\tau} \qquad 7.4$$

with

$$\tau = \frac{V}{Q} \qquad x_A = 1 - \frac{C_A}{C_{Ao}} \qquad Q = \frac{F_{Ao}}{C_{Ao}}$$

where

τ = residence time of reactant A into the bed (sec)

X_A = fractional conversion of reactant A

Q = volumetric flow rate of reactant A (cm^3/sec)

Thus for a flat plate fluidised bed photoreactor if the light absorption by the whole bed, the residence time of reactant A and the kinetic constant are known, then the conversion of reactant A can be calculated using equation 7.4.

However, the distribution of photons within the reactor may vary with bed height, it is therefore more representative to consider the reaction at different bed heights. For this reason a compartmentalised model was developed.

The fluidised photoreactor was divided in several compartments, each of which was taken as a CSTR. Fig. 7.1 shows a schematic representation of the compartmentalised fluidised bed photoreactor model.

For a fixed reactor thickness, particle size and gas flow rate, the light absorption in each compartment ($\hat{E}'_{a_n}$) can be evaluated from the $E_t(h_n)$ and $E_r(h_n)$ plots by applying a radiation balance of energy. The residence time in the compartment n (τ_n) is obtained by the volumetric flow rate and the volume of the compartment n. Thus for a fixed kinetic constant the conversion in each compartment (X_{A_n}) is obtained by applying equation 7.4 to that compartment n. The total conversion (X_A) from the compartmentalised model of the fluidised photoreactor is given by:

$$x_A = 1 - \prod_{i=1} (1 - x_{Ai}) \qquad 7.5$$

The total conversion X_A obtained as described above will be compared with that obtained by treating the reactor as a single compartment CSTR.

Photoreactor A was chosen for study with 13X zeolite particles of diameter 0.165 mm at a flow rate of 6.72 times to that required for minimum fluidisation. The fluidised bed was divided into six compartments and the values of $\hat{E}'_{a_n}$ and τ_n in each compartment were evaluated. For a fixed kinetic constant and by applying equation 7.5, X_A was calculated and compared with X_A obtained from equation 7.4 taking the reactor as a single compartment. It should be noted that computational experiments using different number of compartments showed that six compartments were adequate.

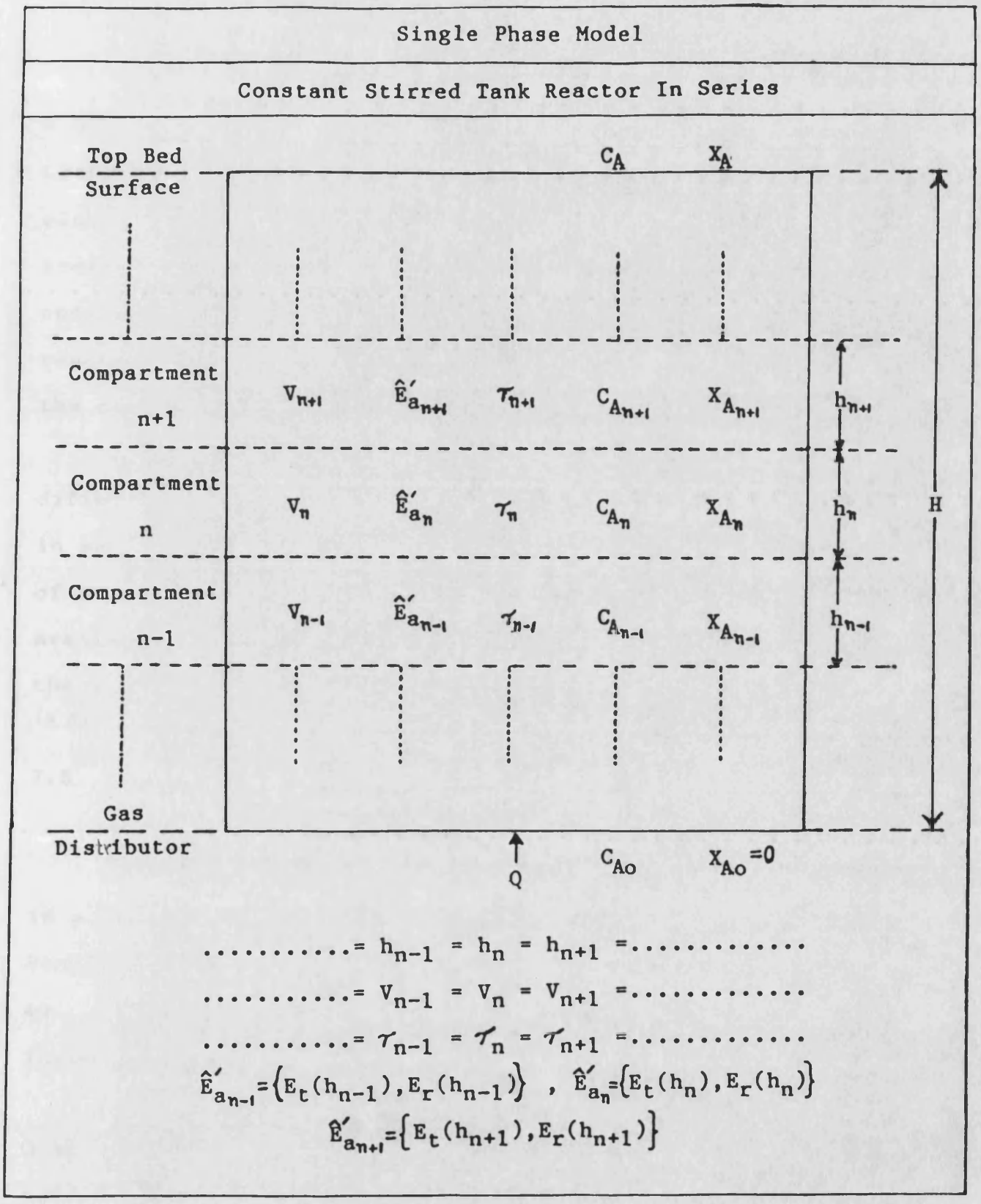

Figure 7.1. Compartmentalised model of a fluidised bed photoreactor

Six values of the kinetic constant k were chosen for study: 0.001, 0.01, 0.03, 0.05, 0.08 and 0.1. Figure 7.2 shows the plots obtained between conversion and different values of k. From these plots, it can be seen that the fluidised photoreactor can be treated as a single compartment CSTR for values of kinetic constants less than 0.01, because the final concentration of reactant A coincides with that obtained from the compartmentalised model.

For values of k greater than 0.01 the conversions are different, and it is essential to model the photoreactor as CSTR's in series. The choice of model is clearly dependent on the value of k. Whenever values of E_a at different bed heights are available, or if an equation of E_a as a function of h is known, the multi-compartment model should be used. The conclusion of course is also true in general regardless of whether the reactor is a photoreactor or not.

7.5 Effect of Flow Rate on Reactant Conversion

The effect of flow rate and hence the degree of fluidisation in a fluidised bed reactor on the reactant conversion was studied. Reactor A was chosen with 13X zeolite particles of diameter 0.116 mm. The volumetric flow rate was plotted against conversion for three different values of the kinetic constant k.

Figure 7.3 shows Q versus X_A for values of k equal to 0.01, 0.05 and 0.1 $cm^3/\mu J$. From these plots it can be seen that conversion declines with flow rate. At low values of k, i.e. k = 0.01, a sharp decrease of X_A with flow rate is observed. The rate of decrease of X_A with Q becomes less as higher flow rates are approached.

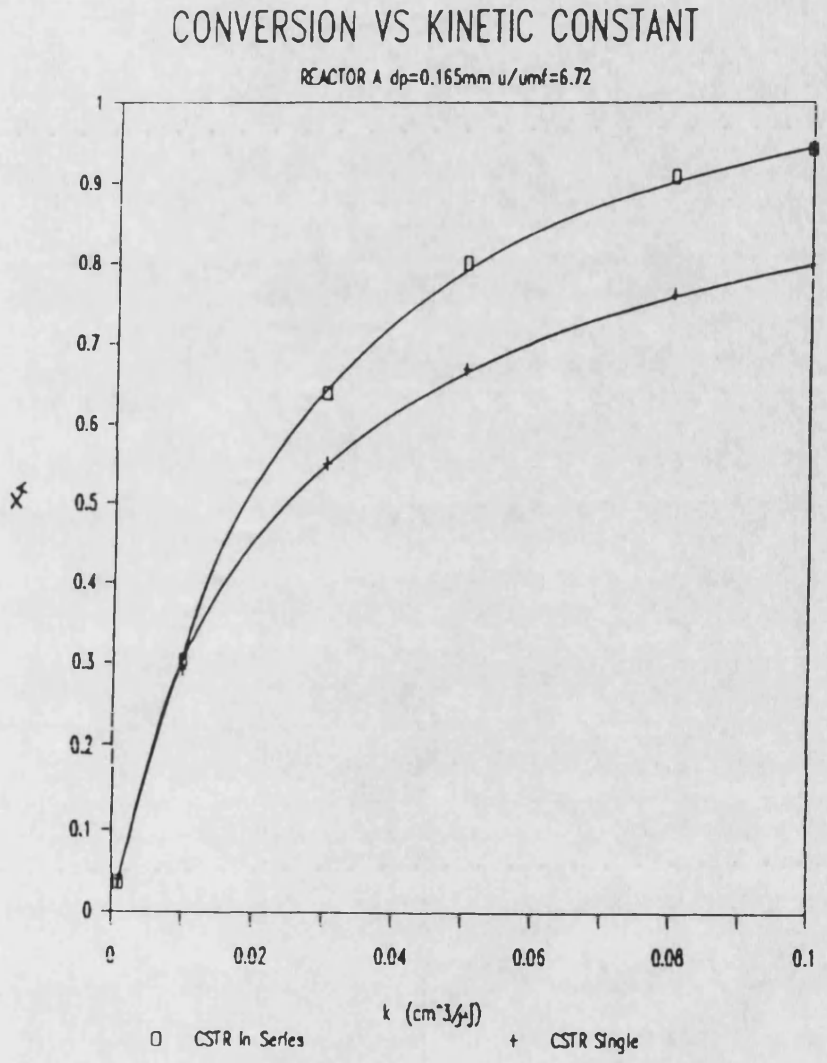

Figure 7.2. Variation of reactant conversion with values of kinetic constant. Reactor A, u/umf=6.72, dp=0.165mm and 13X zeolites

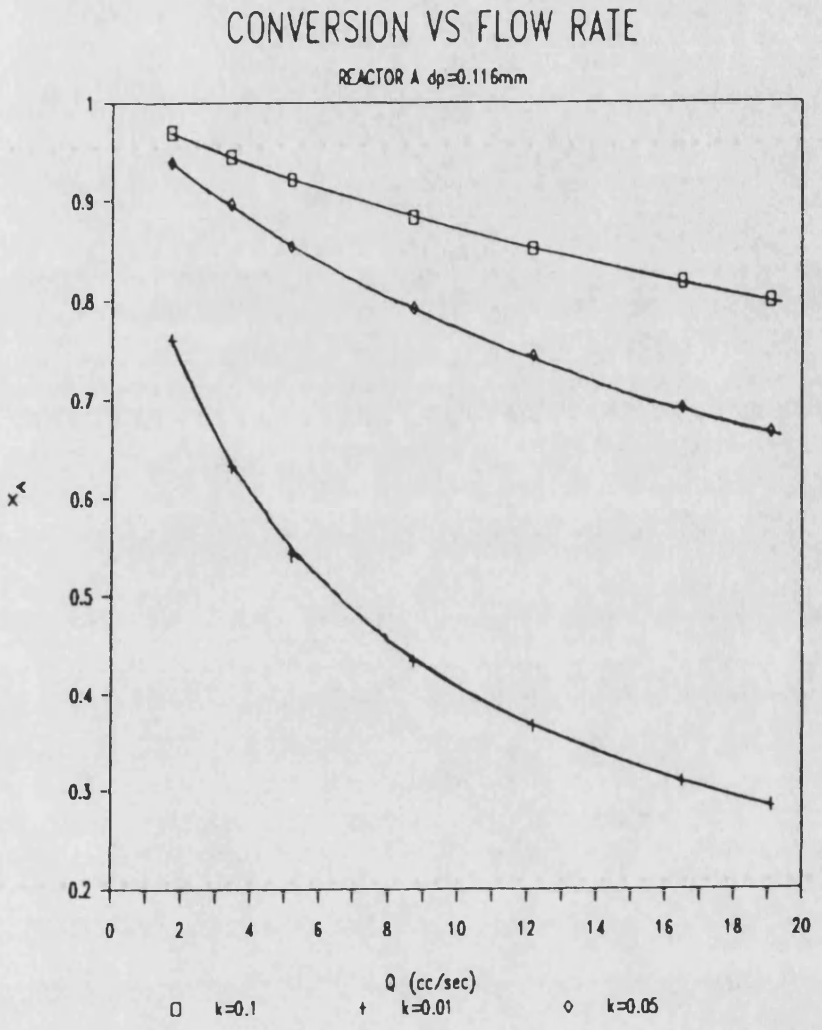

Figure 7.3. Variation of reactant conversion with flow rate. Reactor A, dp=0.116mm, 13X zeolites

The dependence of flow rate on conversion becomes more linear as higher values of the kinetic constant are approached. The decline of conversion with flow rate is due to decreasing residence time of the reactant A within photoreactor.

7.6 Effect of Light Absorption on Reactant Conversion

In section 7.4, it was shown how the experimental values of light absorption for 13X zeolites were used to simulate a hypothetical pseudohomogeneous photoreaction. Since reactant conversion depends on light absorption by the system, the effect of volumetric rate of light absorption ($\hat{E}'_a$) on reactant conversion (X_A) was investigated.

For a fixed kinetic constant and residence time, the volumetric rate of light absorption was varied and the conversion X_A was evaluated by using the single compartment model, equation 7.4. Five values of the kinetic constant k were considered for the simulation study. The residence time (τ) was assumed to be 1.3 sec. The value of τ was randomly selected within the range of the residence times of the different fluidised bed reactors used. The same value of (τ) was used by Cassano et al[29] to show the performance of different types of photoreactor geometry.

Figure 7.4 shows the dependence of X_A with $\hat{E}'_a$. From these graphs it can be seen that conversion X_A increases with the volumetric rate of light absorption ($\hat{E}'_a$). For low values of k, i.e. 0.001, 0.005 and 0.01, the dependence of X_A versus $\hat{E}'_a$ is approximately linear.

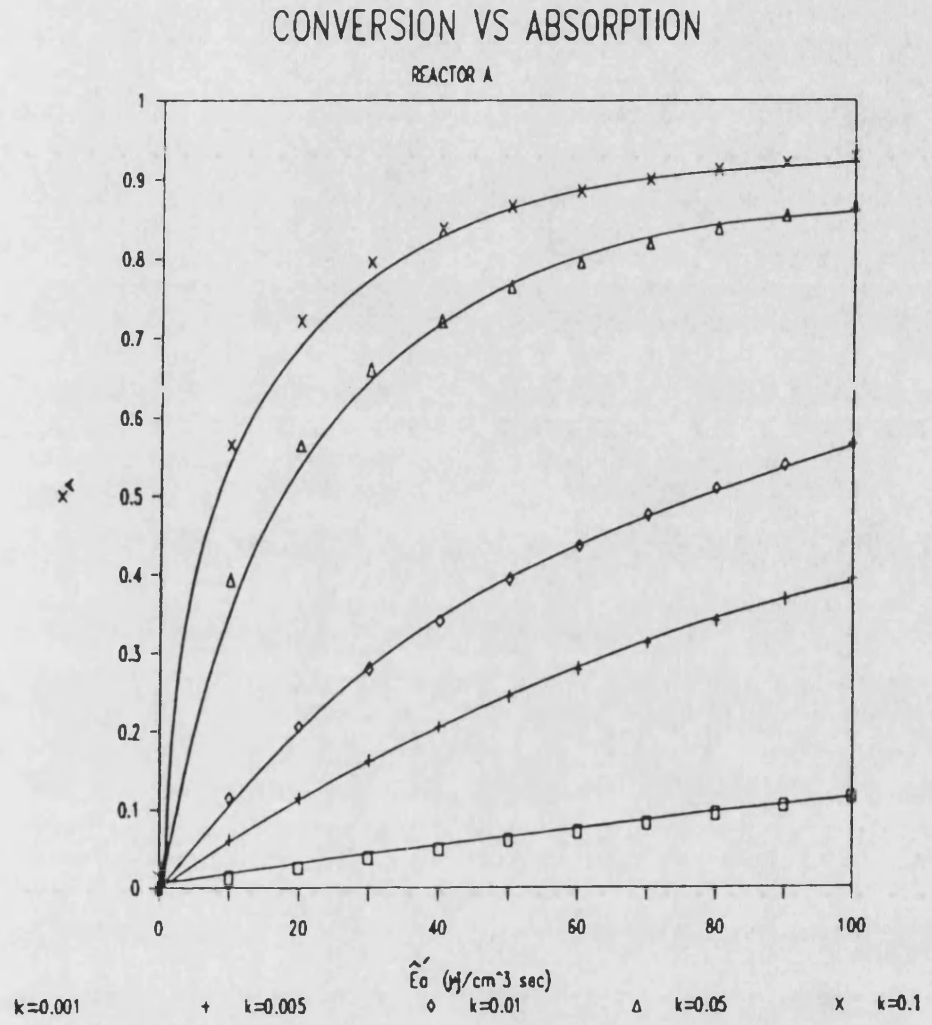

Figure 7.4. Variation of reactant conversion with volumetric rate of light absorption for reactor A and residence time of 1.3sec

For photoreactions with higher values of the kinetic constant, a sharp increase in the X_A vs $\hat{E}_a'$ curves is observed. At high values of $\hat{E}_a'$, X_A approaches some assymptotic values.

7.7 Discussion of the Fluidised Bed Photoreactor Model

The local volumetric rate of light absorption in a homogeneous system can be evaluated by applying a radiation balance. This parameter is essential for any analysis and design of a photoreactor and it is generally a function of the spatial parameters of the system.

The non-homogeneity of radiation field due to the photon-scattering of particles has been examined by different research groups[68-74]. They used the Monte-Carlo technique to evaluate the heterogeneous radiation field, resulting in considerable mathematical complexity despite the high number of assumptions made.

The use of the new optical technique employed by the present study made possible the evaluation of volumetric rate of light absorption ($\hat{E}_a'$) by the measured values of light transmittance and reflectance through a radiation balance without the need of complex radiation formulations.

In section 7.4 it had been shown how the treatment of a fluidised bed as a single phase model was coupled with the heterogeneous radiation field. Obviously in the single phase model, no segregation between dilute and dense phase is considered and the whole bed is treated as one phase.

The use of more complex fluidised bed models describing perhaps with greater fidelity the fluidisation flow and particle patterns within the bed such as the two phase and three phase models, requires the knowledge of the local volumetric rate of light absorption in the separate phases (bubble phase, dense phase and cloud phase).

The heterogeneous radiation field can then be coupled with the reactor material balance equations. The type of flow, i.e. plug flow, perfect mixing, etc, through the separate phases is another parameter which has to be considered. In addition to that, mass transfer between the phases have to be taken into account as well as the controlling steps of the photoreaction on the catalyst surfaces. Heat transfer may also have to be taken into account and accordingly the temperature effects on product selectivity should be considered.

CHAPTER 8

DISCUSSION, CONCLUSIONS AND RECOMMENDATIONS

8.1 Summary of Discussion

The actinometric technique is commonly used for the experimental study of light absorption in photoreactors. However, such a technique cannot be applied to the gas-solid system used by the present study, because there is not as yet any suitable test reaction of well known kinetics. A new optical technique has been devised in the present study. This measurement technique made possible the evaluation of light transmittance and reflectance. This technique makes use of optical measurements of the total light transmittance through and light reflectance from the reactor and this technique can be applied to other heterogeneous systems such as gas-liquid and gas-liquid-solid photoreactors. However, the incident light beam must be compatible with the detection devices. The dimensions of incident light beam must ensure that the total light transmittance through and light reflectance from the reactor are completely collected by the detection devices. This can be achieved by the use of integrating spheres.

In fluidised photoreactors light transmittance increases with flow rate because of the creation of large voids within bed. Large voids allow more light to penetrate further into the bed

leading to higher light transmittance. As particle diameter increases bed voidage increases and hence light transmittance through the bed increases. Light transmittance decreases with increasing reactor thickness. This is due to the effect of longer light path travelled through the reactor and higher photon-scattering within the bed. Light reflectance decreases with flow rate because more photons penetrate into the bed.

A simple simulation of a fluidised photoreactor has been studied here. Useful information on the behaviour of such reactors has been derived when a single photoreaction was performed. However, in an industrial process more complex photoreactions are involved and it is essential to have information on the local values of the design variables as discussed in section 7.7.

8.2 Conclusions

The important conclusions drawn from this research are as follows.

(1) A flat plate fluidised bed reactor is ideal for photoreactions because fluidisation enchances contact between reactants, photocatalyst and photons (see section 2.7).

(2) The local light transmittance increases with bed height above the distributor. The mean light transmitted through the whole irradiated area of the reactor increases with flow rate and with particle diameter. A semilogarithmic dependence between mean light transmittance and reactor thickness was found. For the two

types of particles used, two correlations (equations 4.2 and 4.3) were found. These correlations show that mean light transmittance is directly proportional to bed expansion, square root of particle diameter and inversely to reactor internal thickness. The coefficients of the above correlations are dependent on the type of particles used.

(3) The local light reflectance decreases with bed height above the distributor. The mean light reflectance decreases with gas flow rate and particle size. Light reflectance does not vary significantly with reactor thickness. A linear dependence between light reflectance and bed expansion has been found. Two correlations between light reflectance and fluidisation parameters have been found. The coefficients on the above correlations are dependent on the type of particles.

(4) The light energy available within photoreactor, i.e. light absorption, has been evaluated by the measured optical variables, i.e. light transmittance and light reflectance, by applying a radiation balance (equation 6.1) to the whole reactor system. Light absorption increases with gas flow rate, particle diameter and bed expansion. The light reflectance relative to transmittance increases with reactor thickness. Two correlations for light absorption have been proposed. The fluidisation parameters involved were bed height, particle diameter and reactor thickness. The coefficients of the equations are dependent on the type of particles used.

(5) The fluidised photoreactor was modelled as a single phase (with respect to fluidisation) single compartment constant flow

stirred tank reactor. A hypothetical photochemical reaction which is first order with respect to light absorption and reactant concentration was simulated. The kinetic constant was shown to be an important parameter in the modelling the photoreactor as a CSTR in series. The photoreactant conversion decreases with flow rate and increases with light absorption.

8.3 Recommendations

It is recommended that further improvements towards the modelling and design of photoreactors would be made if the present research could be extended to the following areas.

The minimisation of light lost from the photoreactor will increase the light energy available within reactor. Thus the transparent back wall of the reactor can be replaced by a flat plate reflector (for example a mirror) which will reduce the light transmittance to zero and the only term to be measured will be the light reflectance for the evaluation of light absorption through 6.1 equation. Such an arrangement might lead to an increase in light absorption. The correlations found in the present study may be modified and tested. It should be noted that since a mirror will receive irradiation from all directions and will reflect accordingly, the experiments must ensure that all the light reflected from the reactor is collected by the integrating sphere for reflectance measurements.

The increase of light absorption will be enchanced by irradiating the flat plate photoreactor from both sides. If an

increase on light absorption is proved to be so, then such an arrangement can be experimentally investigated. Thus two integrating spheres should be used simultaneously with each integrating sphere measuring both transmittance and reflectance.

The present research has shown how a flat plate fluidised bed might behave as a photoreactor. The correlations obtained for light transmittance, reflectance and absorption have only been tested with the ranges of values of the variables used. For large-scale modelling and design of a photoreactor to be used in an industrial photochemical process, the above correlations must be tested over a broader range of values of the variables.

The new optical technique developed in the present study for light transmittance and reflectance measurements can also be used for the modelling and design of gas-liquid-solid fluidised systems, a subject which has not received much attention.

REFERENCES

1. Baginski, F.C., 1952, Eng. Dissertation, Yale University, U.S.A.

2. Cassano, A.E. and Smith, J.M., 1966, A.I.Ch.E.J., 13, No. 5, p. 915.

3. Hutson, T., Logan, R.S., 1972, Chem. Eng. Prog., 68, p. 76.

4. Matsuura, T., Smith, J.M., 1970, Ind. Eng. Chem. Fund.,9, No. 2, p. 253.

5. Matsuura, T., Smith, J.M., 1970, A.I.Ch.E.J., 16, No. 6, p. 1064.

6. Schorr, V., Smith, J.M., 1971, Ind. Eng. Chem., 10, No. 4, p. 570.

7. Zamaraev, K.I., Parmon, V.N., 1980, Catal. Rev. Sci. Eng., 22, p. 261.

8. Zamaraev, K.I., Parmon, V.N., 1980, Russian Chem. Reviews 49, p. 695.

9. Markham, M.C., Laidler, K.J., 1953, J. Phys. Chem., 57, p. 363.

10. Heidt, L.J., McMillan, A.F., 1953, Science, 117, p. 75.

11. Mann, K.R., Lewis, N.S., Miskowshi, V.M., Erwin, D.K., Hammond, G.S., Gray, H.B., 1977, J. Am. Chem. Soc.,99, p. 5525.

12. Kiwi, J., Gratzel, M., 1979, Nature, 281, p. 651.

13. Fujishima, A., Honda, K., 1972, Nature, 238, p. 37.

14. Schrauzer, G.N., Guth, T.D., 1977, J. Am. Chem. Soc., 99, p. 7189.

15. Van Damme, H., Hall, W.K., 1979, J. Am. Chem. Soc., 101, p. 4373.

16. Hemminger, J.C., Carr, R., Somorjai, G.A., 1978, Chem. Phys. Lett., 57, p. 100.

17. Inoue, T., Fujishima, A., Konishi, S., Honda, K., 1979, Nature, 277, p. 637.

18. Sakata, T., Kawai, T., Okuyama, M., 1980, Third Hydrog. Energy Prog. Proceedings. World Hydrogen Energy Conf., eds. Veziroglu, T.N., Fueki, K., Ohtar, T., Pergamon Press, 2, p. 773.

19. Carr, R.G., Somorjai, G.A., 1981, Nature, 290, p. 576.

20. Augugliaro, V., Lauricella, A., Rizzuti, L., Schiavello, M., Sclafani, A., 1982, Int. J. of Hydrog. Energy, 7, No. 11, p. 845.

21. Augugliaro, V., D Alba, F., Rizzuti, L., Schiavello, M., Sclafani, A., 1982, Int. J. of Hydrogen Energy, 7, No. 11, p. 851.

22. Kasal, P.H., Bishop, R.J., 1977, J. Phys. Chem., 81, p. 1527.

23. Jacobs, P.A., Uytterhoeren, J.B., Beyer, H.K., 1977, J. Chem. Soc. Chem. Comm., p. 128.

24. Leutwyler, S., Schumacher, E., 1977, Chimia, 31, p. 475.

25. Khan, F., Yue, P.L., Rizzuti, L., Auguliaro, V., Brucato, A., 1983, Ind. Eng. Chem., 22, No. 2, p. 238.

26. Khan, F., 1983, Ph. D. Thesis, Bath University, U.K.

27. Bhagwat, W.V., Dhar, N.R., 1932, J. Indian Chem. Soc., p. 335.

28. Hill, F.B., Felder, R.M. 1965, A.I.Ch.E.J., 11, No. 5, p. 873.

29. Cassano, A.E., Silverton, P.L., Smith, J.M., 1967, Ind. Eng. Chem., 59, No. 1, p. 18.

30. Harrano, Y., Smith, J.M., 1968, A.I.Ch.E.J., 14, No. 4, p. 584.

31. Harrano, Y., Smith, J.M., 1972, Int. Chem. Eng., 12, No. 1, p. 131.

32. Jacob, S.M., Dranoff, J.S., 1966, Chem. Eng. Prog. Symp. Ser., 62, No. 68, p. 47.

33. Jacob, S.M., Dranoff, J.S., 1968, Chem. Eng. Prog. Symp. Ser., 64, No. 89, p. 54.

34. Jacob, S.M., Dranoff, J.S., 1970, A.I.Ch.E.J., 16, No. 3, p. 359.

35. Williams, J.A., Ragonese, F.P., 1970, Chem. Eng. Sci., 25, p. 1751.

36. Scarbo, R., Williams, J.A., 1973, Chem. Eng. Sci., 28, p. 83.

37. Matsuura, T., Smith, J.M., 1970, A.I.Ch.E.J., 16, No. 2, p. 321.

38. Zolner III, W.J., Williams, J.A., 1971, A.I.Ch.E.J., 17, No. 2, p. 502.

39. Williams, J.A., 1976, A.I.Ch.E.J., 22, No. 4, p. 811.

40. Akehata, T., Shirai, T., 1972, J. Chem. Eng. of Japan, 5, No. 4, p. 385.

41. Costa, L.J., 1977, Afinida (Spanish), 34, No. 3-4, p. 19.

42. Tournier, A., Deglise, X., Andre, J.C., Niclause, M., 1982, A.I.Ch.E.J., 28, No. 1, p. 156.

43. Roger, M., Villermaux, J., 1979, Chem. Eng. Journal, 17, p. 219.

44. Roger, M., Villermaux, J., 1983, Chem. Eng. Journal, 26, p. 85.

45. Alfano, M.O., Romero, L.R., Cassano, A.E., 1986 Chem.Eng. Sci., 41, No. 3, p. 421.

46. Schechter, R.S., Wissler, E.H. 1960, Appl. Sci. Res.,9, p. 334.

47. Santarelli, F., Stramigioli, C. 1975, Ing. Chim. Italiano, 11, p. 63.

48. Williams, J.A., 1978, A.I.Ch.E.J., 24, p. 335.

49. Harada, J. Akehata, T., Shirai, T., 1971, Kagaku Kogaku, 35, p. 233.

50. Harris, P.R., Dranoff, J.S., 1965, A.I.Ch.E.J., 11, p. 497.

51. Magelli, F., Santarelli, F., 1978, Chem. Eng. Sci., 33, p. 611.

52. Spadoni, G., Bandini, E., Santarelli, F., 1980, Chem. Eng. Sci., 35, p. 925.

53. Pasquali, G., Santarelli, F., 1978, Chem. Eng. Commun., 2, p. 271.

54. Stramigioli, C., Spadoni, G., Santarelli, F., 1983, Int. J. Heat Mass Transfer, 26, p. 539.

55. Akehata, T., Shirai, T., Ishizoki, N., Ito, K., 1973, Kagaku Kogaku, 37, p. 1026.

56. Cerda, J., Irazoqui, H.A., Cassano, A.E., 1973, A.I.Ch.E.J., 19, p. 963.

57. Cerda, J., Marchetti, J.L., Cassano, A.E., 1977, Lat. Am. J. Heat Mass Transfer, 1, p. 33.

58. De Bernardez, E., Cassano, A.E., 1982, Lat. Am. J. Heat Mass Transfer, 6, p. 333.

59. Romero, R.L., Alfano, O.M., Marchetti, J.L., Cassano, A.E., 1983, Chem. Eng. Sci., 38, p. 1593.

60. Alfano, O.M., Romero, R.L., Cassano, A.E., 1985, Chem. Eng. Sci., 40, p. 2119.

61. Stramigioli, C., Santarelli, F., Foraboschi, F.P., 1975, Ing. Chim. Italiano, 11, p. 143.

62. Stramigioli, C., Santarelli, F., Foraboschi, F.P., 1977, Appl. Sci. Res., 33, p. 23.

63. Bandini, E., Stramigioli, C., Santarelli, F., 1977, Chem. Eng. Sci., 32, p. 89.

64. Yokota, T., Iwano, T., Tadaki, T., 1976, Kagaku Kogaku Roubunshu, 2, p. 298.

65. Sugawara, T., Omori, K., Ohashi, H., 1979, J. Chem. Eng. of Japan, 12, No. 2, p. 143.

66. Bhattacharya, A., Deshpande, P.K., 1978, J. Indian Inst. Sci., 327, p. 43.

67. Rudd, D.F., 1960, Chem. Eng. Sci., 12, p. 51.

68. Santarelli, F., Stramigioli, C., Spiga, G., Ozisik, M.N. 1982, Int. J. Heat Mass Transfer, 25, p. 57.

69. Stramigioli, C., Spadoni, G., Santarelli, F., 1978, Int. J. Heat Mass Transfer, 21, p. 660.

70. Spadoni, G., Stramigioli, C., Santarelli, F., 1980, Chem. Eng. Commun., 4, p. 643.

71. Spadoni, G., Bandini, E., Santarelli, F., 1978, Chem. Eng. Sci., 33, p. 517.

72. Ozisik, M.N., Siewert, C.E., 1969, Int. J. Heat Mass Transfer, 12, p. 611.

73. Lii, C.C., Ozisik, M.N., 1973, Int. J. Heat Mass Transfer, 16, p. 685.

74. Boffi, V.C., Santarelli, F., Spiga, G., Stramigioli, C., 1979, Int. J. Heat Mass Transfer, 22, p. 1705.

75. Akehata, T., Ito, K., Inokawa, A., 1976, Kagaku Kogaku Ronbunshu, 2, p. 583.

76. Inokawa, A., Akehata, T., 1980, Kagaku Kogaku Ronbunshu, 6, p. 178.

77. Rizzuti, L., Yue, P.L., 1983, Chem. Eng. Sci., 38, p. 1241.

78. Yue, P.L., Rizzuti, L., Augugliaro, V., 1986, Chem. Eng. Sci., 41, p. 171.

79. Alfano, O.M., Romero, R.L., Cassano, A.E., 1986, Chem. Eng. Sci, 41, p. 1137.

80. Yokota, T., Iwano, T., Tadaki, T., 1977, Kagaku Kogaku Ronbunshu, 3, p. 248.

81. Yokota, T., Iwano, T., Tadaki, T., 1978, Kagaku Kogaku Ronbunshu, 4, p. 103.

82. Yokota, T., Iwano, T., Deguchi, H., Tadaki, T., 1981, Kagaku Kogaku Ronbunshu, 7, p. 157.

83. Yokota, T., Iwano, T., Saito, A., Tadaki, T., 1981, Kagaku Kogaku Ronbunshu, 7, p. 164.

84. Lii, C.C., Ozisik, M.N., 1973, Int. J. Heat Mass Transfer, 16, p. 685.

85. Sugawara, T., Tadaki, T., Maeda, S., 1971, Kagaku Kogaku, 35, p. 461.

86. Shirotsuka, T., Nishiumi, M., 1971, Kagaku Kogaku, 34, p. 1363.

87. Shirotsuka, T., Nishiumi, M., 1972, Kagaku Kogaku, 36, p. 300.

88. Shirotsuka, T., Mishiumi, M., 1972, Kagaku Kogaku, 36, p. 307.

89. Shirotsuka, T., Nishiumi, M., 1972, Kagaku Kogaku, 36, p. 328.

90. Otake, T., Tone, S., Higuchi, K., Nakao, K., 1981, Kagaku Kogaku Ronbunshu, 7, p. 57.

91. Otake, T., Tone, S., Higuchi, K., Nakao, K., 1983, Int. Chem. Eng., 23, p. 288.

92. Geldart, D., 1975, in Geldart, D. (eds.), "Fluidisation Technology", Vol. 1, McGraw-Hill, New York.

93. Yue, P.L., 1985, NATO-ASI Series, in Schiavello, M. (ed.), "Photoelectrochemistry, Photocatalysis and Photoreactors", p. 527, Reidel, D.Publishing Company, Netherlands.

94. Braun, A.M. 1988, NATO-ASI Series, in Schiavello, M. (ed.), "Photocatalysis and Environment Trends and Applications", p. 601, Kluwer Accademic Publishers, Netherlands.

95. Grace, J.R., 1971, A.I.Ch.E., Sympos. Series, 67, p. 159.

96. Grace, J.R., 1986, "Gas Fluidisation Technology" edited by D. Geldart.

97. Sheu, C.Y., Johnstone, H.F., 1955, A.I.Ch.E.J., 1, p. 349.

98. Kato, K., Wen, C.Y., 1969, Chem. Eng. Sci., 24, p. 1351.

99. Kunii, D., Levenspiel, D., 1969, "Fluidisation Engineering", Wiley, New York.

100. Yue, P.L., Khan, F., Rizzuti, L., 1983, Chem. Eng. Sci., 38, p. 1893.

101. Miyama, H., Fujii, N., Nagae, Y., 1980, Chem. Phys. Lett., 74, p. 523.

102. Pichat, P., Herrmann, J.M., Courbon, H., Disdier, J., Mozzanega, M.N., 1982, Can. J. of Chem. Eng., 60, p. 27.

103. Movahed,H., 1978, M.Sc.Thesis, University of Manchester Institute of Science and Technology, U.K.

104. Rizzuti, L., Brucato, A., Brucato, V., 1985, Proc. 2nd Ibero American Conf. on Catal.

105. Wen, C.Y., Yu, Y.H., 1966, A.I.Ch.E.J., 12, p. 610.

106. Kunii, D., Levenspiel, O., 1977, in Kunii, D., and Levenspiel, O., (eds.), "Fluidisation Engineering", Krieger, R.E., Publishing Co., Inc., New York.

107. Richardson, J.F., 1971, in Davidson, T.F. and Harrison, D., (eds.), "Fluidisation", Academic Press, New York.

108. Calvert, J.G., Pitts, J.N., 1966, "Photochemistry", p. 780, Jolan Wiley and Sons, Inc., New York.

109. Leighton, W.G., Forbes, G.S., 1930, J. Am. Chem. Soc., 52, p. 3139.

110. Parker, C.A., Hatchard, C.G., 1956, Proc. Roy. Soc., (London), A235, p. 518.

111. Grim, F., Luckay, W.G., 1968, Appl. Opt., 7, p. 2289.

112. Fendley, J., 1985, Solar Energy, 35, No. 3, p. 281.

113. Iatridis, D., Yue, P.L., 1988, NATO-ASI Series, in Schiavello, M. (ed.), "Photocatalysis and Environment Trends and Applications", p. 603, Kluwer Accademic Publishers, Netherlands.